NASA TECHNICAL MEMORANDUM NASA TM-88583

THEORY AND DESIGN OF FLIGHT-VEHICLE ENGINES

V. T. Zhdanov and R. I. Kurziner, Eds.

Translation of Teoriya i konstruktsiya dvigateley letatel'nykh apparatov, USSR Academy of Sciences, Moscow, 1979. 158 pages.

NATIONAL AERONAUTICS AND SPACE ADMINISTRATION
WASHINGTON, D.C. 20546 APRIL 1987

TABLE OF CONTENTS

From the Editors

A great deal of attention in the Soviet Union is being paid to elaborating on the scientific legacy of the founders of rocket and space science and technology. Since 1966 annual scientific lectures have been held in Kaluga, dedicated to elaborating the creative legacy and developing the ideas of K. E. Tsiolkovskiy; since 1970 the F. A. Tsander memorial scientific lectures have been held in Moscow, Leningrad, Riga, and Dnepropetrovsk; since 1971 various scientific and social organizations, the USSR DOSAAF [Voluntary Society for Collaboration with the Army, Air Force, and Navy], and institutions of higher learning have been conducting lectures dedicated to some pioneers in the conquest of space.

In 1977 the Presidium of the USSR Academy of Sciences adopted a resolution concerning the holding of a scientific session dedicated to the 70th anniversary of the birthday of S. P. Korolev. Participating in the work of this session of lectures were prominent Soviet scientists who worked with S. P. Korolev, researchers into the scientific creativity of this remarkable scientist, veterans of Soviet rocket technology, and the scientific societies of Moscow and other cities in the nation.

The second set of S. P. Korolev memorial lectures took place between 29 March and 4 April 1978. About 50 reports were given at the plenary session and at the sessions of four sections. In addition, the symposium "The Role of the Researcher's Personality in the Genesis of Cosmonautics Theory and Liquid-Fuel Rocket Technology" was held within the framework of the symposium.

Later, in connection with the creation of the USSR Academy of Sciences Commission on Elaboration of the Legacy of Pioneers in the Conquest of Outer Space (Corresponding Member of the USSR Academy of Sciences V. V. Raushenbakh, Commission chairman), entrusted with study of the scientific creativity of Academician S. P. Korolev, Academician M. K. Yangel', Corresponding Member of the USSR Academy of Sciences G. N. Babakin, and other founders of space rocket science and technology, a resolution was adopted to conduct joint scientific lectures dedicated to the memory of the outstanding Soviet scientists and pioneers in the conquest of outer space.

The 1979 scientific lectures were held in Moscow from 26 February to 2 March. Over 1000 people took part in them, including prominent Soviet scientists and experts in space rocket technology, aviation and cosmonautics historians, veterans of Soviet rocket building, pilot-cosmonauts of the USSR, and talented junior scientists.

About 80 reports were given at the plenary and section sessions. They dealt with development of the scientific legacy of the founders of space rocket technology, problems of applied celestial mechanics and guidance, and topics in the theory and construction of aircraft engines and the history of aviation and cosmonautics. Three thematic sessions dedicated to the scientific creativity of A. M. Isayev, B. S. Stechkin, and S. A. Chaplygin were also held.

The collection before the reader includes reports read at the sessions of the "Theory and Construction of Aircraft Engines" section and three reports on this subject given at the 1978 lectures. The basic content of the collection consists of results of research on various aspects of the theory of operation of jet engines at high supersonic speeds: high-temperature gas-turbine jet engines (GTD), hypersonic ramjet engines (GPVRD), and liquid-fuel rocket engines.

Discussions involve the problems of testing modern complex high-temperature GTD and trends in the development of testing methods, and requirements for the principles of testing future aircraft engines are formulated. Methods of selecting the basic parameters of cooled high-temperature turbines of aircraft GTD are examined.

An approximate model of the operation of high-speed PVRD [ramjet engines] (SPVRD [supersonic ramjets] and GPVRD) is examined, the results from analysis of errors in experimental determination of these engines' parameters and results from computational study on selecting the optimal geometry of the GPVRD air inlet are cited, the effect of irregularity of a supersonic flow with shock waves on friction and heat exchange in the GPVRD duct is investigated, and the results of numerical calculation of plane supersonic flows in ducts are cited.

An analysis is made of means of hydrodynamic modeling of operation in ZhRD [liquid-fuel rocket engines] in the launch mode; the hierarchy of mathematical models of aircraft control ZhRD is examined.

The collection is aimed at the use of specialists working in the field of reaction engines for aviation and space systems. It may also prove useful to scientists, teachers, and students at aviation institutes.

THEORY AND DESIGN OF FLIGHT-VEHICLE ENGINES
(Proceedings of the Joint Scientific Lectures
Dedicated to the Memory of Soviet Scientist-Pioneers in the
Conquest of Outer Space: Moscow, 26 February-2 March 1979)

V. T. Zdanov and R. I. Kurziner, Eds. /5*

CURRENT PROBLEMS IN TESTING AVIATION ENGINES[1]

V. M. Akimov

The new and greater capabilities opening up before designers and researchers because of the introduction of computers and assorted powerful numerical methods are in many cases creating the illusion that the role of experiment is diminishing, especially in the design of aviation and space technology. For aircraft engines the problem of testing is quite an acute one and requires answers to many new and complicated questions. We shall examine this subject using the example of aircraft jet engines, bearing in mind that the problem is characteristic of rocket engines as well -- with the difference, of course, produced by the specific features of both engine types.

Gas-turbine jet engines began being produced when the theory and calculation methods of engine and element operation had already been basically developed (in our country this was accomplished primarily by Academician B. S. Stechkin and such other scientists as Prof. B. V. Uvarov, Prof. K. V. Kholshevnikov, and their scientists). Fairly refined methods of calculating gas-turbine engine strength also developed rapidly. Despite this, experimental work on operational development and testing /6
of engines under construction did and continues to constitute the basic content of gas-turbine engine construction with regard to time and cost. One of the major reasons for this situation is the inadmissibility of any markedly excess weight and size for engines and aircraft components in general. This necessitates experimental testing of the adequacy of selected performance margins for engine components and systems, which in most cases are notable for high load levels.

---

*Numbers in the margin indicate pagination in the foreign text.

[1]In preparing this report the author employed articles from various authors published in Ispytaniye aviatsionnykh dvigateley [Aviation Engine Testing], UAI Press, Ufa: No. 1, 1972; No. 2, 1974, No. 3, 1975; No. 4, 1976; No. 5, 1977; No. 6, 1978.

5,6

Data characterizing the process of experimental operational development of aviation GTD [gas-turbine engines] are given in Figs. 1-3. The many years' experience of engine-building firms indicates that the period of operational development tests averages 50-60 months (Fig. 1). Note that 30 to 50 months pass from the first test-bed tests to the first test flight. Several dozen experimental engines are used in the operational development process. A look at Fig. 2 reveals that there is a tendency towards reduction of their number, but the total accrued operating time is not decreased (Fig. 3) because the average accrued operating time for each example is increased. Out of 10^4 hours of total accrued operating time, $(1 + 2) \cdot 10^3$ hours are spent on engine operation under simulated field conditions in altitude chambers and wind tunnels. The total cost of operational development for an experimental engine is 130-150 times greater than the cost of full-scale production of one engine model in sustained production. This ratio is 30/60 for the airframe.

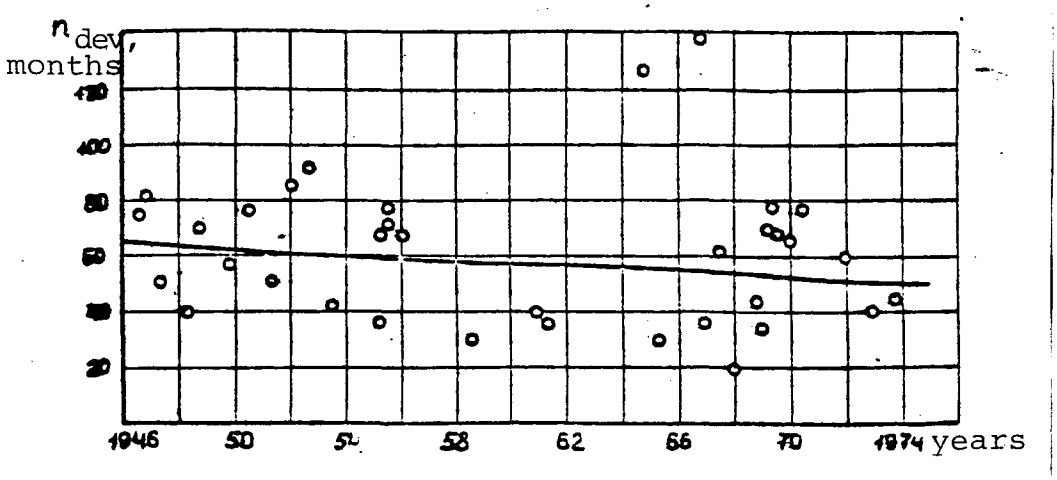

Fig. 1. Experimental operational development periods for various types of GTD in months (before beginning operational use) from the year operational development begins.

—— -- trend line.

Development of numerical methods based on use of powerful modern computers led to an abrupt increase in assorted parameters, defined in computed design, characterizing operation of all GTD components. The total number of computation operations in the design of an engine has increased from 10^6 to 10^{12} in 30 years. Universal methods allowing high-precision computation of the stressed state of extremely complicated parts, methods of optimizing an engine and its components at all levels of design (engine -- in the aircraft, assembly -- in the engine, part -- in the assembly), simulation models, such as operations

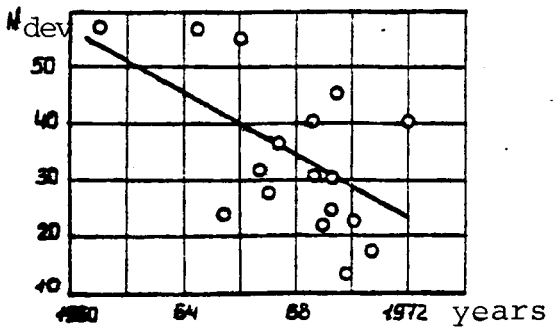

Fig. 2. Number of experimental GTD models relative to year operational development begins.

models, allowing, in particular, tracing the possible consequences of various failures, and other such possibilities presumably should have simplified the tasks of tests and reduced their required number. This did not occur in /8 practice, however. The complication of engines and their requirements, occurring together with refinement of computation and design methods, was so significant that experimental operational testing tasks also became constantly more complex. In the last few years a number of sometimes conflicting factors have made the problem of engine testing rather acute and necessitated involvement of new approaches and new methods for its solution.

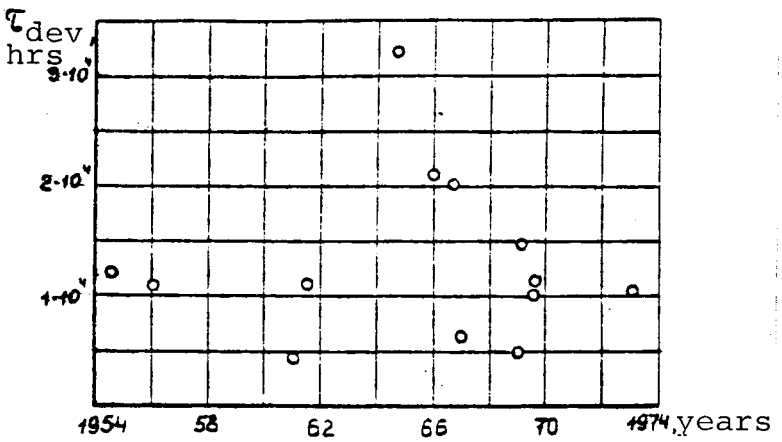

Fig. 3. Total running time of GTD during operational development relative to year operational development begins.

We shall examine the factors determining the current requirements for aviation engine tests; we shall deal first with the factors requiring increased volume and complexity of data obtained in testing.

First among such factors is the constantly increasing design and parametric complication of GTD. We shall use simple examples to show the effect of complication of engines on the complication of their tests. For instance, in modern GTD the temperature level of the gas ahead of the turbine is approximately 1600K (it will reach 1800-1900K in the next generation of engines), so only cooled turbine blades, notable for construction complexity, are employed. A cooled-blade thickness variation within 0.1 mm leads to a wall-temperature difference of ∿50K, impermissible with relatively small strength margins from the standpoint of required blade reliability and lifetime. Since such technological variability cannot be precluded in experimental models, the wall temperature of each operating blade has to be measured during operational

testing. On the other hand, all modern GTD are two- and three-shaft. Obviously, it is practically impossible to tap sensor signals from the internal rotor using traditional current-collectors. Consequently, fundamentally new means of gathering data are needed. Furthermore, the specific unit weight of modern engines has reached a level on the order of $\gamma_{sw} = 0.125$, corresponding to a thrust/weight ratio of 8. This requires designating minimum performance margins, and thus maximum experimental testing of the construction. In sum, we have to obtain a constantly increasing volume of information, which at the same time becomes more and more difficult to obtain.

Second among such factors is the complication of use conditions, including engine operation for most of a flight with inlet air parameters above atmospheric on the test-bed (an SPS [SST] engine) and integration of the powerplant components and airframe/9 (for example, the powerplant of V/STOL [vertical/short take-off and landing] aircraft with a surface-blown wing). Both these factors require testing to provide complex simulation of flight conditions on special, expensive and power-consuming stands.

Third among the factors complicating GTD testing would be the extremely high reliability of modern engines. For passenger-aircraft engines, firmly established in operation and production, this is characterized by mean times-between-failures-in-flight of $(3 + 5) \cdot 10^4$ hours, and sometimes even more, and for some specific failures, by values on the order of $0.5 \cdot 10^6$ hours. Confirmation of this reliability at the testing stage using traditional statistical methods with any acceptable trustworthiness would require a multiple increase in engine running time during operational testing, and a very large increase, as seen in Fig. 3. The practical impossibility of such a formulation of the question led to the need to develop and introduce special indirect methods of evaluating engine-component and system reliability, before launching full-scale production, in a relatively short time of testing.

Fourthly, difficulties arise in life testing because of the very large lifetime values of many modern engines. For passenger-aircraft engines the specified life (added up from several overhaul periods) is $3 \cdot 10^4$ hours, and this is now common. If the engine performance for the entire specified life were checked on a full time scale, operating $\sim$10 hours a work day, such life tests would take about 10 years. The senselessness of this situation made it necessary as engine lifetimes increased to develop and employ new, accelerated methods of testing engines, so-called equivalent tests.

Fifthly, new requirements for engines, associated with environmental protection, led to the need for GTD tests new to the engine-builder -- tests to determine the content of harmful materials in the combustion products exiting the engine and to

evaluate engine noise. New testing methods and new equipment were needed.

Sixthly, the implementation of "Standards for Airworthiness of USSR Civil Aviation Aircraft" (NLG SSSR [USSR Airworthiness Standards]), which met the requirements of the International Civil Aviation Organization (ICAO), necessitated some review of testing procedures and methods testing the characteristics of new engines. /10 Some new types of tests (tests on autorotation without lubrication, for instance) were introduced as part of these tests, the results of which were used to assess the suitability of an engine for flight operations, and the programs and procedures of certain tests had to be reviewed (e.g., the two-hundred-hour tests, traditional for our country, were replaced by one-hundred-fifty-hour tests, which better meet the generally accepted international requirements).

Along with the above factors necessitating expansion of experimental data, tendencies are found to hinder meeting of these requirements. First of these is the constant increase in the cost of experimental developments, associated with the complications of engines. This cost has increased $\sim$20 times since the first gas-turbine engines were built. Obviously, this circumstance forces us to try to reduce the number of experimental models used up in the experimental operational development of an engine.

Secondly, requirements for fuel and energy-resource economy face us with the task of constantly finding possibilities of decreasing the extent of testing (including in special high-altitude installations).

Thus, two conflicting groups of factors are making it necessary to obtain increasingly extensive data on a decreasing number of experimental models and in a shorter time of testing. The practice of engine-building has now developed certain approaches to solution of these problems, considering the above conflicts. A number of trends have been mapped out in order to provide effective solution of the engine-testing problem. Here are some of them:

-- introduction of non-contact measurements and combining of tests;

-- planning of the experiment;

-- extensive automation of the experiment and use of mathematical models of engines in tests;

-- production of special test-beds simulating an increasingly wide range of flight conditions;

-- advancement of accelerated equivalent and cyclic tests for testing lifetime;

-- rejection of certain types of testing;

-- development and use of special certification tests for engine operational reliability;

-- development and introduction of new types of tests (for noise and emissions). /11

We shall deal briefly with the above topics, and we shall go into somewhat greater detail on some which, in our view, may be of some interest also beyond the field of aviation gas-turbine construction.

Non-contact measurements. Various methods of non-contact measurement of GTD parameters have become widespread in recent years. We shall examine several such methods.

One interesting instrument for non-contact measurements is that which has been termed ELURA (cathode-ray device for recording blade-vibration amplitudes). The instrument's operation is based on the discrete-phase method. A fixed pulse-transducer (2 in Fig. 4) generates a pulse at the time some stimulus with an angle pitch equal to the blade's passes by it. Such stimuli may be holes, teeth, etc. Another pulse-transducer (1 in Fig. 4) generates a pulse when the tip of a blade whose vibrations are being measured passes by it. The time interval between pulses of the actuating and synchronizing transducers τ_{imp} is proportional to the path transition time Δl_i (see Fig. 4)

$$t_{imp} = \Delta l_i / u_к. \qquad (I)$$

where u_k is the circumferential velocity at the rotor periphery. In turn, linear marks made by an electron beam on the screen of the recording device $\Delta l_i'$ are proportional to τ_{imp}, so $\Delta l_i' \sim \Delta l_i$ (2).

If there are no blade vibrations, the Δl_i degenerate into points. Several new types of instruments have been created with the use and in the development of this principle. Both transducers can be placed in the housing above the rotor. By placing the transducers over different points on the blade face, measurements can be made of different forms of vibrations, including some torsional ones.

Use of ELURA-type instruments may not always be effective, however, e.g., when studying high-frequency blade vibrations by certain complex shapes. In such cases it remains necessary to read signals from transducers mounted on the internal rotors of

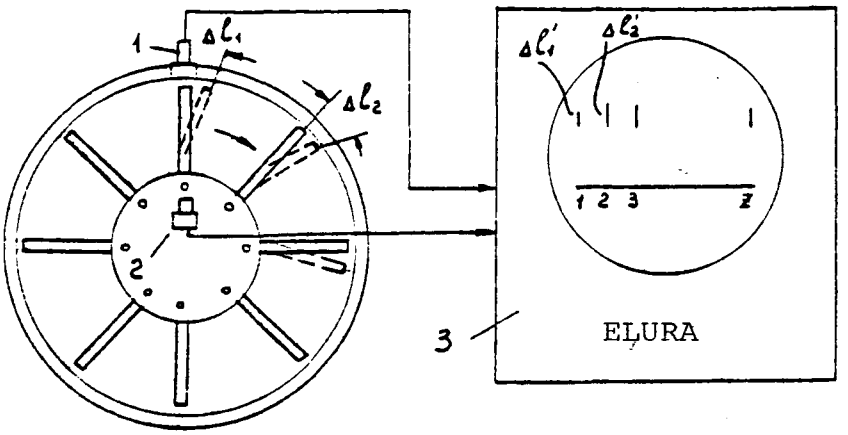

Fig. 4. Schematic diagram of blade-vibration amplitude measurement using the ELURA instrument.

1 -- actuating pulse transducer, 2 -- reference synchronizing pulse transducer, 3 -- cathode-ray recording device.

multishaft GTD. Then we have to resort to microtelemetry, i.e., use of miniature transducers that rotate together with the rotor. /13 Requirements for them are very strict: for example, one adopted model provides for operation at a centrifugal acceleration of $3 \cdot 10^4$ g and allows a transducer temperature of 125°C. Use of microtelemetry is one of the developing trends in non-contact retrieval of data during engine tests.

Optical pyrometries (Fig. 5) have recently become widespread for measurement of operating blade temperatures. The operating principle of the optical pyrometer is quite familiar. Difficulties encountered when using this instrument for aviation GTD measurements are also fairly characteristic. In particular, they are associated with the presence of soot in the flame. In most cases the error (when measuring blade-wall temperatures up to $\sim$1000°C) can be considered not to exceed approximately 10°C. Use of a scanner allows measuring the temperature of each operating blade, something practically impossible when measuring with thermocouples. The lower right corner of Fig. 5 shows an example of the type of recorded data: the temperature of each of z blades is measured separately.

Note that research is under way on use of optical methods such as Raman spectrography, which should allow, in particular, measurement of the temperature of any level at a point in a stream of high-speed gas.

We shall mention two other promising methods of non-contact measurement. First of these is vibroacoustic analysis, including

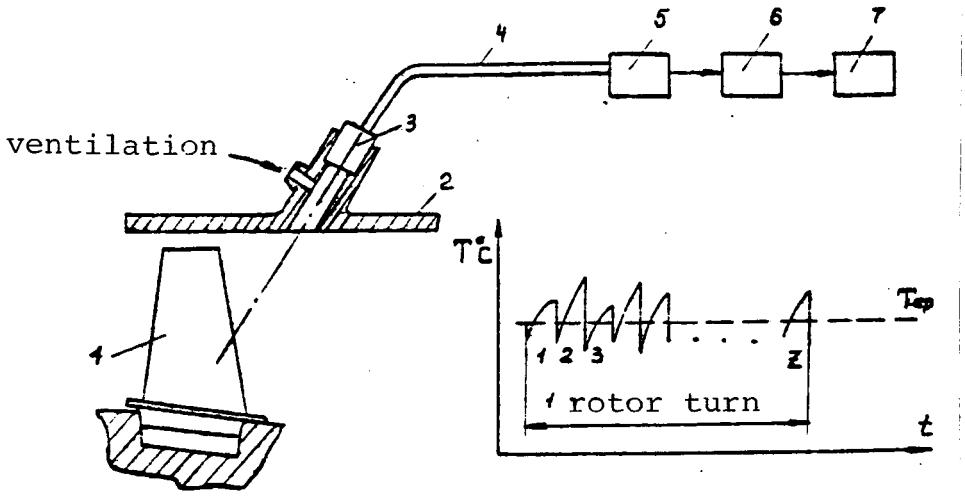

Fig. 5. Non-contact measurement of operating turbine-blade temperatures using an optical pyrometer.

1 -- blade, 2 -- turbine housing, 3 -- objective lens, 4 -- optical fiber, 5 -- photodetector, 6 -- amplifier, 7 -- recorder.

analysis of noise emitted by the engine. In this case, microphones mounted outside the engine are used to draw an acoustic portrait in different operating modes. Noise analysis can, in principle, be used to evaluate, for instance, closeness to surge, bearing defects, breakage of a small piece of blade, and many other data. One difficulty is separating the very weak signal when there is a very high general noise level. Analysis of the noise spectrum requires complicated and sometimes narrowly specialized equipment.

Also being developed are methods of laser Doppler velocity measurement (LDIS), which allow detailed study of flow structures. Some successes have already been achieved in using LDIS to study flows, even those of complex structure, such as the flow in the channels of an axial-flow compressor.

Non-contact measurements not only provide information difficult to obtain with other methods, but also permit combining /15
GTD tests with different objectives. For example, tensometric measurement of internal-stage blades, transmitting sensor signals using microtelemetry, study of low-pressure stage blade vibrations using the ELURA instrument, pyrometer measurement of turbine blade temperatures, reading of the engine's acoustic portrait, etc., can all be accomplished simultaneously. Consequently, non-contact measurements are a powerful method for meeting the conflicting requirements placed on testing of modern avaiation gas-turbine engines.

Experiment planning. Experiment planning methods recently finding use in aviation engine-building (previously employed in other branches of technology) have provided an appreciable effect in solution of problems arising in testing modern GTD. The theory of experiment planning is, of course, based on the concept of a multifactor experiment, while the traditional experiment in tests of engines and their components was always a single-factor one. Combination of factors (x_1, x_2, ..., x_k) in measurements is chosen in accordance with certain rules, and processing of the experimental data produces regression equations of the $y = f(x_1, x_2, \ldots, x_k)$ type, which associate the characteristic being sought with the factors determining it.

Experiment planning allows, first of all, reducing the required volume of experimental data with a given accuracy of results and, secondly, it opens up great possibilities for optimizing the system being tested, e.g., for finding the most suitable adjustment of engine components. Figure 6 illustrates the former using as an example the results of expensive tests to read the high-altitude characteristics of an engine in an altitude chamber. The graphs in this figure show that ten points were needed to draw the throttle characteristics at five altitudes (instead of the minimum thirty with a single-factor experiment). The agreement of characteristics obtained using regression equation $R = f(H, n)$, where H is the flight altitude and n is the r.p.m., with the results of control single-factor experiments for two values of H is good.

The idea of one method of optimization (simplex) is shown for a two-factor (x_1 and x_2) experiment in Fig. 7. First, experiments corresponding to combinations of factors at points 1, 2, and 3 of the factor plane are set up. The vertex of the simplex (point 2) where the worst value of parameter y was obtained, is mirror-reflected and coordinates x_1 and x_2 of new vertex 4, for which the next experiment is performed, are found. The points of the new simplex 1-3-4 are used to select the worst one according to the results, and it is again mirror-reflected (point 5), etc. In most cases the simplex method allows entering the optimum region in a few steps. Most effective are such optimization methods in experiments whose results had previously been sometimes difficult to assess even roughly, in the operational development of combustion chambers, for example. /17

Experiment automation and use of mathematical models of engines. A great deal has been written about experiment automation, in connection with which we shall only briefly mention one aspect of this question. We note that when discussing automation we most often mean automation of the collection and processing of measurement results, which earlier had been performed manually. Labor productivity thus increases and the

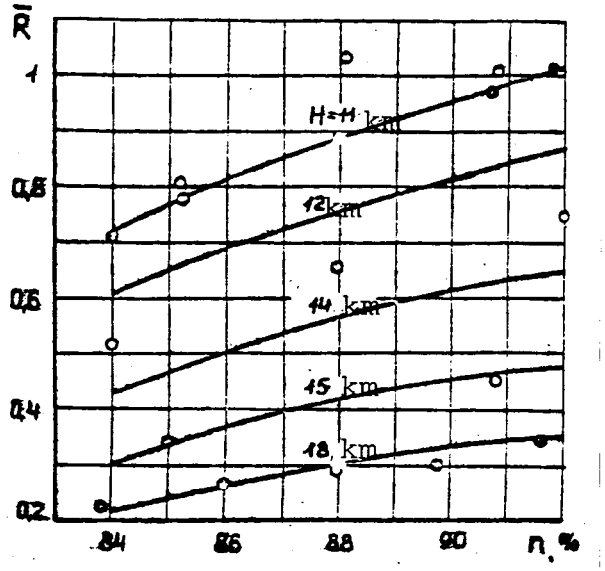

Fig. 6. Throttle characteristics of an engine at M = const. and H = var., obtained using regression equation (——).

o -- combinations of factor values used to conduct experiment.
o -- experimental points obtained in control single-value experiments.

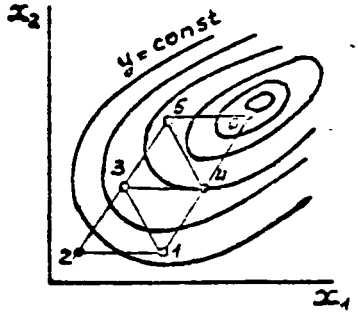

Fig. 7. Diagram of optimization with simplex method.

efficiency of equipment use is enhanced; the time consumed by the experimenter in making decisions is reduced if processing takes place at the rate of the experiment. There is, however, no sharp reduction in the volume of testing if the approach to organization of the experiment is not altered. A decisive effect can be obtained with a fundamental change in methods of obtaining data about the item being tested and in methods of evaluating the test results. For example, if in a multi-level automation system powerful, high-level computers compare the experimental data with various mathematical models (thermal gas-dynamic, dynamic, etc.) of the test engine, fairly complete identification of the engine with its models can be accomplished using the results of a limited number of measurements. Use of such methods of evaluating test results according to limited information, when models of an engine or one of its assemblies are matched with experimental material, allows reducing the required volume of experimental data. Prospectively, with use of non-contact measurements, combination of goals of different tests, and use of a set of mathematical models in an automated system we can expect a marked reduction in the volume of tests done to assess the achieved parameters of the assemblies, and of the entire engine, and /18 a choice of directions to take in further operational development.

Simulation of flight conditions. The expansion of engine-use conditions and the increase in air-mass flows demand constant complication and increased cost of special installations for altitude-velocity tests. Thus, one of the main directions to take in bringing these requirements into line with economic

ones is employment, in all possible cases, of simplified experimental installations for partial simulation of flight conditions. We have in mind, for instance, simulation of velocity at slowed air parameters, heating of incoming air by mixing it with the exhaust gases of another engine operating on an adjacent test-bed, use of pulsed tunnels, etc., etc. This is a huge area, fairly specific for aviation engines, and there is no reason to dwell upon it in more detail within the framework of this article.

Equivalent and cyclic tests. Here the main question is that of equivalence (with respect to failure rate) of equivalent test conditions to operational conditions. We shall examine some possible approaches to assessing equivalence of GTD conditions.

1) Often it is expedient to employ the measure of lifetime, associated with strength margins. Then the principle of equivalence is reduced to equality of safety margins in accelerated and operational tests. Since we can consider that the lifetime of a GTD is determined primarily by the turbine blades and disks, the equality of statistical safety margins at increased temperature is adopted as the measure of the equivalence of conditions. At each temperature T for a given material we can write equation

$$\sigma^m t^* = C, \qquad (3)$$

where t* is the prefailure time with exposure to static stress σ. The equivalence principle, based on equality of safety margins, is illustrated in Fig. 8. If T_i, t_i, and σ_i are the temperature, operating time, and effective stress under the conditions simulated by the equivalent tests, and $\sigma_{B/t_i}^{T_i}$ is the long-term strength limit at these T_i and t_i, then the safety margin in this condition

$$k_i = \sigma_{B/t_i}^{T_i} / \sigma_i. \qquad (4)$$

If in another (t - m) condition t_1 is the operating time with which the safety margin

$$k_1 = \sigma_{B/t_1}^{T_1} / \sigma_1 \qquad (5)$$

equals that in the ith condition, then this (1st) condition is /19
equivalent to the ith. Using the statistical failure model (3) and a linear model of damage summation we can obtain the equivalence condition

$$t_{1\,eq} = t_1 \sum_{i=1}^{n} (k_1/k_i)^{m_1}. \qquad (6)$$

where t_{1eq} is the equivalent time in the 1st (selected as equivalent) condition and n represents all conditions simulating the equivalent. Equation (6) provides a decisive curtailment of testing time. For example, if we double the operating time of an aviation engine in the maximum condition, in many cases we

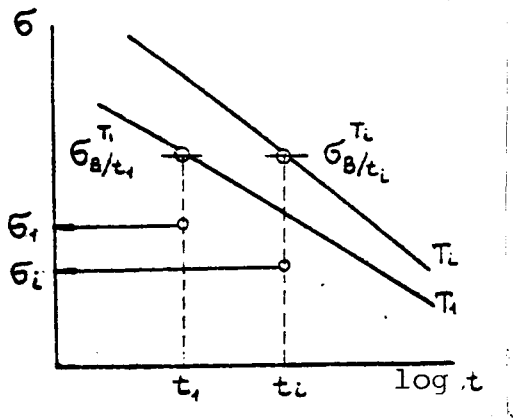

Fig. 8. For evaluating the equivalence of long-term strength conditions.

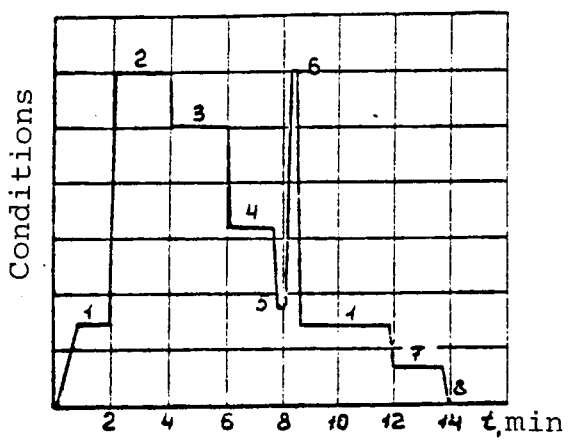

Fig. 9. Examples of TRDD test cycles.

1 -- idle, 2 -- take-off mode, 3 -- cruise mode, 4 -- descent mode, 5 -- idle in flight, 6 -- thrust reversal, 7 -- intermediate idle, 8 -- shutdown.

can consider that, by vulnerability to damage of the hot portion, this is practically equivalent to a lifetime of engine operation.

2) Widely prevalent are cyclic tests in which equality of the number of cycles of low-endurance fiatigue in a lifetime and in cyclic tests is taken as a measure of equivalence. The effect of other conditions on failure rate of the hot area and rotor of a GTD is considered less substantial. Loading cycles of the cycle type shown in Fig. 9 for a passenger aircraft TRDD [fanjet] engine are reproduced in the tests. The short duration of the cycle allows reproducing many thousands of them in a short time. Normally in cyclic tests the statistical scatter of the results of low-cycle tests is taken into account. Based on the possible difference in the properties of materials, tests are done with a margin against the number of start and shutdown cycles per lifetime:

$$N_{test} = CN_{res}/\eta \qquad (7)$$

where N_{res} is the number of cycles per lifetime, N_{test}, per test; C is the margin by number of cycles considering scatter, and η is the correspondence factor of the operating and test cycles.

The value of C is determined using the scatter field of the results of tests on prototypes (see Fig. 10). If a crack appears in a disk at N_{test} number of cycles, it is assumed that this is the best disk. The worst disk at the same load fails at N' cycles (see Fig. 10). Hence, $C = N_{test}/N'$. The value of coefficient C can in practice approach C = 2-3. Also possible is an overstress version of testing. If a bad disk fails at N' cycles and σ'_{-1} stresses (Fig. 10), the best runs N' at stress σ''_{-1}. Then with N' operating/21 cycles we can avoid increasing the number of test cycles (N_{test} =N'),

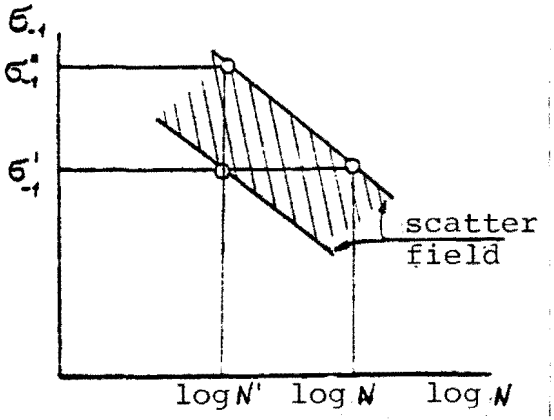

Fig. 10. For accounting for scatter of results of low-cycle tests in GTD cyclic tests.

but increase it $\bar{C} = \sigma''_{-1}/\sigma'_{-1}$ times in stress tests.

3) The statistical approach to assessing equivalence of conditions reduces essentially to equality of probabilities of failure-free operation in equivalent tests and in a lifetime:

$$P(t_1, z_1) = P(t_2, z_2). \qquad (8)$$

where $P(t_1, z_1)$ is the probability of failure-free operation in time t_1, in mode z_1, and $P(t_2, z_2)$ is the same in time t_2 in mode z_2.

Using the mean statistical indices, we write

$$\lambda_{cp}(z_1)t_1 = \lambda_{cp}(z_2)t_2, \qquad (9)$$

where $\lambda_{cp} = \int_0^t \lambda(t)dt$ is the mean failure rate. Since $\lambda_{cp} = I/T$, where T is the mean running time per failure, we can write instead of (9)

$$t_1/T(z_1) = t_2/T(z_2). \qquad (10)$$

Studies by the author and A. A. Morozov found statistical relations linking engine running time per failure to its operating conditions, especially flight durations (t_{fl}) and proportions of heavy duty conditions per lifetime ($\bar{z}$). Specifically, for a large number of engines it was shown that

$$\tau \sim t_{fl}^{0.967}\,\bar{z}^{-0.161}. \qquad (11)$$

Substituting (10) in (9), we find that if subscript 1 in (9) means equivalent tests and subscript 2 means flight:

$$t_{eq}/\tau = (t_{test}/t_{fl})^{0,967}\,(\bar{z}_{test}/\bar{z})^{-0,161} \qquad (12)$$

where τ is the engine lifetime, t_{test} is the duration of the test cycle, and $\bar{z}_{test}$ is the relative proportion of heavy duty conditions in the tests. From (12) it follows that the greater the proportion of heavy duty conditions and the shorter the test cycle, the shorter the time of equivalent tests.

Note that, ignoring the second relation in the right part of (12), bearing in mind the small value of the exponent in it and considering the closeness to unity of the exponent in ratio t_{test}/t_{fl}, we can write as an approximation

$$t_{eq}/t_{test} \approx \tau/t_{fl}. \qquad (13)$$

But $t_{eq}/t_{test} = N_{test}$, and $\tau/t_{fl} = N_{fl}$. Then from (13) we obtain/22 the condition for equivalence of conditions

$$N_{test} \simeq N_{fl} \qquad (14)$$

i.e., we come to the idea of cyclic testing.

Practical use of the statistical approach to equivalent tests is difficult because of the absence of models of the (11) type for new engines. Compromise approaches, combining equivalent (by long-term strength of combustion area) and cyclic tests, are usually used in practice.

Rejection of some tests. We always have to seek out possibilities for reducing the volume of tests and to review the range of GTD tests. For example, in many cases it has proven possible to eliminate some tests in mass-production plants, replacing them with some kind of control. Commission tests, as a means of monitoring control over the stability of production of certain engines long in production, can be replaced by other methods of stability control, e.g., dynamic vibration tests of blades, etc. Two-step routine delivery tests using modern methods of diagnosing engine condition are replaced by single-step ones in many cases. Without dwelling further upon these questions, we note merely that, in addition to the necessary complication of the testing system, we must constantly work to make it smaller and simplify it in all cases where this is possible.

Special tests to check the operational reliability of engines. The system of tests to check indirectly the reliability of an engine and all its systems has been developed, is in operation, and is constantly being improved. The requirements for these tests have been formulated in the airworthiness standards, and their positive results are a mandatory condition for engine certification.

The basic idea of tests is that they are a brief check of engine components and systems under assorted influences and operating conditions in order to determine the presence and adequacy of performance margins.

Three questions always arise when developing and refining such a system of tests: what to test (test list), how to test (methods and programs), and how to assess the results of the tests.

The main, but not the only condition for formulating the /23 list of tests is checking of performance margins as applied to typical failures (for example, fatigue failures of blades, surges, icing, foreign-object damage to the compressor, etc., etc.) or rare but more dangerous ones (disk failure, for example).

The system of testing now in effect contains several dozen types of tests. Therefore, despite the relatively short duration of most tests, a full set of them takes one or two years and requires use of several engines. Some tests, such as determination of blade vibration characteristics, checking of gas-dynamic stability margins, and examination of the lubrication system, blend into a whole set of operations including several engine overhauls, complex preparation, and many placements of the engine on test-beds, including in altitude chambers.

The decisive question when developing test procedures is the choice of the level of loads (conditions and external influences) that the engine should withstand and at which its performance margins should be checked. For example, with strain measurement of turbine blades (operating) and compressors (operating and turning) we determine the effect on vibration stress level of such factors as greatest possible irregularities of total air pressures in operation, maximum possible working medium pressures and temperatures under high-altitude and -speed conditions, etc. The strain measurement should be performed throughout the entire range of r.p.m.'s, from idle to maximum, since both resonance and stall vibrations may arise at any r.p.m. values, as shown in Fig. 11, for example.

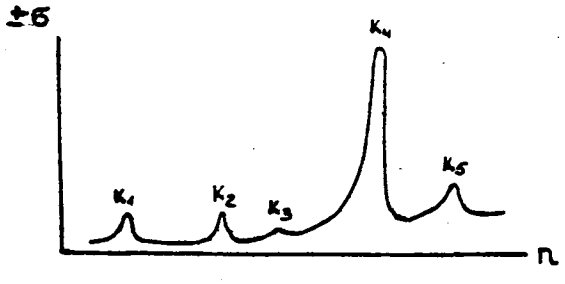

Fig. 11. Sample variable stress curve.

Testing, for instance, of anti-icing system effectiveness should, in accordance with adopted standards, be performed under air-temperature and artificial icing conditions corresponding to the graph in Fig. 12. In nature it is very rare, but possible, to encounter icing conditions more severe than those shown in Fig. 12. It is suggested that when such rare situations do develop in some areas, flights into them should be avoided at that time, since protection against icing is extremely difficult under these conditions.

We shall examine one other case: testing of engine performance after a bird strike. These tests check engine operation when several birds of average size (weighing 0.5-0.7 kg) and small size (weighing up to 115 g) or one large bird (weighing at least 1.8 kg) strike the engine. These conditions were selected based on analysis of worldwide experience in operating aircraft with GTD. The tests are conducted on an installation whose diagram is shown in Fig. 13. An air-driven gun has to be used to impart to the bird enough speed so that its velocity of impact with the engine /25

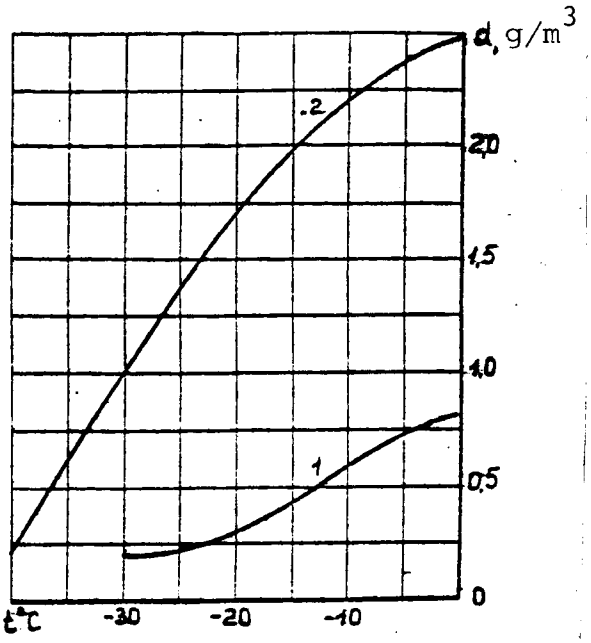

Fig. 12. Recommended curves of water content for testing anti-icing systems.

1 -- prolonged action, 2 -- action lasting up to ∿1 min.

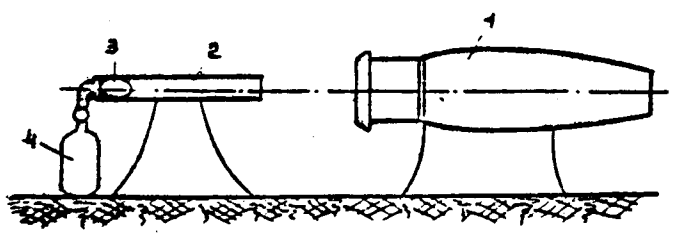

Fig. 13. Bird-launching installation.

1 -- GTD being tested, 2 -- pneumatic cannon, 3 -- bird, 4 -- compressed air bottle.

equals the aircraft's cruising speed at the altitude where a bird strike is still possible.

Assessing test results requires a very well-founded regard for the consequences of some influence (if it takes place) and for the level of performance margins established by the tests. True, in some cases the assessment of consequences is unambiguous and causes no difficulties -- and in these cases the assessment of test results proceeds according to the "yes or no" principle. Such is the situation in tests on housing impenetrability during blade breaks -- if the broken blade does not pierce the housing and all secondary damage is localized within the engine, the test results are positive.

An opposite example can be served by assessment of damage from a bird sucked into the engine. Some damage is unavoidable under these circumstances, but which to consider tolerable is not obvious without analyzing later flight situations. The following assessment criteria have been adopted. A bird weighing 1.8 kg, after striking the engine, should not inflict damage dangerous to a multi-engine aircraft. Spontaneous or forced shutdown of one engine is not viewed as dangerous to the aircraft. Impact of several medium-sized or small birds should not lead to engine shutdown or to inadmissible (for flight continuation) deviations of parameters, since small birds may hit several engines.

Tests measuring engine noise and emission of toxic materials. These types of tests, comparatively new for aircraft-engine building, have given rise to a number of new questions. The major one

for noise measurement is that tests to determine GTD acoustic characteristics require creation of a free acoustic field, i.e., these tests are impossible on common test-beds. There should be no noise-reflecting structures by open test-beds for acoustic measurements, even 100 m from the engine. If service structures are present at distances up to 100 m from the line of the engine axis, their walls should be covered with sound-absorbing material./28

In tests measuring toxic emissions the difficulties are associated with some equipment and procedural questions. First to be determined in these tests are engine exhaust concentrations of nitrogen oxides (NO_x), carbon monoxide (CO), unburned hydrocarbons (HC), and smoke. Figure 14 shows examples of change in the concentrations of these compounds relative to engine settings. These concentration levels, in g per kg of fuel, indicate that quite infinitesimal contents of these compounds, relative to the total volume of engine exhaust gases, have to be measured. For example, the required range of NO_x measurements is 0-0.1%, of HC, 0-0.2%. On the other hand, there are ICAO-recommended standards for total content of toxic substances emitted in an airport region over a rather prolonged standard cycle (Fig. 15), including taxiing and waiting on a taxiway, take-off and climb to ∿900 m, descent from this altitude, landing run, and taxi to park. Considering the changes in the concentration of hazardous materials with engine settings, this requires exceptionally high accuracies of instantaneous measurements of these concentrations. Modern methods have been developed to detect up to 10^{-6} to 10^{-7} parts-by-volume of toxic substances in exhaust gases. There was a need, however, to employ different measurement principles for each compound: chemiluminescence for NO_x, flame-ionization for HC, and a method based on nondispersed infrared absorption for CO. As a result, complex and expensive equipment has to be used in tests to measure emissions of hazardous substances.

Engine complication has led to the fact that the total cycle for producing aviation GTD, including time studying separate components, developing the experimental prototype, and, finally, building and developing an experimental model put into large-scale production, has stretched to 15 years. And experimental work continues to play a dominant role at all stages of this cycle.

* * *

To sum up, we can formulate certain conclusions from the above material.

Firstly, the complication of aviation engines and requirements for them are outpacing progress in design and calculation /29 methods, leading to complication and increase in the volume of tests. Thus, we need to have further intensive and purposeful improvement of, on one hand, design methods and, on the other, means and methods of experimental engine development. Otherwise

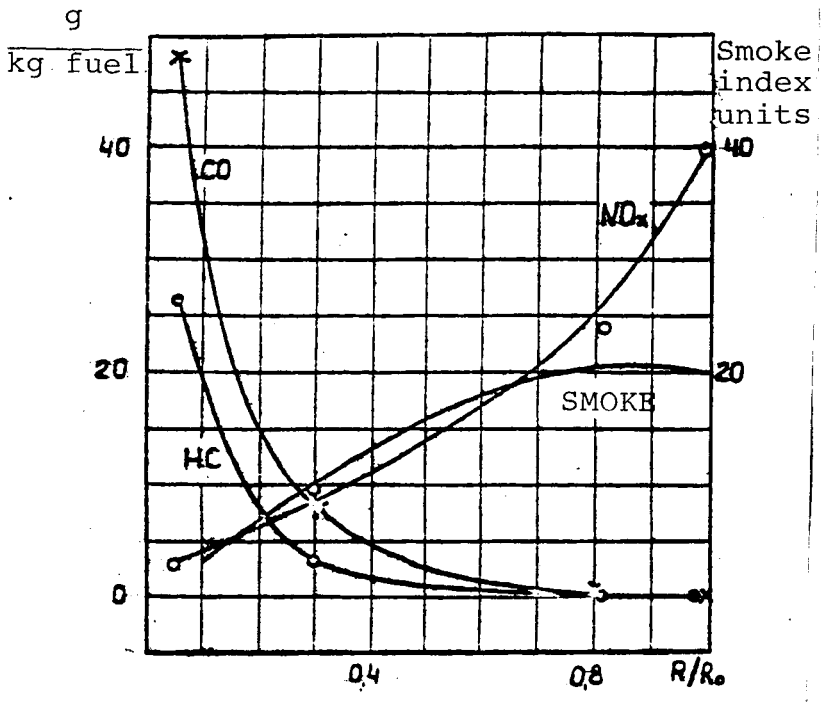

/26

Fig. 14. Example of change in the concentration of toxic substances with engine setting.

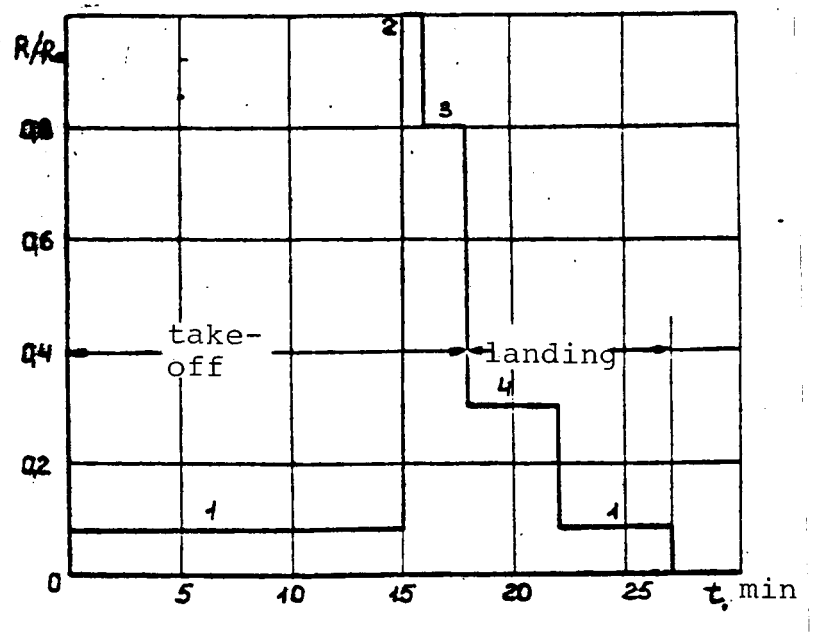

/27

Fig. 15. Conventional standard "take-off - landing" cycle, for which total emission of toxic substances is determined.

1 -- taxiing, 2 -- take-off, 3 -- climb, 4 -- descent.

a further increase in conflicts between requirements and the capabilities of experimental operational development is unavoidable.

Secondly, in connection with the very large time period between the beginning and end of the engine-development cycle, there has to be very reliable prediction of a wide range of required engine properties, so as to reduce to a minimum the development of changes whose need develops and is discovered in the process of developing and testing an engine and its components.

Thirdly, further, long-term development of engines merely through constant complication of them is impossible. An active search must be undertaken for fundamentally new solutions involving the work process, design-technology solutions, and materials.

ERRORS IN EXPERIMENTAL DETERMINATION OF HIGH-SPEED RAMJET PARAMETERS

Yu. M. Shikhman, M. V. Strokin, V. A. Uvarov

One of the pioneers in cosmonautics and rocket technology, /30
F. A. Tsander, focused considerable attention on refining the thermodynamic cycles of jet engines and pointed out the promise for use of VRD [jet engines] in high-speed flight [1, 2]. Some confirmation of his prediction is found in ramjet engines designed for use as powerplants of aricraft flying at Mach numbers from 3 to 6 and more [3-5, 7].

Now, of course, serious attention is being paid to experimental research on the operation, parameters, and characteristics of GPVRD [hypersonic ramjet engines], and tests of GPVRD on flying laboratories are under discussion [5]. The complexity of conducting tests at high airflow M, both on ground-based test-beds and on flying laboratories, is what lends importance to the study of possible errors in experimental determination of high-speed ramjet parameters. The results of such research may be of help in choosing more accurate methods of processing experimental data and developing requirements for measurement accuracy. In this article we attempt to undertake such research.

We use as an example a GPVRD operating at M 3 -- a so-called dual-mode GPVRD (DGPVRD) [3]. One possible design for a DGPVRD flow duct is shown in Fig. 1. Its distinguishing feature is that/31 the fuel combustion process can take place in a sub- or supersonic flow, depending on the fuel consumption or M. Accordingly, we shall call these the sub- and supersonic combustion modes.

The basic parameters measured in tests of these engines are the static pressures P_i, measured on the walls of the flow duct, the temperature of these walls T_{wi}, and data on fuel consumption G_T. Assume we also know the static pressure of the incident air flow P_H, its stagnation temperature T_H^*, and the pressure behind a normal shock $P_H^{*\prime}$. In addition to these three parameters, we may also know others which also characterize the energy factors of the air flow, e.g., P_H^*, T_H^*, and $P_H^{*\prime}$ [*sic*].

We need the measured parameters to determine engine and incident-flow parameters: incident-flow Mach number M_H and angle of attack i_H, air-mass flow through the engine G_B, the inlet coefficients of flow, resistance, and total pressure (ϕ, C_x, ν_B), Mach number in the inlet opening -- M_g, the efficiency of the fuel combustion process in the combustor -- the combustion efficiency in the outlet section and its change along the combustor [illegible],

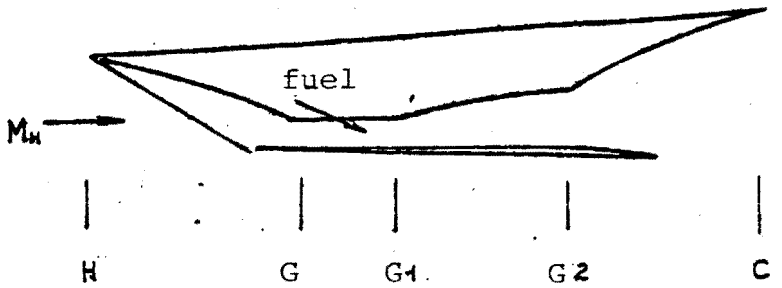

Fig. 1. Diagram of GPVRD.

the total pressure, temperature, and stagnation coefficients, flow Mach number along the combustor duct, the exhaust nozzle impulse-loss coefficient, the engine thrust parameters, the values of the pressure and friction forces, and other characteristics. We shall examine the determination of just some basic values.

We shall set up a characterization of the error in determining parameters by the realtive or absolute standard deviation (σ or $\bar{\sigma}$). Then, if $f(x_1, x_2, \ldots, x_K)$ is the value under examination and depends on the measured parameters $x_1, x_2, \ldots, x_K$,

$$\sigma_f = \sqrt{\sum_{i=1}^{K} \left(\frac{\partial f}{\partial x}\right)^2 \sigma_{x_i}^2} = \sqrt{\sum_{i=1}^{K} \left(\frac{\partial f}{\partial x_i}\right)^2 \bar{\sigma}_{x_i}^2}, \quad \bar{\sigma}_f = \frac{\sigma_f}{f}$$

and the value of f falls into the range of values $f \pm \sigma_f$ with an error 0.68 relative to σ, if the values of σ_{x_i} characterize the mean-square random error of the measured parameters.

Assume we are measuring P_H^* and $P_H^{*\prime}$. Then M_H is determined by expression

$$\frac{P_H^{*\prime}}{P_H^*} = \left(\frac{\gamma+1}{2}\right)^{\frac{\gamma+1}{\gamma-1}} \left(\frac{2}{\gamma-1}\right)^{\frac{1}{\gamma-1}} \frac{M_H^{\frac{2\gamma}{\gamma-1}}}{\left(\frac{2\gamma}{\gamma-1} M_H^2 - 1\right)\left(1 + \frac{\gamma-1}{2} M_H^2\right)^{\gamma/(\gamma-1)}},$$

and $\bar{\sigma}_{M_H}$, determined under condition $\frac{2\gamma}{\gamma-1} M_H^2 = \frac{2\gamma}{\gamma-1} M_H^2 - 1$ (which is valid at $M_H \gg 1.0$), can be found from equation

$$\bar{\sigma}_{M_H} = \frac{M_H\left(1 + \frac{\gamma-1}{2} M_H^2\right)}{|2 - M_H^2|} \sqrt{\bar{\sigma}_{P_H^*}^2 + \bar{\sigma}_{P_H^{*\prime}}^2}. \qquad (I)$$

The incident flow angle of attack i_H can be calculated using/32 familiar relations for the degree of static pressure increase in the first wedge of the inlet, $\bar{p} = p_1/p_H$. By simplifying these relations, assuming smallness of wedge and shock angles, we can

obtain an approximated expression for calculating angle of attack i_H:

$$i_H = \frac{\frac{\gamma+1}{2\gamma}\bar{p} - 1}{M_H\sqrt{\frac{\gamma+1}{\gamma}\bar{p}}} - \omega, \qquad (2)$$

where ω is the wedge angle of the inlet. Comparison of this approximated expression with precise solutions (Fig. 2) revealed the possibility of employing it to determine the error of i_H. The value of σ_{i_H}, following (2), is calculated using equation:

$$\sigma_{i_H} = \sqrt{\left(\frac{\omega+\omega}{2} + \frac{1}{M_H\sqrt{\frac{\gamma+1}{2}\frac{p_1}{p_H}}}\right)^2(\bar{\sigma}^2_{p_1} + \bar{\sigma}^2_H) + (\omega + i_H)^2\bar{\sigma}^2_{M_H} + \omega\bar{\sigma}^2_\omega}. \qquad (3)$$

Obviously, the error of determining M_H has the basic effect on σ_{i_H}.

The basic inlet parameters ϕ, ν_B, C_x, and M_g are calculated using the measured distribution of pressures on the stagnation surfaces. For a flat inlet with any number of shocks on the stagnation surfaces we can write a system of equations determining the flow diagram and the values of ϕ and C_x. For the sake of simplicity and clarity, at $i_H = 0$ we shall examine the case where all shocks other than the first approach under the lip. Then

$$\varphi = \frac{\operatorname{tg}\alpha_1(\gamma - \chi\operatorname{tg}\omega_1)}{\gamma[\operatorname{tg}(\alpha_1 - \omega_1)]}, \qquad (4)$$

where α_1 is the shock slope, ω_1 is the wedge angle of the inlet. Using the relation for determining α_1

$$\sin^2\alpha_1 = \frac{\gamma+1}{2\gamma}\frac{1}{M_H^2}\left(\frac{p_1}{p_H} + \frac{\gamma-1}{\gamma+1}\right)$$

and the condition of smallness of angle α_1 ($\operatorname{tg}\alpha \approx \sin\alpha \approx \alpha$), we obtain

$$\bar{\sigma}_\varphi = \frac{\omega_1}{\alpha_1 - \omega_1}\bar{\sigma}_{\alpha_1} = \frac{\omega_1}{\alpha_1 - \omega_1}\sqrt{\bar{\sigma}^2_{M_H} + \frac{1}{4}(\bar{\sigma}^2_{p_1} + \bar{\sigma}^2_{p_H})}. \qquad (5)$$

But since $C_{x\max} = \frac{\left(\frac{p_1}{p_H} - 1\right)(1 - \varphi_{\max})}{\frac{\gamma}{2}M_H^2}$, then with I

$$\bar{\sigma}_{C_{x\max}} = \sqrt{\varphi^2\bar{\sigma}^2_{M_H} + \frac{\varphi}{1-\varphi}\bar{\sigma}^2_\varphi + \left(\frac{p_1/p_H}{\frac{p_1}{p_H} - 1}\right)^2(\bar{\sigma}^2_{p_1} + \bar{\sigma}^2_{p_H})}. \qquad (6)$$

If $\varphi_{\max} \to 1$, it is more correct to determine the absolute error σ_{C_x}.

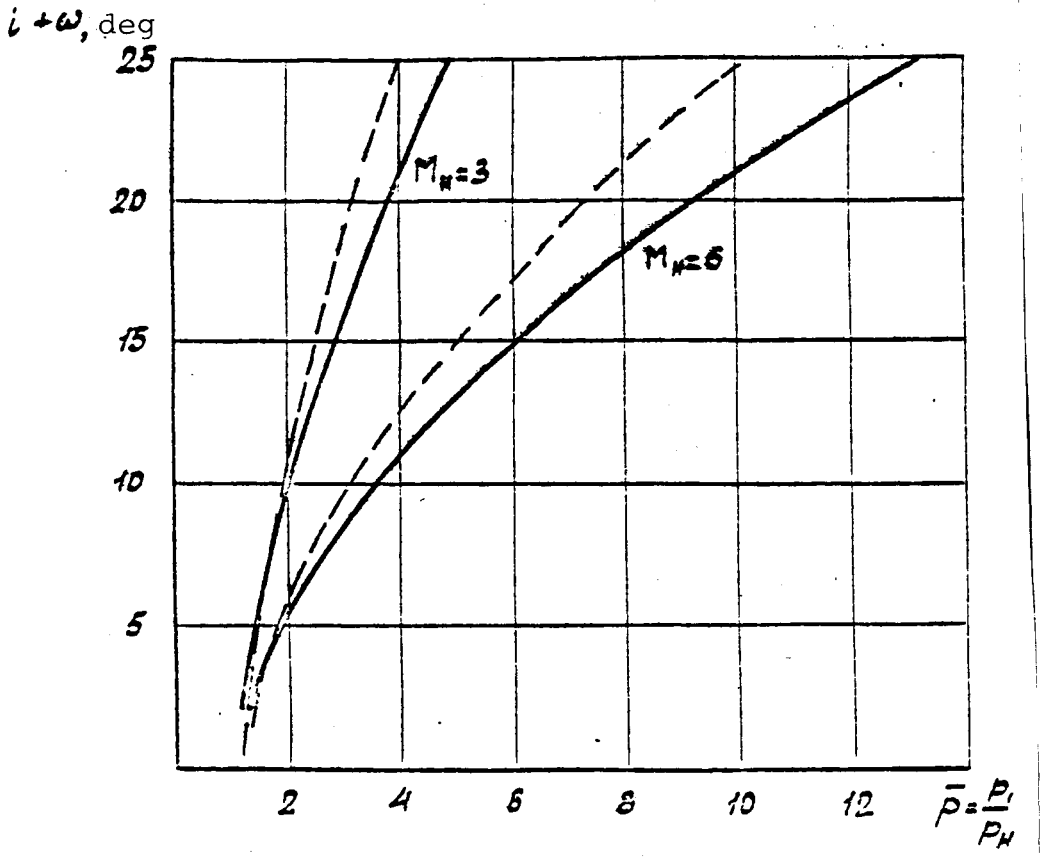

Fig. 2. Comparison of approximated relation (2) with precise solution.

—— precise solution [6];
---- equation (2), this article.

For analytic determination of the error of the total pressure coefficient ν_B and M_G, we shall write a system of equations using/34 gas-dynamic functions (assuming $T_H^* = T_G^*$)

$$f(\lambda_H) F_{BX} \varphi - f(\lambda_B) \gamma_B F_G = \frac{R}{p_H}$$
$$q(\lambda_H) F_{BX} \varphi - \gamma_B q(\lambda_G) F_G = 0$$

and solving it with respect to γ_B and λ_g we obtain

$$z(\lambda_G) = z(\lambda_H) - \frac{R}{F_{BX} \varphi p_H y(\lambda_H) j_{mp}}$$

$$\gamma_B = \frac{q(\lambda_H) F_{BX} \varphi}{q(\lambda_G) F_G}$$

Here $y(\lambda)$, $f(\lambda)$, and $z(\lambda)$ are gas-dynamic functions, F_{BX} is the area of the engine inlet, $R = \frac{k}{2} c_x M_H^2 p_H F_{BX} + R_p + R_{mp}$, R_p are the pressure forces, and R_{mp} represents the friction forces on the

stagnation surfaces of the air inlet.

After determining the partial derivatives and simplifying the obtained expressions, considering the contribution of each term, we obtain the following relations for errors of M_g and ν_B:

$$\bar{\sigma}_{M_g} = \frac{\left[1+\left(\frac{\gamma-1}{2}M_G^2\right)\right]}{1\cdot\tau(\lambda_G)^{k-1}}\sqrt{\frac{M_H^2\left(1+\frac{k}{2R\varphi_H}\right)^2}{2(\gamma+1)\left(1+\frac{\gamma-1}{2}M_H^2\right)}\bar{\sigma}_{M_H}^2+\left[\tau(\lambda_H)-\tau(\lambda_G)\right]^2\left(\bar{\sigma}_{\varphi_H}^2+\bar{\sigma}_{\varphi}^2+\bar{\sigma}_{R}^2\right)} \qquad (7)$$

$$\bar{\sigma}_{M_H} = \sqrt{\left[\frac{M_H^2-1}{1+\frac{\gamma-1}{2}M_H^2}\bar{\sigma}_{M_H}\right]^2+\bar{\sigma}_{\varphi}^2+\left[\frac{M_G^2-1}{1+\frac{\gamma-1}{2}M_G^2}\bar{\sigma}_{M_G}\right]^2}. \qquad (8)$$

Thus, examination of expressions (5)-(8) provides evidence that the basic effect on the error of determining air inlet parameters is exerted by the error in determining M_H of the incident flow. It is also clear that the errors in pressure and friction forces on the stagnation surfaces $\bar{\sigma}_R$ have little effect on flow parameters in the air inlet opening, since

$$\tau(\lambda_H)-\tau(\lambda_G) \ll 1.$$

Analysis of the errors in parameters determining the efficiency of operation in the combustor shall be performed using the example of combustion efficiency η_{nc}, which is a most important characteristic of operation.

We should distinguish the peculiarities of methods of processing experimental data using a thrust-measurement device (permitting measurement or determination by calculation of the total flow momentum at the outlet from the combustor 1 ks) and without it.

We shall examine the possibilities of studying DGPVRD in the subsonic combustion mode without a thrust-measurement bench. The condition $M_{g2} = 1$ at known air-mass flows G_B and with an excess-air coefficient α is necessary and sufficient for calculating flow parameters in section "G2". In fact, the mass-flow equation /35

$$\tau_{G_2} - \frac{\tau(\varphi_{G_2}, T_{G_2})\,g}{R(\varphi_{G_2}, T_{G_2})}\left(\frac{FP}{G}\right)_{G_2}^2 = 0$$

is used to determine temperature T_{G_2} and the flow enthalpy J_{G_2}. Then, from the energy equation, assuming an amount of heat not released upon incomplete combustion of 1 kg of fuel,

$$\Delta J_\eta = H_u(1-\eta'_{nc}) \text{ at } \alpha \geq 1$$
$$\Delta J_\eta = H_u(1-\eta_{nc})\alpha \text{ at } \alpha < 1, \qquad (9)$$

we obtain at $\alpha \geq 1$

$$\eta_{nc} = 1 - \frac{1}{H_u}\left[J^*_{a_2} + \alpha L_0 J^*_0 - (1+\alpha L_0)\left(J^*_{G_2} + \bar{Q}_{cyc}\right)\right] \qquad (10)$$

at $\alpha < 1$

$$\eta_{KC} = 1 - \frac{1}{H_u \alpha}\left[J^*_{G_2} + \alpha L_0 J^*_6 - (1+\alpha L_0)(J^*_{G_2} + \bar{Q}_{cyc})\right]. \qquad (II)$$

Here Q_{cyc} is the amount of heat given off by the engine cycle.

We shall examine the case $\alpha \geq 1$. Then, from (10), we obtain the formula for the relative error of η_{KC}:

$$\bar{\sigma}_{\eta_{KC}} = \frac{1}{\eta}\sqrt{\left(\frac{C_p T^*_{H_2}}{H_u}\bar{\sigma}_{T_{H_2}}\right)^2 + \left(\alpha L_0 \frac{C_p T^*_H}{H_u}\bar{\sigma}_{T_H}\right)^2 + \left((1+\alpha L_0)\frac{\bar{Q}_{cyc}}{H_u}\bar{\sigma}_{\bar{Q}_{cyc}}\right)^2 + \left[\alpha L_0 \frac{(J^*_{G_2} + \bar{Q}_{cyc} - J^*_6)}{H_u}\sigma_\alpha\right]^2 + \left[2\frac{(1+\alpha L_0)(A\frac{\gamma}{2}RT_{G_2} + C_p T_{G_2})}{H_u}\right]^2 \times \sqrt{\bar{\sigma}^2_{P_{G_2}} + \bar{\sigma}^2_{P_{G_2}} + \bar{\sigma}^2_{G_{G_2}}}}. \qquad (I2)$$

This formula can be substantially simplified. In fact:

$$\sigma_{G_2} \approx \sigma_6 ; \quad \frac{C_p T^*_{H_2}}{H_u} \ll 1 ; \quad \frac{\alpha L_0}{H_u}\left|J^*_{G_2} + \bar{Q}_{cyc} - J^*_6\right| \ll 1.$$

We can also show that

$$2\frac{1+\alpha L_0}{H_u \eta}(A\frac{\gamma}{2}RT + C_p T)G_2 = 2\left(\frac{\alpha L_0 C_p T^*_H}{H_u \eta} + 1\right).$$

Then $$\bar{\sigma}_{\eta_{KC}} = \sqrt{\left(\alpha L_0 \frac{C_p T^*_H}{H_u \eta}\bar{\sigma}_{T_H}\right)^2 + \left[(1+\alpha L_0)\frac{\bar{Q}_{cyc}}{H_u \eta}\bar{\sigma}_{\bar{Q}_{cyc}}\right]^2 + 4\left(\frac{\alpha L_0 C_p T^*_H}{H_u \eta} + 1\right)^2(\bar{\sigma}^2_{P_{G_2}} + \bar{\sigma}^2_{\sigma_6} + \bar{\sigma}^2_{P_{G_2}})}. \qquad (I3)$$

Defining $$\bar{\sigma}_{\sigma_6} = \sqrt{\bar{\sigma}^2_\varphi + \bar{\sigma}^2_{P_H} + \bar{\sigma}^2_{\sigma_H} + \bar{\sigma}^2_{P_{BX}} + \frac{1}{4}\bar{\sigma}^2_{T_H}}$$

and considering the results of calculated estimates showing that the basic contribution to $\bar{\sigma}_{\eta KC}$ is made by the error of calculating total enthalpy J^*_{G2}, i.e., the third term in the radicand in (13), we obtain an approximated formula for $\bar{\sigma}_{\eta KC}$ at $\alpha \geq 1$:

/36

$$\bar{\sigma}_{\eta_{KC}} = 2\left(\frac{\alpha L_0 C_p T^*_H}{H_u \eta} + 1\right)\sqrt{\bar{\sigma}^2_{P_{G_2}} + \bar{\sigma}^2_{\sigma_H} + \bar{\sigma}^2_\varphi + \bar{\sigma}^2_{P_H} + \bar{\sigma}^2_{P_{BX}} + \bar{\sigma}^2_{P_{G_2}} + \frac{1}{4}\bar{\sigma}^2_{T_H}}. \qquad (I4)$$

An analogous relation, but without α in the factor in front of the square root, is obtained also for the second case at $\alpha < 1$. We can see from equation (14) that, besides $\bar{\sigma}_{M_H}$, the error of measuring P_{G2} also substantially affects the error of η_{KC}.

A more complicated expression for $\bar{\sigma}_{\eta KC}$ is obtained when studying the supersonic combustion mode without thrust measurements. We should stress the need in this case to calculate the friction forces along the combustor duct, especially with low heat inputs (low engine thrusts).

Questions of determining the error of η_{KC} in tests with thrust measurement, and also questions of comparing both testing methods with and without thrust measurement require special experimental examination and go beyond the framework of this article. We shall merely note that use of condition $M_{G_2} = 1$ when processing the measurement results in engine tests with thrust measurement in subsonic combustion modes introduces an additional error in the final result, for example, of $B_{\eta KC}$. For instance, we can show that in this case the error in calculation of total enthalpy would be more than 1.5 times higher than $\bar{\sigma}_{J^*_{G2}}$, determined based on a data-processing method not employing condition $M_{G_2} = 2$.

Examination of the errors in parameters determinig operating efficiency in a jet nozzle (for example, the impulse-loss coefficient) in tests of it in an engine system revealed that the value of the absolute error σ_{ξ_1} is comparable to the value of the impulse-loss coefficient itself. This fact demonstrates the difficulties of accurate quantitative study of a jet nozzle in the engine system.

Calculations at M_H = 4-6 were made to determine the level of the analyzed errors. It was assumed that the pressure-measurement errors in different sections of the flow duct are the same and the errors of geometric-value measurement equal zero. Friction forces in the combustor and nozzle were ignored in calculations of thrust errors in the first approximation. The results of the calculations are shown in Figs. 3-6.

/37

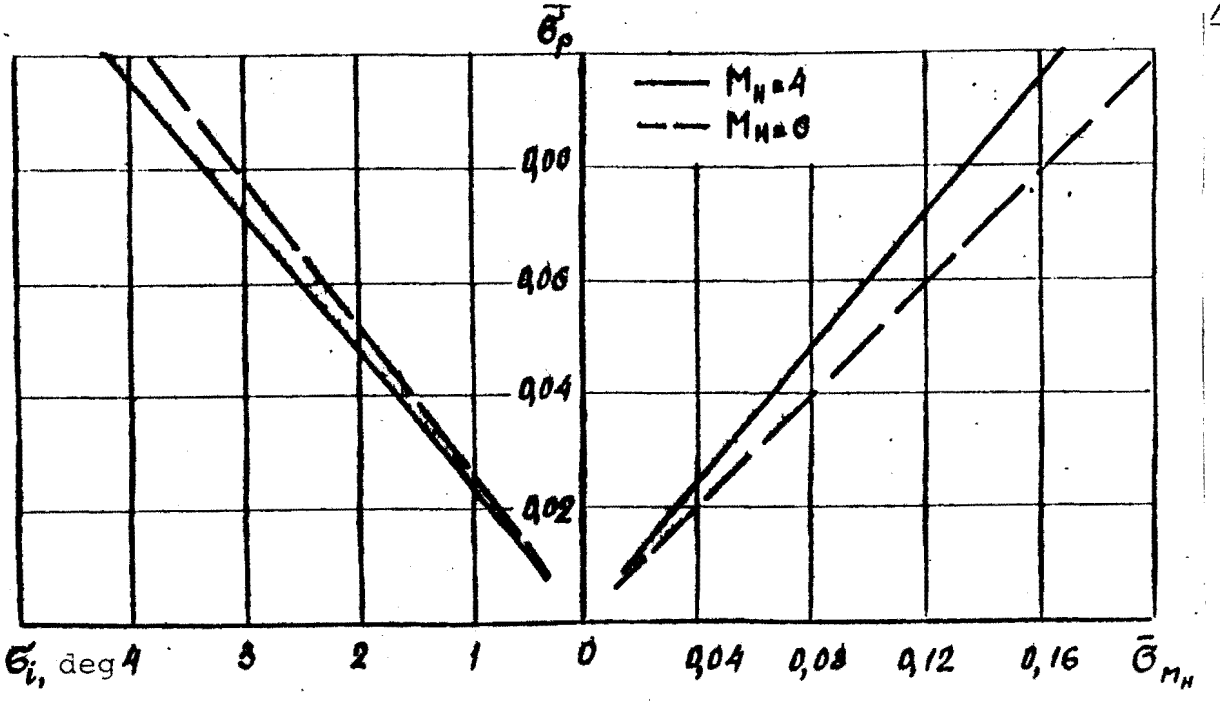

Fig. 3. Relation of M_H and σ errors to static pressure measurement error.

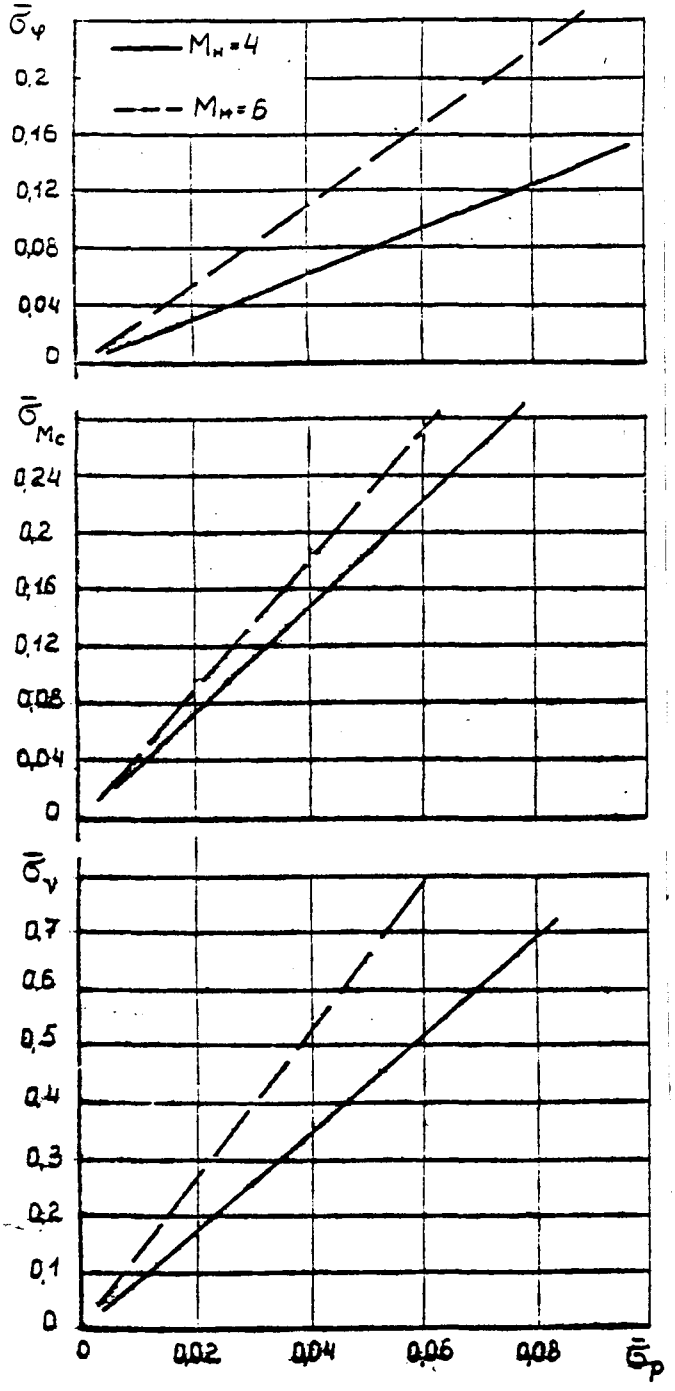

Fig. 4.

The data presented illustrate the effect of M_H on the errors of certain parameters (an increase of M_H generally leads to an increase in σ). The slight reduction of the angle-of-attack error with increase in M_H /41 is explained by the more flattened path of relation (2) at high M_H. The effect of M_H on the errors of air-inlet and combustor parameters depends substantially on the M_H. This is because of accumulation of errors in flow parameters along the duct.

For example, if the ratio $\bar{\sigma}_{M_c}/\bar{\sigma}_p \leq 2$ in the M_H measurement range under examination, then at $M_H = 6$ in the air inlet the analogous ratios reach values $\bar{\sigma}_\varphi/\bar{\sigma}_p = 2{,}9$; $\bar{\sigma}_{M_c}/\bar{\sigma}_p = 4{,}5$, a $\bar{\sigma}_v/\bar{\sigma}_p = 13{,}5$ (Fig. 4).

As calculations revealed, research on a combustor in an engine system becomes difficult when measuring pressures with $\bar{\sigma}_P = 0.02 + 0.03$ if air-mass flow is not measured (Fig. 5). The significant increase of the error of $\bar{\sigma}_{KC}$ with increase in M_H or $\alpha/2$ is explained by reduction of the contribution of heat release to total energy flow when fuel is burned. The cited data show that a substantially more accurate value of combustion efficiency η_{KC} can be achieved by measuring the air-mass flow through the engine when testing in an attached duct or by prior calibrations in engine tests in wind tunnels (errors in other parameters are also reduced in this way).

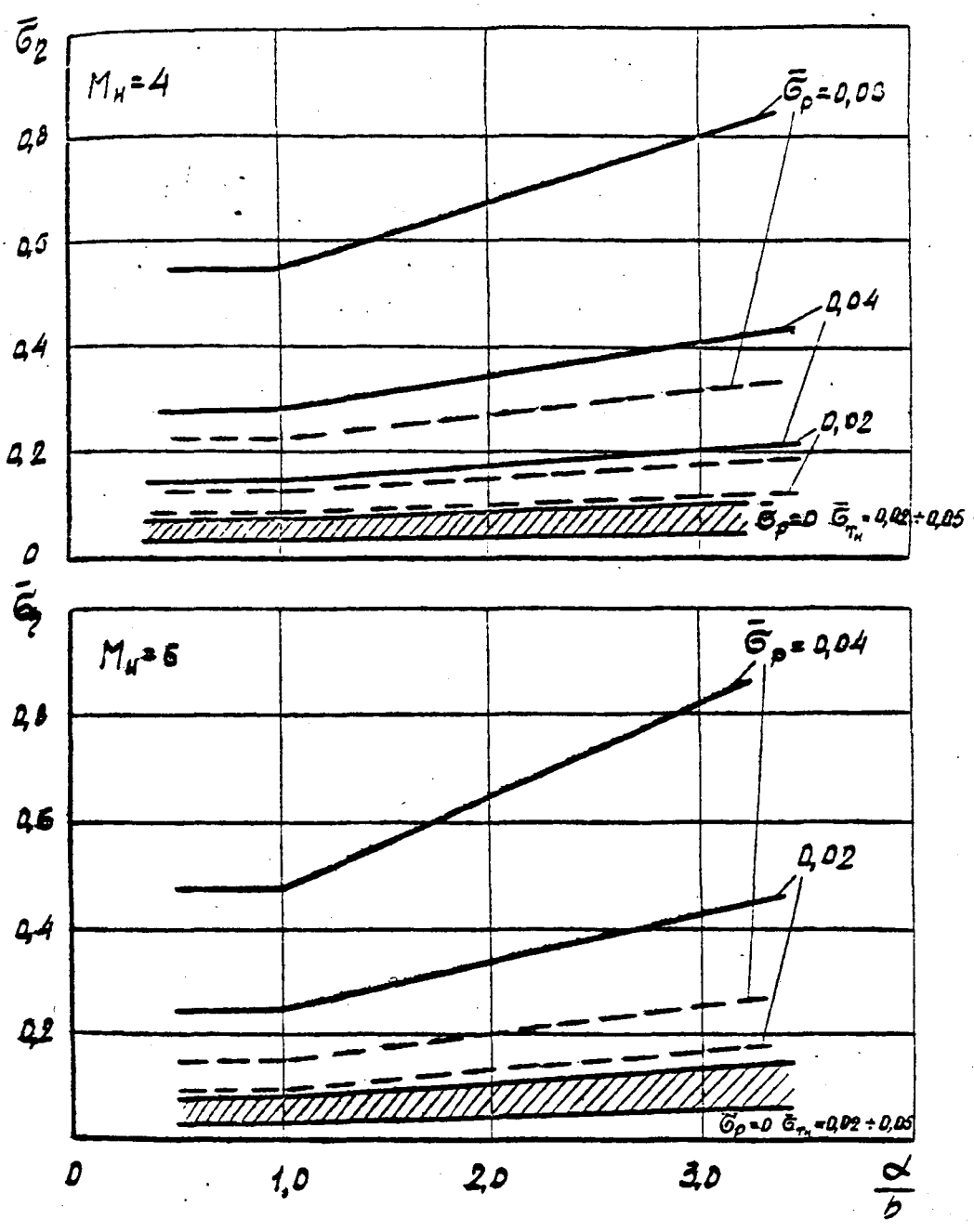

Fig. 5. Dependence of combustion-efficiency error on excess-air coefficient at various M_H and σ_η.

—— without measuring air-mass flow,
---- with measurement of air-mass flow, = 0.02.

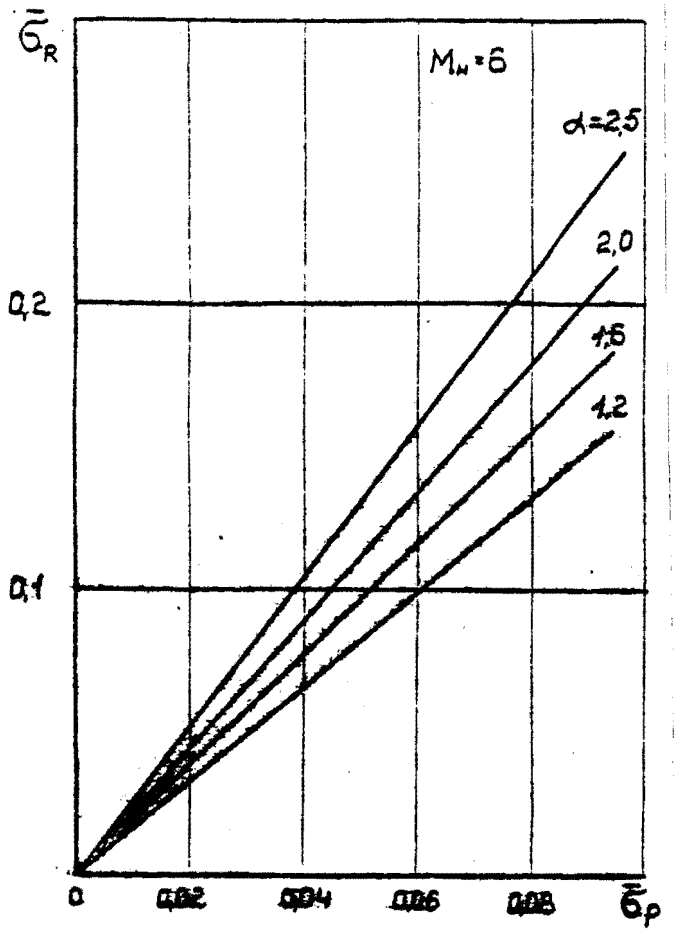

Fig. 6. Dependence of error in calculating internal thrust of a PVRD on pressure-measurement error.

Possible errors in determining engine thrust were estimated by integrating the distribution of static pressure along the walls of the flow duct (Fig. 6) in the supersonic combustion modes. We mentioned above the importance of correctly calculating friction forces, especially at high α or low η_{KC}, i.e., at low values of engine thrust. Thus the actual $\bar{\sigma}_R$ may be somewhat higher than those shown in Fig. 6.

Therefore, determination of the errors in parameters of PVRD operating in the M = 4-6 range revealed that errors in measurement of pressures in the flow and on the walls of the flow duct have a substantial effect on errors in operation parameters and engine characteristics. Inaccuracy in determining incident-flow M_H has a definite effect on the values of these errors.

Our analysis demonstrated that pressure measurement with $\bar{\sigma}_p < 0.02$ provides acceptable accuracy of determining PVRD parameters and characteristics.

The authors thank R. I. Kurziner for his useful advice.

REFERENCES

1. Tsander, F. A., "The problem of flight using jet-propelled vehicles," in Pionery raketnoy tekhniki. Kibal'chich, Tsiolkovskiy, Tsander, Kondratyuk. Izbrannyye trudy [Pioneers in Rocket Technology: Kibal'chich, Tsiolkovskiy, Tsander, Kondratyuk. Selected Works], Moscow, 1964, pp. 435-441.

2. Tsander, F. A., "A comparison of fuel consumption when oxygen is taken from the atmosphere and when it is stored in a rocket," in Problemy poleta pri pomoshchi reaktivnykh apparatov [Problems of Flight Using Jet-Propelled Vehicles], Moscow, 1961, pp. 261-266.

3. Curran, E. T., and F. T. Stull, "Ramjet engines: Highlights of past achievements and future promise," paper presented at the 2d International Symposium on Air-Breathing Engines, III, Sheffield, 1974.

4. Bendot, I. G., "Composite propulsion systems for an advanced reusable launch vehicle application," paper presented at the 2d International Symposium on Air-Breathing Engines, III, Sheffield, 1974.

5. Waltrup, P. I., G. I. Anderson, F. D. Stull, "Supersonic combustion ramjet (scramjet) engine development in the United States," paper presented at the 3d International Symposium on Air-Breathing Engines, 1976.

6. Kibardin, Yu. A., S. I. Kuznetsov, A. N. Lyubimov, B. Ya. Shumyatskiy, Atlas gazodinamicheskikh funktsiy pri bol'shikh skorostyakh i vysokikh temperaturakh vozdushnogo potoka [Atlas of Gas-Dynamic Functions at High Air Flow Velocities and Temperatures], 1961.

7. Kurziner, R. I., Reaktivnyye dvigateli dlya bol'shikh sverkh-zvukovykh skorostey poleta [Jet Engines for High Supersonic Flight Speeds], Moscow, 1977.

EFFECT OF IRREGULARITY OF A SUPERSONIC FLOW WITH SHOCK WAVES ON FRICTION AND HEAT EXCHANGE IN A HYPERSONIC RAMJET ENGINE DUCT

O. V. Voloshchenko, V. N. Ostras', V. A. Eysmont

The problem of determining friction and heat exchange in the/43 duct of a GPVRD [hypersonic ramjet engine] is among the most important ones when designing an engine. The flow in the duct of such an engine, especially at the beginning of the combustor, is substantially irregular along the height and length of the duct. The typical calculated pattern of flow in a GPVRD duct in "cold" mode is shown in Fig. 1. The pattern was obtained by calculating frictionless flow using the method in [1]. As Fig. 1 shows, there are shock waves and rarefaction waves all along the duct. In the real case this pattern is aggravated by viscous interaction and formation of a boundary layer separation zone at the walls of the duct. Determination of friction and heat exchange for such a flow is an extremely complex task.

In such situations friction and heat flows are calculated with the assumption of flow one-dimensionality, using familiar boundary layer calculation methods for supersonic main flows [2]. The correctness of this approach when determining friction for axially symmetric irregular flows in ducts $l/d \geq 5$ long was experimentally tested and confirmed in [3]. Bearing in mind Reynolds' hydrodynamic analogy, normally used in boundary layer calculations [2], the results in [3] permit the hope that a similar procedure is valid for heat exchange as well. However, the possibility of employing this determination of friction, and /45 especially heat exchange, for asymmetric irregular supersonic flows, characteristic of GPVRD ducts, required additional testing. Furthermore, determination of heat exchange from averaged parameters is known not to provide the distribution of local heat flows along the duct walls when shock waves are present, something necessary when developing engine cooling systems.

The purpose of our work was to carry out a calculation study of friction and heat flows in a flat duct with supersonic irregular flow, characteristic of GPVRD ducts, considering the detailed structure of irregular flow. The possibility of employing friction and heat flow calculation from averaged parameters was tested simultaneously.

Selected as the model for investigation was a constant cross-section duct with dimensionless length $l/h = 25$. A duct height $h = 0.03$ m was assumed as a characteristic dimension. The width of the duct was assumed fairly large ($b/h = 33$), which

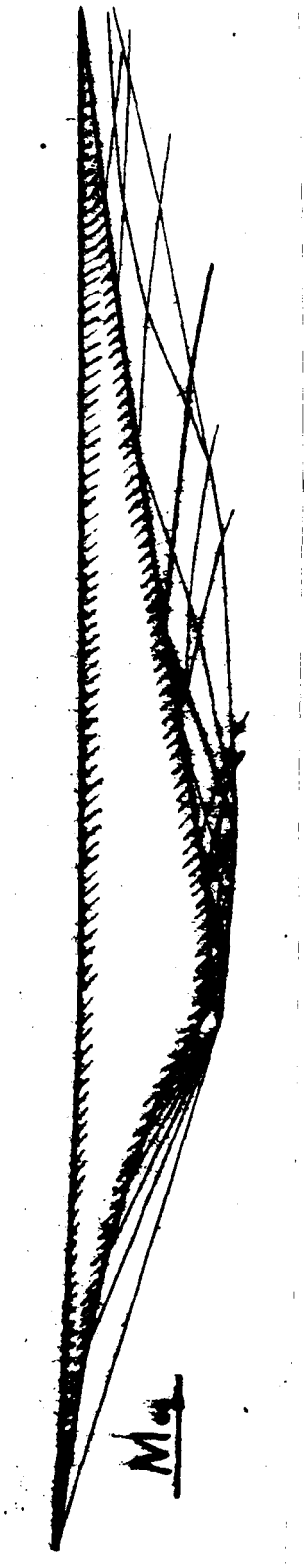

Fig. 1.

made it possible to avoid consideration of the side walls in the calculations. Irregularity and asymmetry of flow at the inlet to the duct was provided by unilateral deflection of the incident flow by a wedge with an angle $\theta = 15°$.

The supersonic flow formed in the duct with shock waves and rarefaction waves was calculated using the method in [1]. In the calculations it was assumed that outside the boundary layer the gas is non-heat-conducting, inviscid, and perfect (æ = 1.4), there is no interaction between the frictionless flow and the boundary layer, and the rise of a boundary layer at the walls is compensated for by duct expansion to the thickness of the boundary layer displacement.

The distributions of Mach number M, pressure P, and temperature T parameters along the duct walls, obtained through the calculations, were taken as the initial data for computing the boundary layer. The boundary layer in the duct was considered turbulent, formally achieved through appropriate choice of pressure at the inlet. The integral method [2] was used to calculate the turbulent boundary layer. Calculation of the boundary layer characteristics with its passage through shocks was performed using the effective-length method [4]. In distinction to [4], the effective length was determined not from the condition of retaining the momentum thickness $\delta_1^{**} = \delta_2^{**}$ with the transition of the boundary layer across the shock wave, but from the condition of retaining friction forces $Xfr_1 = Xfr_2$. This procedure, together/46 with satisfactory agreement with experiment when calculating friction in a duct with irregular flow and the more physical idea of change in friction force upon transition across the shock waves, provides, as demonstrated by calculations, satisfactory agreement with experiment [6] as regards the amount of friction stress and specific heat flow. The boundary layer was calculated assuming $\bar{T}_w = \text{const}$. Calculations were performed for incident flow $M_\infty = 4 + 8$, to which corresponded a Mach number of an even flow, equivalent by momentum and energy expenditure, in the channel $M = 2.64\text{-}4.35$.

Figure 2 shows a typical computation pattern of supersonic flow with shock waves and a flow structure in some sections of this duct for $M_\infty = 8$. As Fig. 2 shows, considerable irregularity of pressure P, M number, and velocity direction [illegible] is retained throughout this extent of duct. There are four shock reflections from each wall in all the modes examined in this article with respect to M_∞, as well as in the mode shown in Fig. 2. Estimates revealed that in all the modes the first two shock reflections on the upper wall and on the lower produce boundary layer separations. Assessing the effect of separations will be discussed below.

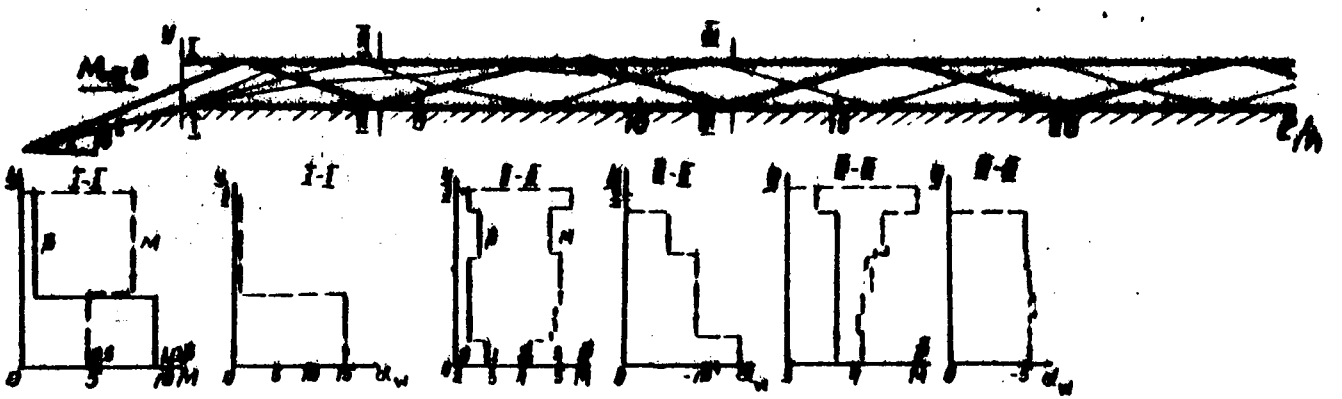

Fig. 2.

Weak attenuation of irregularity along the duct is indirectly seen in Fig. 3, which shows for M = 8 the distribution at the duct walls of relative pressure P/P_∞, M, and the parameters $\bar{P}_p$ and M_p of the uniform flow equivalent to it. Figure 3 shows that the amplitudes of variations in $\bar{P}$ and M change fairly weakly along the duct. Also shown here are the results of a calculation of specific heat flows q_w along the duct walls for an irregular and uniform flow equivalent to it.

The results of friction force calculations for each wall are presented in Fig. 4 as relations between the momentum loss factor $\bar{J}$ = [illegible] and duct relative length $\bar{l} = l/h$ and $l_d = l/d$, where X_{fr} = the force of friction, J is the flow total momentum in the inlet section of the duct, equal to the momentum of a uniform flow equivalent to non-uniform with respect to rate, momentum, and energy; d is the hydraulic diameter of the duct, for a planar duct equaling d = 23h/[illegible] + h. This figure shows the total values of the planar-channel momentum loss factors, $\bar{J} = \bar{J}_{up} + \bar{J}_{low}$.

We shall first examine the results with respect to friction, /50 shown in Fig. 4. The distribution of friction forces along the duct graphically indicates the effect of shock and rarefaction waves on friction force. This effect is strongest at the beginning of the duct at the points where the shock waves diverge and reflect from the duct walls. At these points we find a more intensive increase in friction force, which then weakens the rarefaction wave. A similar pattern occurs in the rest of the duct, but with less intensity, a fact associated with weakening and damping of shock waves along the duct. A comparison of the friction forces at the upper and lower walls reveals that in the initial portion of a duct $l/h = 2 + 4$ long there arises a substantial differential of friction forces at the upper and lower walls at all the M_∞ numbers investigated, and this differential is then retained all along the duct. The genesis of this differential of friction forces at the walls in the inlet section of the duct is associated with flow irregularity and asymmetry in the inlet section of the duct. Also apparent from the data given in Fig. 4 is that the curves of the friction-force distributions of uniform flows equivalent to non-uniform at $l/h > 2$ occupy an intermediate place between the values of the friction forces for the upper and lower walls.

There is practical interest in comparing the total momentum loss factors in a planar duct with irregular and uniform flows, and also with the experimental data in [3] with respect to friction in tunnels. This comparison reveals (see Fig. 4) that at $l/h > 2$ the calculated values of friction-related momentum-loss factors of an irregular flow differ only slightly from friction-related momentum loss of a uniform flow equivalent to irregular with respect to rate, momentum, and energy. The obtained calculation data also agree satisfactorily with the experimental data

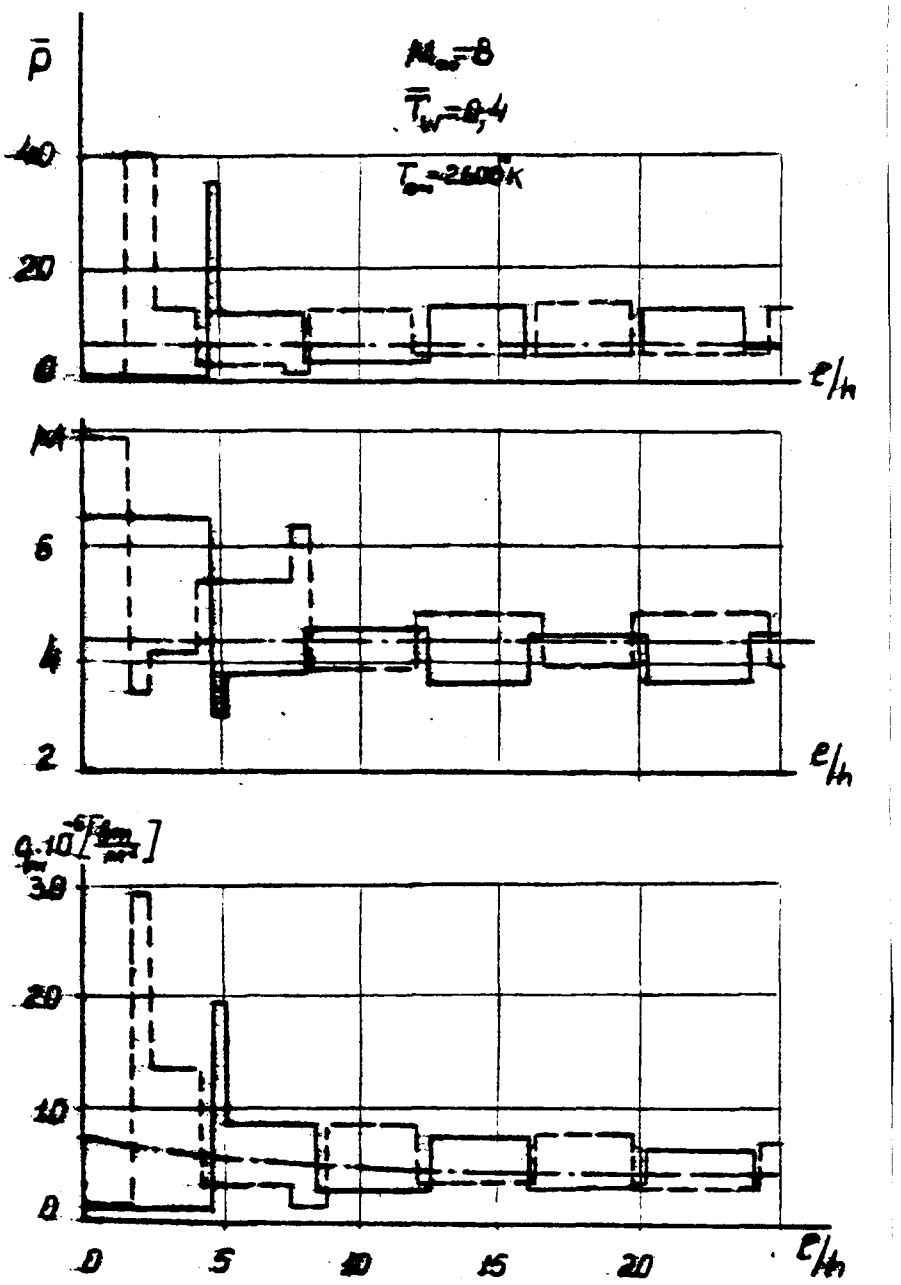
$\bar{p}$
$M_\infty = 8$
$\bar{T}_w = 0{,}4$
$T_\infty = 2600°K$
40
20
0
ℓ/h
8
6
4
2
ℓ/h
$q_w \cdot 10^{-6} [\frac{kcal}{m^2 s}]$
30
20
10
0
0
5
10
15
20
ℓ/h

Fig. 3.

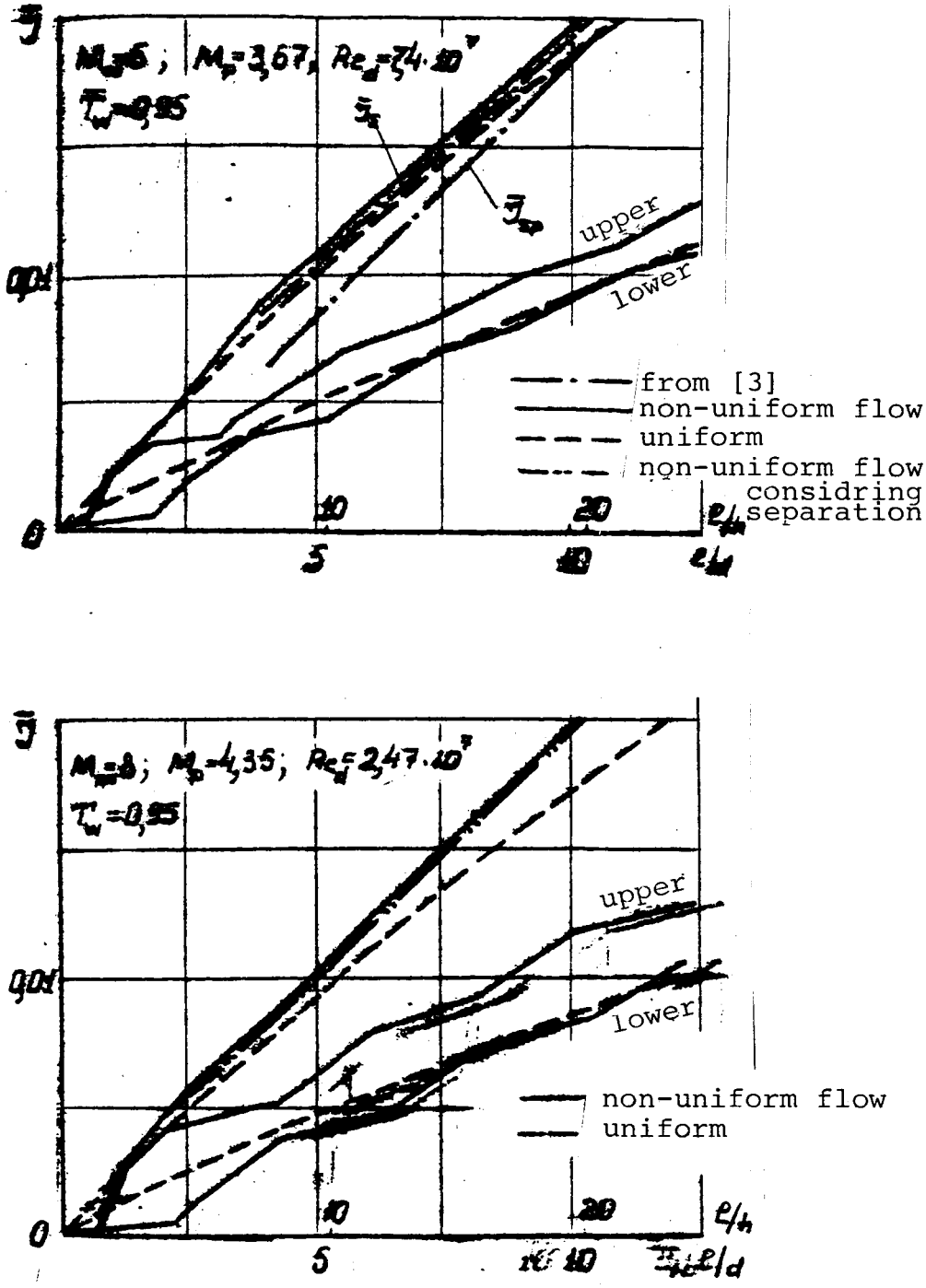
upper
lower
from [3]
non-uniform flow
uniform
non-uniform flow considring separation
0
5
10
20
upper
lower
non-uniform flow
uniform
0
5
10
20

Fig. 4.

in [3]. The slight increase of calculated values over the experimental, and also the greater increase in friction along the tunnel in [3], apparently is associated with the presence of a boundary layer at the tunnel inlet, increasing in the nozzle, and the effect of boundary layer increase in length with flow deceleration in the tunnel.

The above results from calculation of irregular flow friction in a planar duct were obtained without considering possible boundary layer separations at the walls. As already mentioned, an approximate estimation of the effect of separations on the total flow-friction force in the duct was made. Analysis/51 of the pressure drops in shocks for the irregular flows examined in this article revealed that boundary layer separations are possible at the upper wall only in the first two shocks, but at the lower only in the first shock. Here the relative length of the separation zones $\tilde{l}_{sep} = l_{sep}|h$, determined from [5], may be $\tilde{l}_{sep} \approx 0.04\text{-}0.8$. If we assume that there is no friction in the separation zones and that the separation zones do not affect later flow, but the boundary layer characteristics behind the separation zone are calculated similarly to the separationless case, then the reduction of friction through separations does not exceed 10%, even with relatively short ducts, as we can see from Fig. 4.

The effect of shock and rarefaction waves on local heat flows is graphically apparent when examining the curves of q_w distribution along the walls of the duct in Fig. 3. Where the shock waves fall and reflect from the walls the local specific heat flows increase irregularly and exceed by 3-4 times the level of heat flows determined from uniform-flow parameters. A similar pattern is seen throughout the duct, but with a reduction in the maximum level of local heat flow, associated with damping of the shock wave intensities. The difference in distribution of specific heat flows at the upper and lower wall of the duct is associated with irregularity and asymmetry of flow in the inlet section. As a whole, the distribution of specific heat flows at the duct walls reflects the nature of pressure distribution by length in an irregular flow and can be approximated by relation

$$q_i|q_{i-1} = (p_i|p_{i-1})^{0,8}.$$

where (P_i/P_{i-1}) is the local pressure increase in the shock at the duct wall.

Figure 5 shows a comparison of the calculated change of heat flows in the shock waves of this duct with the experimental correlation for separation flow $q_i/q_{i-1} = (P_i/P_{i-1})^n$... [6], where the exponent n for the point of separation "attachment" equals

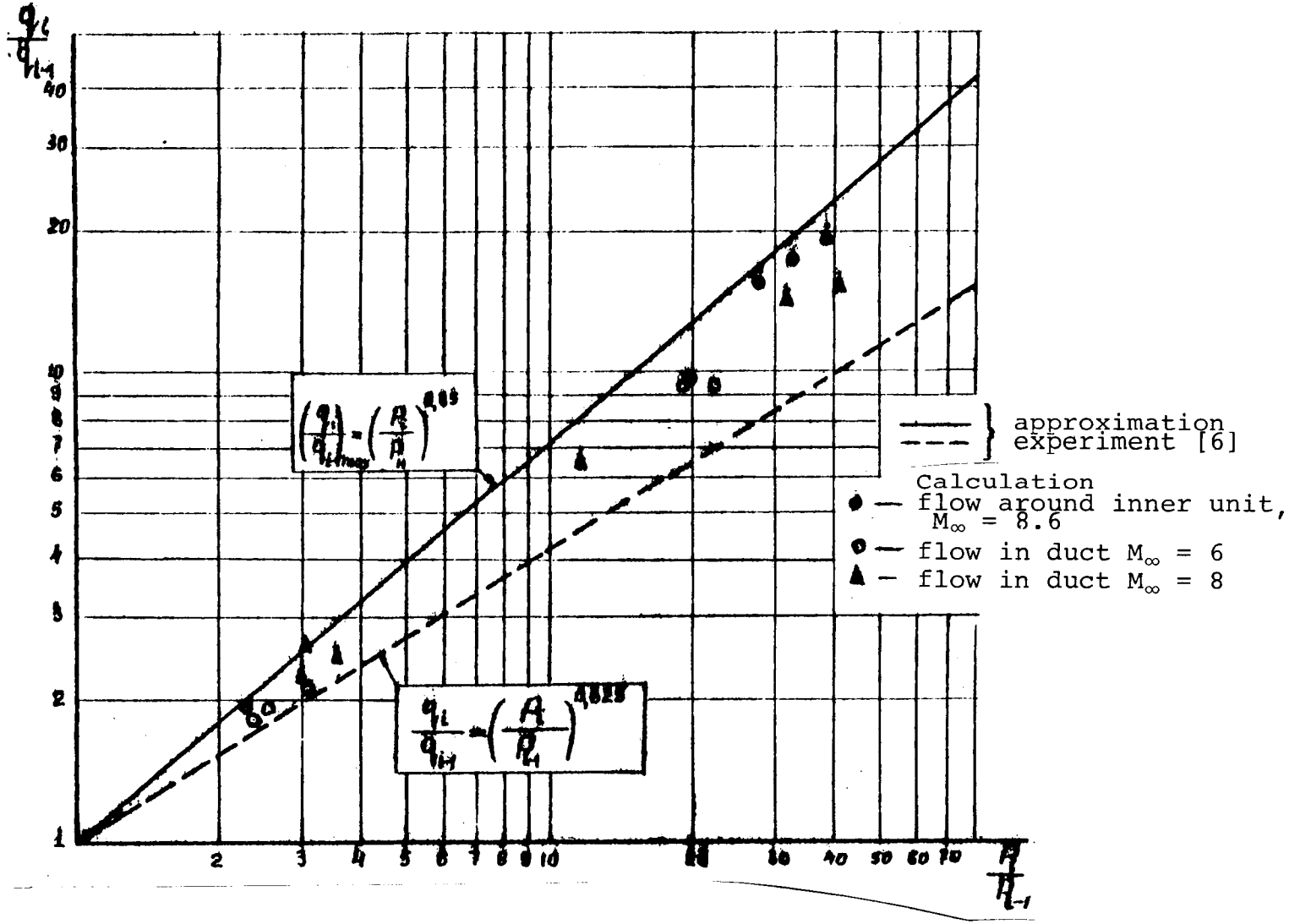
approximation
experiment [6]
Calculation
flow around inner unit, $M_\infty = 8.6$
flow in duct $M_\infty = 6$
flow in duct $M_\infty = 8$

Fig. 5.

/52

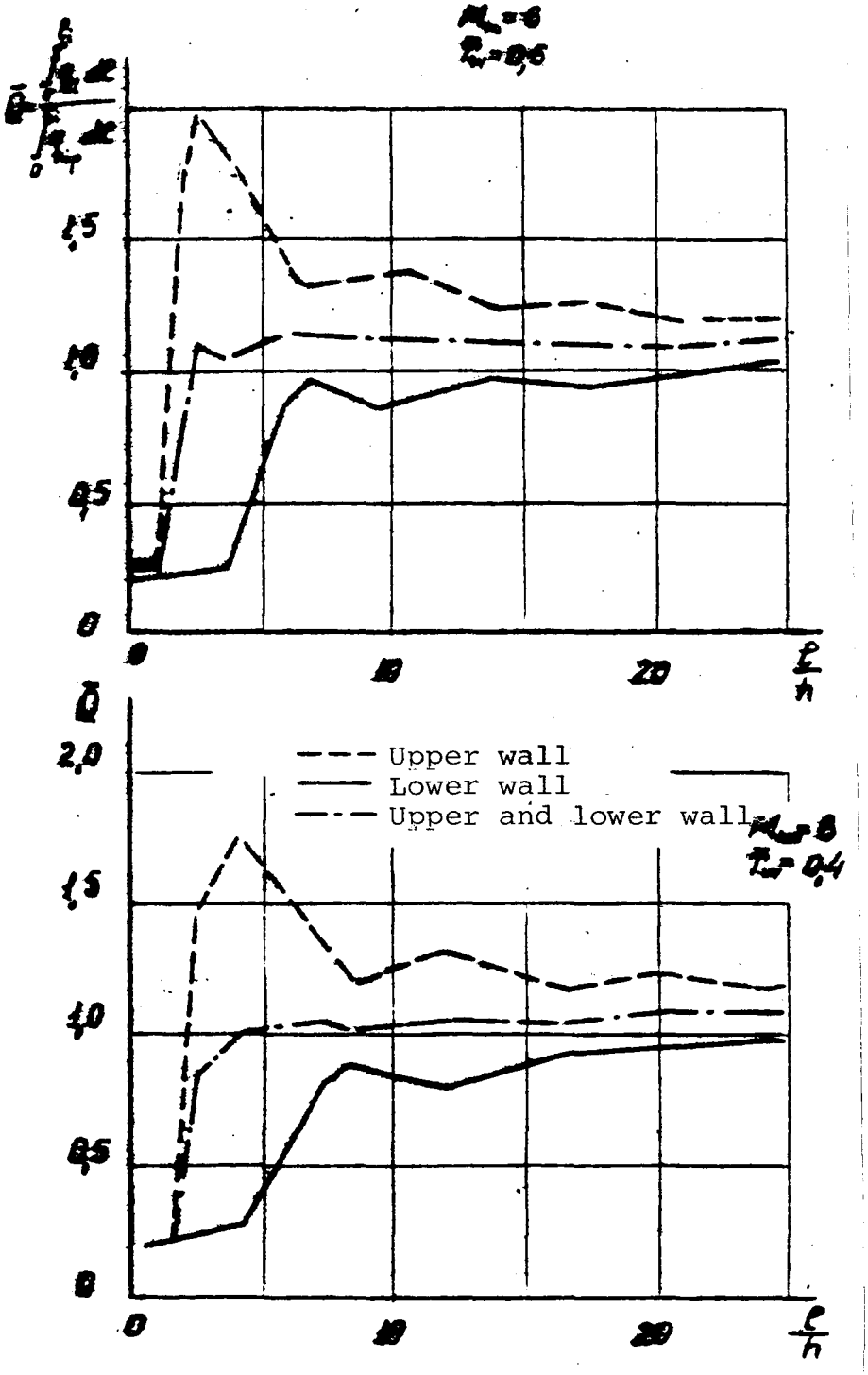

Fig. 6.

0.85, and for the "plateau" region, n = 0.625. Also shown are the calculated points obtained for the conditions of an experiment [6] in which heat flows were measured with M_∞ = 8.6 of a flow over an internal obtuse angle.

As Fig. 5. shows, calculation of local heat flows for a frictionless flow produces intermediate values for heat flows, obtained with separation (between the "plateau" and the "attachment" point). The obtained level of calculated local heat flows is 20-40% below the maximum heat flows at the separation attachment point. /54

Figure 6 shows, for M_∞ = 6 and 8, the ratio of the integral heat flows for each duct wall along its length for an irregular flow and the uniform flow equivalent to it, $\bar{Q} = (\int q_w d\ )/\int q_{wp} d$. We can see that in the initial section of the duct (l/h = 2-7) there is a substantial increase of integral heat flow at the upper wall over that of the lower and uniform flow, and it diminishes at length $l/h \geq 8$. Here the integral heat flows at the lower wall throughout the duct remain somewhat below those at the lower and those calculated using one-dimensional parameters. The total heat flows along the duct, calculated for irregular flow and the uniform flow equivalent to it with respect to rate, momentum, and energy, coincide approximately at length $l/h \geq 4$.

Thus, as research demonstrated, at $l/h \geq 4$ calculation of total heat flows and friction forces in the duct of a GPVRD can be made using the assumption of flow one-dimensionality in the duct and familiar boundary-layer computation methods. This approach produces satisfactory results for both axially symmetric and planar asymmetric flows.

The local specific heat flows should be determined using local flow parameters, since their level may be 3-4 times higher than that of specific heat flows calculated using uniform-flow parameters.

REFERENCES

1. Berlyand, A. T., and F. A. Frost, "A method of calculating two-dimensional supersonic flows with automatic separation of discontinuities and stepwise approximation of rarefaction flow," Informatsionnyy byulleten' "Chislenyye metody mekhaniki sploshnoy sredy" [Information Bulletin "Numerical Methods of Continuous Medium Mechanics"], USSR Academy of Sciences, Siberian Branch, Computer Center, 1972.

2. Avduyevskiy, V. S., "A method of calculating a three-dimensional turbulent boundary layer in a compressible gas," Izvestiya AN SSSR. Mekhanika, 4, 3-12 (1962).

3. Ostras', V. N., and V. I. Penzin, "Experimental study of the force applied to the internal surface of a cylindrical tube with flow into it of a non-uniform supersonic flow created by conic nozzles," Uchenyye zapiski TsAGI 3/4, 29-36 (1972).

4. Repik, Ye. U., and V. Ye. Chekalin, "Convective heat exchange in supersonic conic nozzles," Inzhenernyy zhurnal 2/2, 359-364 (1962).

5. Bogdanov, S. M., and S. Ye. Kepler, "Separation of a turbulent boundary layer in a supersonic flow," VRT 6/36, 50-66 (1956).

6. Holden, M. S., "Shock wave - turbulent boundary layer interaction in hypersonic flow," AIAA Paper No. 72-74, 1972.

FEATURES IN THE SELECTION OF BASIC PARAMETERS OF GAS-TURBINE-ENGINE COOLED TURBINES

O. N. Yemin

1. Peculiarities in calculation of cooled turbines[1] /56

The extensive use of evolved air-cooling of the flow portion of the gas turbines of aviation GTD [gas-turbine engines] has necessitated a more precise procedure for selecting their optimal parameters. As applied to uncooled turbines, parameter optimizations have been fairly thoroughly developed and are discussed in scientific-technical and academic literature [2, 3]. Works [4-6] have cited data needed for preliminary calculation of a cooled turbine or a turbine with cooled stages.

In addition, the initial results from use of cooled turbines indicated a need for considering in the choice of their basic parameters the features of their operation caused by the presence of a system to cool the flow-area components.

Calculations demonstrated, for instance, the need for more accurate assessment of the cooled-turbine r.p.m.'s adopted for the design.

Therefore, this article examines research at the engine department of MAI [Moscow Aviation Institute] concerning the /57 effect of r.p.m.'s on the efficiency of a cooled one-stage turbine.

The analysis was performed for a one-dimensional and the simplest quasi-two-dimensional model of the turbine's operation, i.e., considering its parameters at the mean diameter. The feature of this outline of calculating a cooled turbine using the mean diameter consists in initial calculation of an uncooled stage with determination of the velocity-triangle parameters at the mean diameter, the diametric and fractional (axial) dimensions of the flow-through portion (height and width of the blades, widening angles of the flow-through portion, etc.), and then, for the thusly calculated "uncooled analog" of the turbine being designed, determination of the cooled air flow required to obtain the turbine temperature with which the given long-term strength margins are achieved. Later the working-medium flows

---

[1] The development of aviation and cosmonautics is characterized by a constant increase in parameters of powerplant cycles, especially temperatures in the main combustion chambers of gas-turbine engines [1].

are ascertained in the calculated sections of the stage, in accordance with the cooled-air delivery outline, blade height, and then velocity-triangle parameters.

Thus, although calculation of a cooled turbine according to mean diameter is reduced basically to calculating an uncooled turbine with additions and adjustments, the values of the optimal (expedient) parameters selected when designing a cooled turbine may be substantially different from the parameters of the "analogous" uncooled stage ("uncooled analog"). By "analogous" uncooled stage we shall mean a stage with the same values of basic structural and gas-dynamic parameters ($\bar{H}_{Tu}$, ρ_T, α_1, β_2, u, D_{cp}, $h_{\zeta i}$...), but made uncooled (for example, of a hypothetical superheat-resistant material).

Such a representation is extremely arbitrary, since a cooled turbine, for example, despite the presence of a cooling system (equipment for delivering and distributing cooled air), should be viewed as geometrically similar to an "uncooled" one in which, of course, this equipment is not provided. As will be shown below, however, this comparison is useful, since the efficiencies of uncooled stages and turbines are determined fairly firmly and are well-confirmed by many years of experience in their construction and use. The relation shown in Fig. 1 is used in our analysis [4].

Determination of a cooled turbine's efficiency is difficult, especially in the initial design stage, since it naturally depends on the peculiarities of the cooling system, which are yet unknown./59

Thus, in the first approximation it is suggested that a cooled turbine's efficiency be defined as

$$\eta^*_{T.c} = \eta^*_{T.unc} \cdot \bar{\eta}_c \qquad (1)$$

where $\eta^*_{T.unc}$ is the efficiency of an uncooled turbine stage with basic parameters (H_{Tu}, ρ_T, α_1...) the same as the cooled one under consideration, with the same nozzle-arrangement and impeller geometry, called the "analogous uncooled" stage above; $\bar{\eta}_c$ is the relative efficiency, considering all the peculiarities of the cooled turbine's operation (inequality of flows in stage components, temperature reduction with gas and cooled-air mixing, additional losses with mixing, etc.).

To determine $\bar{\eta}_c$, it is proposed that the experimental (statistical) relation shown in Fig. 2 be employed. Obtained on the basis of processing a relatively small amount of experimental material for the most typical outline of convective-film cooling, it is approximate, but adequate for analyzing turbine parameters at the stage of engine draft design. The value of $\bar{\eta}_c$ depends chiefly on the relative total flow of cooled air -- $G_{c\Sigma}$ (to the stage) -- so the value of $\bar{\eta}_c$ is sometimes arbitrarily

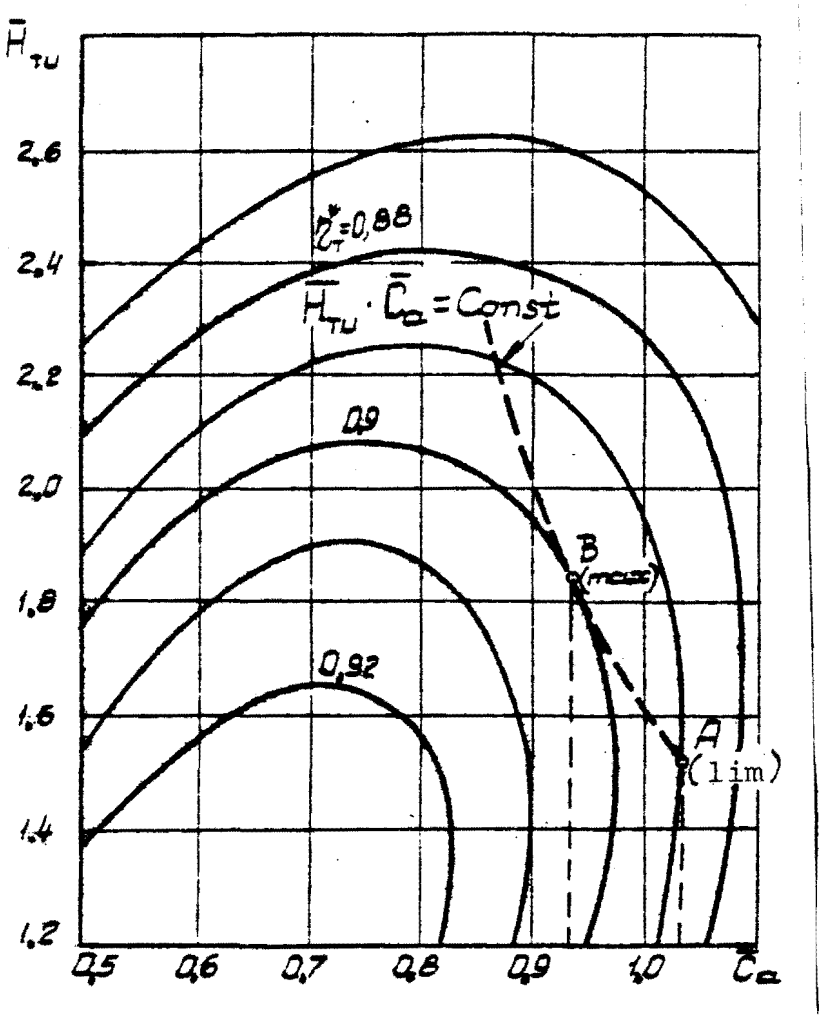

Fig. 1. Efficiency of an "uncooled" turbine stage. The broken line shows the graphic determination of the ratio between r.p.m. and efficiency at maximum setting (A) and in the maximum efficiency mode (B).

represented as the ratio of a turbine with the given total efficiency value to that of the same turbine with $\bar{G}_{c\Sigma} = 0$. /59

$$\bar{G}_{c_\Sigma} = \frac{G_{c.CA} + C_{c.PK}}{G_\Gamma}$$

The required cooled-air flow can be found in the very first step of determining the basic turbine parameters using the familiar relation, the equation associating the coefficient of temperature efficiency of cooling Θ with the relative air flow needed to cool one blade [5]:

$$\Theta = \frac{T_{gas} - T_l}{T^*_{gas} - T^*_c} = f(\bar{G}_c). \qquad (2)$$

/60

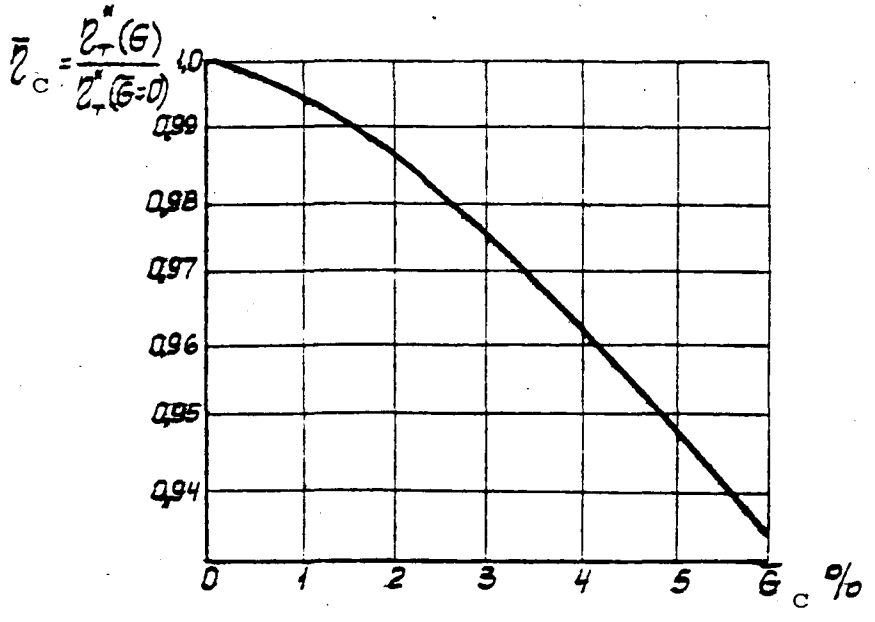

Fig. 2. Effect of total relative amount of cooled air $\bar{G}_{c.CA} + \bar{G}_{c.PK}$ at a stage with convective film cooling of blading on its relative efficiency.

2. Determination of Optimal (Expedient) Turbine Parameters Providing High Efficiencies

/59

Optimization of parameters in accordance with the employed calculation outline assumes obtaining the greatest value of parameter [symbol omitted], consisting of two factors, each of which depends on turbine parameters associated by extremely complicated relations.

/61

The efficiency of an uncooled turbine depends chiefly on the dimensionless parameters describing the process in a simple stage at the mean diameter relative to the height of the flow-through portion and the law of flow-portion profiling by radius.

$$\eta_{T.unc}^{*} = f(\bar{H}_{Tu}; \beta_T; \bar{C}_a; \lambda_u; \frac{D_{cp}}{h_a}; \ldots). \qquad (3)$$

For the given value of theoretical work H_{Tu} of gas flow G and the given or assumed value of the turbine's mean diameter, the choice of some definite value of the flow coefficient $\bar{C}_a$ (or its associated value of angle α_1) determines the value of D_{cp}/h_l, and thus also the degree of reactivity at the calculated mean diameter. In this case the efficiency would be determined by the loading of the stage, i.e., the value of the peripheral velocity or, consequently, the turbine rotor r.p.m.

Reduction of stage loading (i.e., increasing the r.p.m. at a given mean diameter value) usually leads to a decrease in the efficiency of an "uncooled" turbine stage (see Fig. 1). The tensile stress at the root of an operating blade increases because of centrifugal forces [2].

$$\sigma_p = 44{,}7 \cdot 10^{-5} n_T^2 \cdot F_T \cdot \Phi \,. \qquad (4)$$

where F_T is the annular area at the stage outlet, m^2; Φ is the form factor of the operating blades (Φ = 0.58-0.62).

Obviously, to provide the required strength margin for a turbine with a higher r.p.m. we have to ensure fairly high values for the long-term strength of blade material. Of course, high long-term strength values can be provided by reducing the temperature of the blade material, and this requires increasing the cooling air flow. This causes a reduction of $\bar{\eta}_c$.

Recall that the value of $\eta^*_{T.unc}$ increases when r.p.m. increase.

Thus, to obtain a high efficiency value for a cooled turbine the r.p.m. should be chosen so as to produce the highest product $\eta^*_{T.unc} \cdot \bar{\eta}_c$, consisting of values changing in opposite ways with change in n_T. /62

Generally speaking, solution of the problem remains difficult. Thus, in each specific case it is expedient to perform a series of variant calculations.

A typical example of selecting the optimal r.p.m. value is analyzed in detail below.

3. The Concept of Limiting R.P.M.

As an example of the procedure described in [6], calculations were performed for a gas-generator turbine intended for creating a TRDD [ducted-fan turbojet engine] with a total pressure ratio in start conditions $\pi^*_{K\Sigma}$ = 30 and a combustor temperature T^*_Γ = 1700K. The pressure ratio in the gas-generator compressor $\pi^*_{K\Gamma T}$ = 11.5 and the gas flow G_Γ = 65 kg/sec. The convective-film cooled blades are made of alloy ZhS-6, the cooled-air temperature is assumed $T^*_C = T^*_K$ = 880K, and the strength margin K_{σ_p} = 2 for a calculated operating time τ = 250 hrs. The mean diameter of the turbine is assumed D_{cp} = 0.7 m.

We note first of all that experience in performing systematized variant calculations reveals the expediency of varying both the value of the turbine mean diameter and the value of the blade-material temperature, T_ℓ. The temperature of the diaphragm vanes was assumed $T_{\ell CA}$ = 1300K in all calculations.)

/63

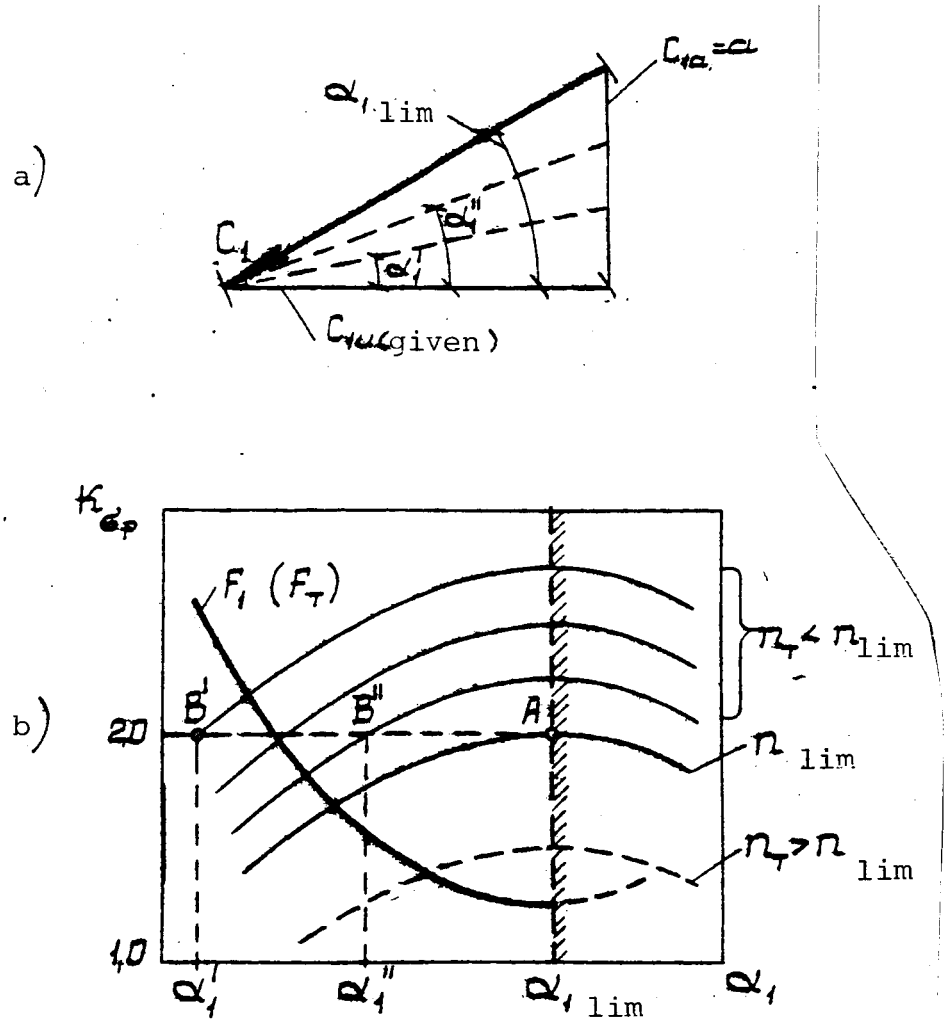

Fig. 3. For defining the idea of limiting r.p.m. of a turbine -- T_l = const.

a) input velocity triangle element;
b) calculation of operating impeller-blade strength margins, under the condition that [expression omitted].

As Fig. 3 shows, to meet condition $K_{\sigma p} = 2$ at the assumed /62 blade material temperature and with the given gas flow value through the stage, increasing the r.p.m. makes it necessary to increase angle α, and thus to decrease blade height. When angle α_1 is increased, however, the velocity in the impeller clearance increases, as does its axial component. When the limiting expanding power of the nozzle equipment is reached (axial component equal to the speed of sound), further reduction of the flow-section area, as shown in Fig. 3a, and thus also of the blade height, is curtailed. Thus, for highly loaded turbines, in which the value of C_{1u} is significant, and especially

for gas-generator turbines, the appearance of limiting r.p.m. becomes characteristic, since there is no need to compensate for further increase in r.p.m. by reducing blade height. In other words, limited nozzle-capacity modes may become characteristic of these turbines, and with these it is obvious that the turbine diameters have to be increased when r.p.m. are increased. The limiting value of angle α_1, determined by the formula following directly from Fig. 3a

/64

$$\tan \alpha_{1\,lim} = \sqrt{\left(\frac{a_{cr_0}}{c_{cr}}\right)^2 - \frac{k-1}{k+1}} \quad (7)$$

Corresponding to the limiting r.p.m. value are the efficiency value points limiting for the given temperature. By connecting the limiting-efficiency points for various temperatures we obtain a curve of limiting efficiencies (Fig. 4). The relation between $\eta_{T\,lim}$ and η_T has a distinct maximum. The presence of a maximum is explained by the opposite effect on efficiency of the loading factor and the amount of cooled air. The nature of the dependence of these values on r.p.m. in limiting modes is shown at the top in Fig. 4. At the same time, for given values of T_ζ the dependences of limiting efficiency on r.p.m. may have an extremum, and we have to determine, in addition to the limiting efficiencies, the values of the maximum efficiencies, which generally may differ from the limiting.

4. Relation Between Maximum and Limiting Efficiencies

As we already mentioned, at T_ζ = const. an increase in angle α_1 (to as much as $\alpha_{1.lim}$) leads to a monotonic increase in r.p.m., corresponding to the assumed strength margin $K_{\sigma p} = 2.0$, right up to the value $n = n_{lim}$.

As we know, however, the turbine-stage efficiency has an extreme character when the calculated value of angle α is changed [2]. The position of this extremum is determined by the configuration of the velocity triangle, which determines the amount of loss in the stage and the exit velocity (C_2 and λ_2). The location of the extremum of function $\eta_T^* = f(\alpha_1)$ is not associated with the strength indices of the projected stage and the value of $\alpha_{1\,opt}$ (by efficiency) can be found "to the left" and "to the right" of the value of $\alpha_{1.lim}$ (by strength), as shown in Fig. 5. A relatively simple method of establishing the relation between maximum and limiting efficiencies is provided by the simplified procedure of evaluating the efficiency of a cooled turbine, in accordance with which the efficiency of an "uncooled" turbine $\eta_T^{*}{}_{.unc}$ is determined using the graphic relation shown in Fig. 2.

/67

Preliminarily, we establish that along line T_ζ = const. in Fig. 4 we can consider valid the following approximated relation:

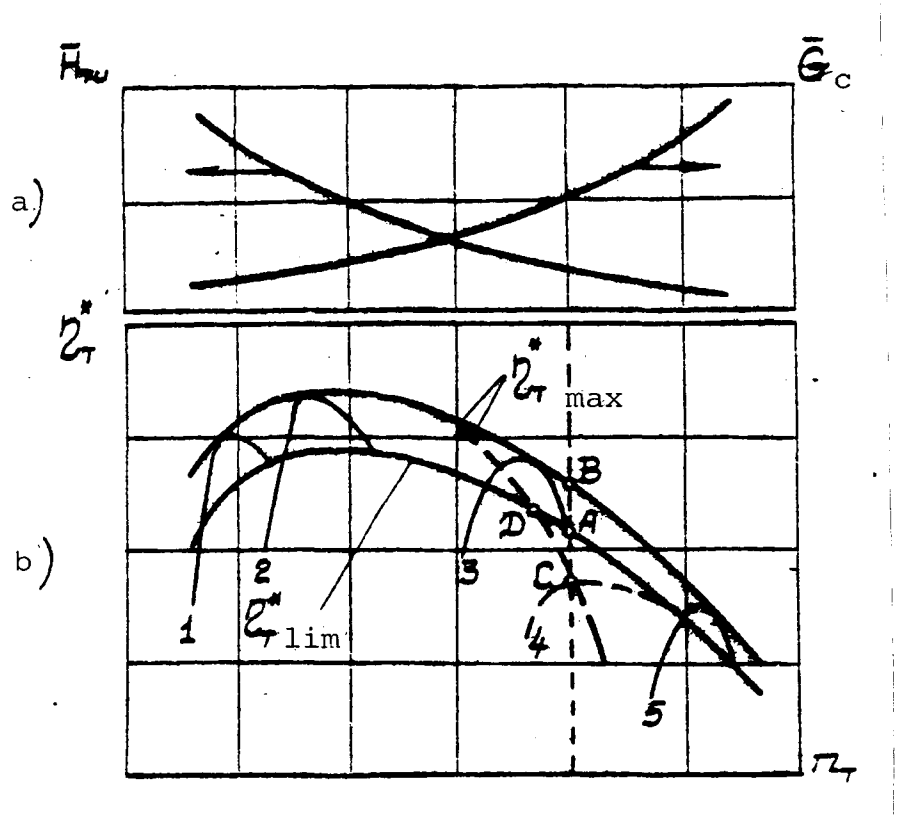

Fig. 4. Explanation of extreme character of relation between cooled-turbine efficiency and r.p.m. (a). Possible relationship of locations of its maximum and limiting efficiencies (b).

Numbers indicate lines of constant values of temperature of blade material ($T_{\ell} > T_{\ell 2} > \ldots T_{\ell 5}$).

$$\sigma_{\text{max}} = \text{idem}; \quad \bar{G}_C = \text{idem}; \quad \bar{\eta}_{t\,C} = \text{idem}.$$

The assumption that the relative flow of cooled air remains unchanged is, generally speaking, approximate, since change in r.p.m., and thus in turbine circumferential velocity u, strictly speaking, leads to a change in the stagnation temperature in relative movement -- T^*_w. /67

In addition, for the assumed condition $K_{\sigma p} = 2.0$ the value of the tensile stresses at the blade root should also be unchanged:

$$\sigma_p = \text{idem}.$$

Converting the simplest formula for determining stresses at the root of an operating blade, we obtain

$$\sigma_p = \text{const}\frac{u^2}{\frac{b_{op}}{h_m}} = \text{const}\frac{u^2 b_{op} h}{} = \text{const}\frac{u^2}{D_{ep}^2}\frac{G_r}{z c_a \gamma} =$$

$$= \text{const}' \frac{\eta_T}{c_a} = \text{idem}.$$

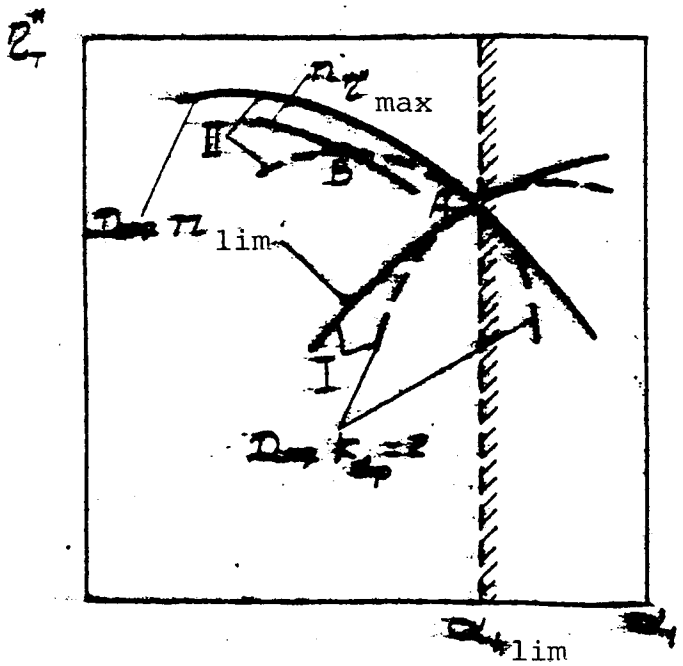

Fig. 5. Relation between η^*_{Tmax} and η^*_{Tlim} case 1, where $n_{\eta^*max} = n_{lim}$ and $\eta^*_{Tmax} = \eta^*_{Tlim}$ case 2, where $n_{\eta^*max} < n_{lim}$ and $\eta^*_{Tmax} > \eta^*_{Tlim}$

Thence it follows that at T_τ = const. we observe condition

$$\bar{c}_a = \text{const}, \quad n_T. \qquad (8)$$

On the other hand, when designing a turbine with a certain value of theoretical work H_{Tu} and a given mean diameter D_{cp}, when the r.p.m. is varied we observe condition

$$\bar{H}_{Tu} = \frac{\text{const}_2}{n^2}. \qquad (9)$$

Combined solution of equations (9) and (8) leads to equation:

$$\bar{H}_{Tu} \cdot \bar{c}_a^2 = \text{const}. \qquad (10)$$

By applying this relation to the graph of the efficiency of an "uncooled" turbine (see Fig. 1) we obtain the possibility of establishing the relation between r.p.m. in limiting mode (point A) and the maximum efficiency mode (point B).

On this graph, point B defines the point where the curve $\bar{H}_{Tu}\bar{c}_a^2$ = const. touches one line of constant values of $\eta^*_{T.unc}$, and at the point of tangency (point B) the maximum value of $\eta^*_{T.unc}$ is achieved. Obviously, the maximum value of the efficiency of a cooled turbine $\eta^*_{T.c}$ would also correspond to this mode. This follows from the fact that all the examination is made along line T_τ = const., for which, as shown above, the relative cooled-air flow $\bar{G}_c$ and the relative efficiency, considering the effect of cooling, $\bar{\eta}_c$, remain unchanged. /68

Thus, with the same values of T_τ, between the parameters of the cooled and uncooled turbines there is an association defined by relations

$$\left.\begin{aligned}\frac{\eta^*_{T\,max}}{\eta^*_{T\,lim}} &= \frac{\eta^*_{T\,unc\,B}}{\eta^*_{T\,unc\,A}}\\ \frac{n_{max}}{n_{lim}} &= \frac{\bar{c}_{a\,B}}{\bar{c}_{a\,A}}\end{aligned}\right\} \qquad (II)$$

To determine a rational value of the turbine rotor r.p.m. of a gas generator, we have to construct the relations of maximum and limiting efficiencies to r.p.m. Using relations (11), we note that for some combination of turbine strength indices and relations between its efficiency and r.p.m. the line $T\zeta$ = const. may be in the form of the broken line in Fig. 4, i.e., with an extremum at point C, lying below pount A on the limiting efficiency curve. Calculations done according to this procedure for a gas generator with the parameters given in section 3 revealed that, to obtain the highest efficiency value, we would have to select the following values of the operating-blade material temperature, turbine r.p.m., stage loading factor, and total relative cooled-air flow:

$$\begin{aligned} T &= 1200K\\ n &= 13{,}000 \text{ r.p.m.}\\ \bar{H}_{Tu} &= 2.0\\ \bar{G}_c &= 4.5 \end{aligned}$$

This would provide a turbine cooled-stage efficiency of $\eta^*_{T.c} = 0.865$.

However, this question of choosing expedient parameters for a gas-generator turbine cannot be considered answered, since we have to introduce into the examination, in addition to turbine efficiency, the compressor operation indices, also determined by the chosen r.p.m.

We can also assume that the expedient r.p.m. would be found near the extreme values of the curves of $\eta^*_{T.lim}$ and η^*_{Tmax}, which /69 are generally quite close to each other.

The above sample calculation allows formulating some concepts about the features of the basic parameters of a high-temperature gas-generator turbine stage.

The calculations demonstrated convincingly that the internal efficiency of a cooled turbine, as opposed to an uncooled turbine, is affected basically by, in addition to the loading factor, the amount of cooled air blowing on the surface of the blade, so the attempt should be made to increase the blade's design temperature and reduce the percentage of discharged air. For reducing $\bar{G}_c$ we can sometimes recommend measures to decrease the cooling-air temperature in a special heat-exchanger [6].

The highest cooled-turbine efficiency is achieved in modes with which the value of the loading factor is higher than that recommended for uncooled turbines.

The minimum value of turbine-blade height for the given temperature of material corresponds to the limiting curve. But in maximum efficiency modes, too, high-temperature turbines of gas generators are characterized by a high value of ratio D_{cp}/h_l = 15-25.

The extreme nature of the relationship between efficiency and r.p.m. leads to the need for designating a "tie" of the engine rotor to determination of the expedient rotor r.p.m. of its gas-generator.

REFERENCES

1. Shlyakhtenko, S. M. (ed.), Teoriya vozdushno-reaktivnykh dvigateley [Jet Engine Theory], Moscow, 1975.

2. Abiants, V. Kh., Teoriya aviatsionnykh gazovykh turbin [Theory of Aviation Gas Turbines], Moscow, 1979.

3. Kholshchevnikov, K. V., Teoriya i raschet aviatsionnykh lopatochnykh mashin [Theory and Design of Aviation Bladed Engines], Moscow, 1979.

4. Khorlok, Dzh. Kh., Osevyye turbiny [Axial Flow Turbines], Moscow, 1972.

5. Kopelev, S. Z, and N. D. Tikhonov, Raschet turbin aviatsionnykh dvigateley [Design of Aviation Engine Turbines], Moscow, 1974.

6. Yemin, O. N., and A. V. Gavrilov, "Procedure for calculating gas turbines in a computer," MAI, (1978).

ON SELECTING THE OPTIMUM TOTAL WEDGE ANGLE FOR A HYPERSONIC RAMJET ENGINE AIR INLET

V. I. Penzin

The most important component of a ramjet engine (PVRD), /70
determining its efficiency, is the air inlet. At high flight speeds, with which it becomes expedient to employ supersonic combustion in the combustor (PVRD), inlet requirements change markedly, since the optimal inlet shape becomes dependent on the engine's operating conditions, i.e., on the excess-fuel ratio (stoichiometric equivalent Φ) [1]. A change in the air inlet's shape entails both a change in the combustor shape and in the level of total pressure loss in the combustor [2]. In [1] an examination was made of a GPVRD [hypersonic ramjet engine] with the simplest two-dimensional, one- and two-shock air inlet. This article investigates the effect of stoichiometric equivalent Φ, number of shocks N, relative inlet throat area $\bar{F}_r$, lip shape, and other parameters in the M_∞ = 6-10 range on the optimum total wedge angle of a multishock air inlet θ_K.

Figure 1 shows a computational outline of a GPVRD with a two-dimensional multishock fixed air inlet. Taken as the optimum value of θ_K was the value at which the thrust coefficient C_a is maximal at the given Φ. The GPVRD thrust calculations considered friction pressure forces on the stagnation surface and internal and external surfaces of the lip. All of these forces are easily calculated for two-dimensional flow. The internal and effective (less external resistance) engine thrusts /72
were determined with the assumption of one-dimensional flow in the combustor and nozzle.

The initial throat area (combustor) of the air inlet was determined without considering the effect of viscosity, assuming the speed of sound in the throat upon start. Then the value of $\bar{F}_{r.init}$ was increased to calculate the effect of viscosity [3] and to provide inlet operation in the M_∞ range, after which the effect of this change on $\theta_{K.opt}$ was determined.

Hydrogen was examined as the fuel, the available heat factor (complete combustion) was assumed equal to 0.9, and the nozzle momentum factor η_n = 0.95. The optimal shape of the GPVRD flow area (air inlet and combustor) does not depend on the area of the nozzle outlet section, and in the calculations the latter was assumed equal to the area of the entrance to the inlet.

An increase in inlet angle θ_K leads to increase in the intensity of shock waves and loss of total pressure in them, but

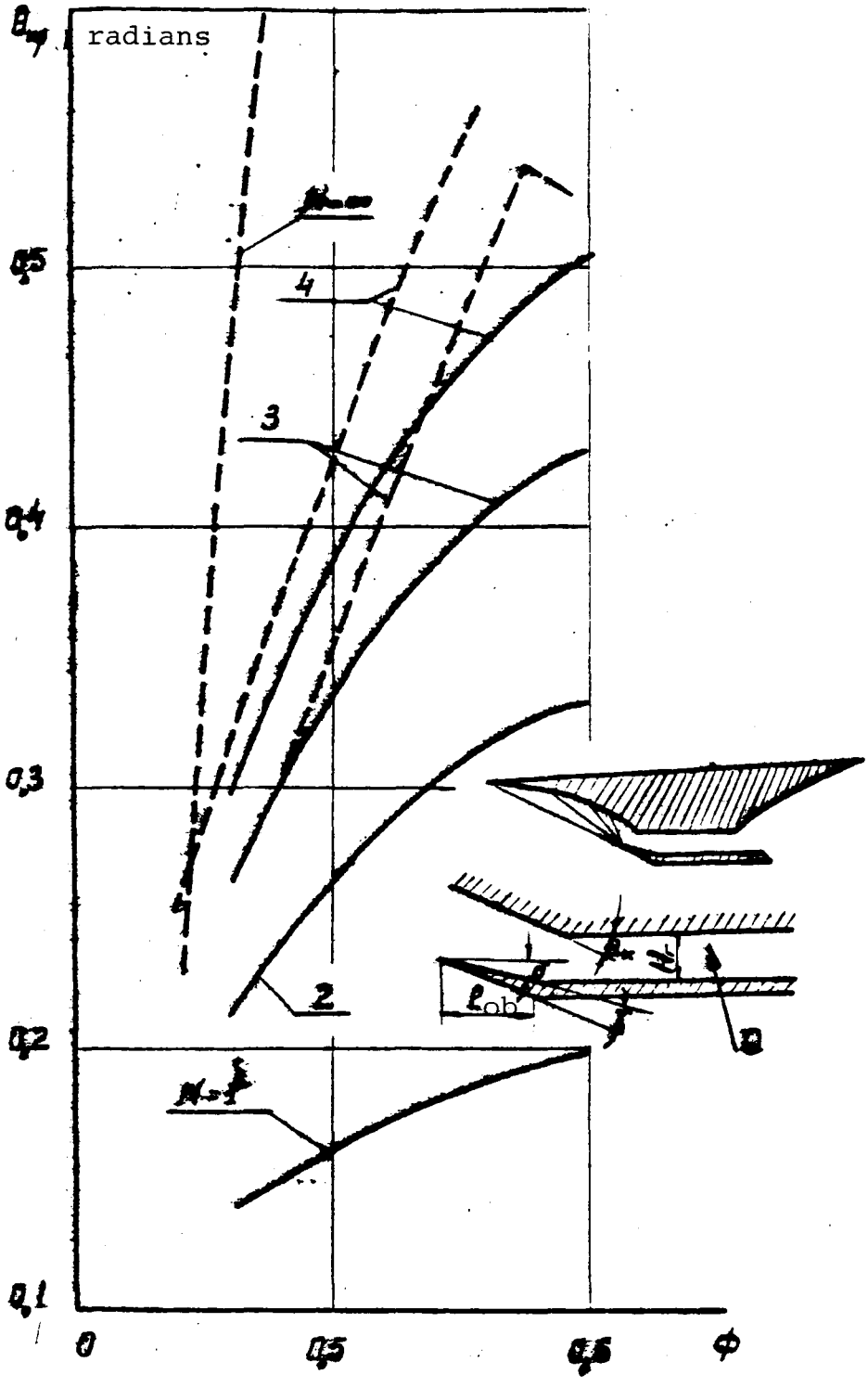

Fig. 1.

heat losses in the combustor decrease, since the flow velocity in the chamber before the fuel-delivery section diminishes. At $\theta_K = \theta_{K.opt}$ the total pressure losses in shocks, and with absorption, reach a minimum, and thrust reaches a maximum.

Figure 1 shows the relation between $\theta_{K.opt}$ and stoichiometric equivalent Φ at $M_\infty = 10$, using an air inlet with 1 to infinity shocks. In the latter case we examined an isoentropic air inlet (inverse of Prandtl-Meyer flow). The graphs shown in Fig. 1 and Fig. 2 correspond to the condition of equal intensity of shocks and are calculated for two cases: 1) the difference between the total wedge angle θ_K and the undercut of the lip are constant ($\theta_K - \delta = 0.16$ radians) (solid lines); and 2) zero undercut of lip, $\delta = 0$ (broken lines). An examination of Fig. 1 reveals that the number of shocks in a multishock air intake substantially alters the optimal value of θ_K. For example, a move from N = 1 to N = 4 changes $\theta_{K.opt}$ at $\Phi = 1$ by $\Delta\theta_K \simeq 0.5$ radians. Reduction of the lip undercut leads to an increase in the value of $\theta_{K.opt}$. But it should be stressed that condition $\delta = 0$ (at $N > 2$) is apparently impossible to bring about in practice because of the high value of $\theta_K - \delta$, which may lead to stall. Increasing the heat input (increasing Φ) leads to an /74
increase in $\theta_{K.opt}$, and moreso as δ is smaller. When Φ is changed from 0.5 to 1.0 the value of $\theta_{K.opt}$ may increase (at N = 3) by 0.1-0.15 radians.

At $M_\infty = 10$ the value of $\theta_{K.opt}$ is reached at practically all values of $\Phi \leq 1$. At $M_\infty = 6$ (Fig. 2) and with $\theta_K = \theta_{K.opt}$ in a constant-section duct, only a relatively small amount of fuel can be delivered ($\Phi_{lim} < 0.2$-0.3). Duct choking occurs when Φ is increased above the limiting value, and the area of the inlet throat and the flow velocity in it increase. The left branches of the curves in Fig. 2 correspond to the optimal value of θ_K, and the right to non-optimal values (choking mode). The conclusions drawn from the results of calculations at $M_\infty = 10$ can be extended to the case where $M_\infty = 6$ if we examine only the left branches of the obtained curves. Additional information in Fig. 2 relates to the effect of lip wedge angle γ (see Fig. 1). In the calculations corresponding to Fig. 2 it was assumed that the length of the lip segment with undercut l_{ob} equals 0.15 times the height of the entrance to the inlet.

It is apparent from Fig. 2 that change in γ from 0.07 to 0.27 radians leads at $\Phi = 0.2$ to an approximately 0.15-radian reduction in $\theta_{K.opt}$. It is also interesting to note that the right branches of relations $\theta_K = \theta_K(\Phi)$ at $N > 3$ are close to each other and can be replaced by one curve for preliminary evaluations.

Generally speaking, it is inexpedient to increase $\Phi > \Phi_{lim}$ by reducing θ_K in a GPVRD, since this reduces engine efficiency.

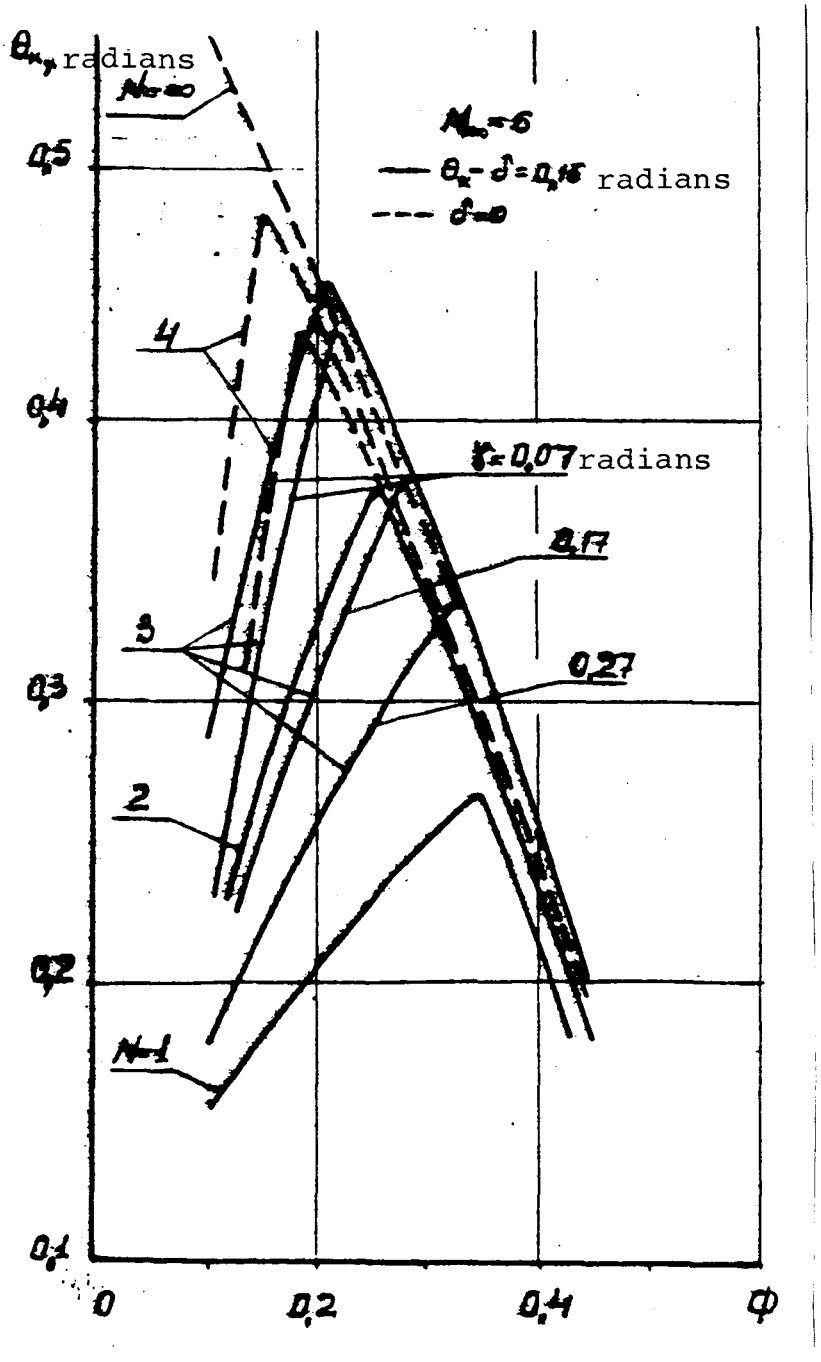
radians
0,5
0,4
0,3
0,2
0,1
0
0,2
0,4
Φ
radians
radians
0,07
0,17
0,27
4
3
2
1

Fig. 2.

It is more proper to accomplish heat input in an expanding combustor after section F = const. In this case, at $\Phi > \Phi_{lim}$ the value of θ_K would be constant and equal to $(\theta_{K.opt})_{max}$. In practice, however, cases are possible where increased heat input into an F = const. chamber may be useful. This may be because of the advantages of simplifying the fuel-delivery system, possible increase in combustion efficiency, etc.

Figure 3 shows generalized relations between $\theta_{K.opt}$ and M_∞ for cases N = 2 and 3 (broken and solid lines) for various values of stoichiometric equivalent Φ. The envelope of the maximum values of $\theta_{K.opt}$ is marked off by the broken/dotted line. An examination of the graph makes it apparent that $\theta_{K.max}$ is reached at $M_\infty = 9$, and it diminishes with further in crease in M_∞, a fact explained by the reduction of relative heat input (under the condition that $\Phi \leq 1$).

Optimization of a GPVRD-powered cruise aircraft at $M_\infty = 8$, /76
10, and 12 is conducted in [4]. A two-shock, two-dimensional air inlet with zero lip undercut was examined. The optimal values of stoichiometric equivalent Φ and the total lip wedge angle θ_K at $M_\infty = 8$ and 10 were obtained as equalling 0.45 and 0.53, 0.295 and 0.23 radians, respectively. These values are marked out by circles in Fig. 3, and thence we can see that the values of $\theta_{K.opt}$ from [4] are somewhat lower (by about 0.05) than those in our work. This can be partially explained by the fact that in [4] the air inlet was assumed variable at start, i.e., with a smaller throat area.

In actual air-inlet constructions, the condition of shock-wave equal intensity is not strictly observed. The slope of the first panel of the deceleration wedge is made larger than is dictated by the condition of equal shock intensity, and the air inlet becomes shorter. Figure 4 shows relations between C_a and the slope of the first panel of a three-shock air inlet θ_1. The slopes of the second and third panels were selected from the condition of equal intensity of the second and third shock waves. A strong dependence of C_a on θ_1 can be seen, when θ_1 is smaller than the optimal value. In the limiting case, at $\theta_1 = 0$, the air inlet degenerates into a two-shock one. At $\theta_1 > \theta_{1.opt}$ the value of C_a changes slightly. Also in Fig. 4, the broken/dotted line marks out the relation between $\theta_{K.opt}$ and θ_1 at $\Phi = 1$. We can see from the graph that an increase in θ_1 leads to an increase in $\theta_{K.opt}$. A change in θ_1 from 0.1 to 0.2 radians leads to a 0.07 increase in $\theta_{K.opt}$. The preceding calculations were performed in the assumption that the inlet throat area is determined under the condition that M in the throat equals unity upon start. The throat area would be greater than initial also in the case where an invariable inlet is used in the M_∞ range.

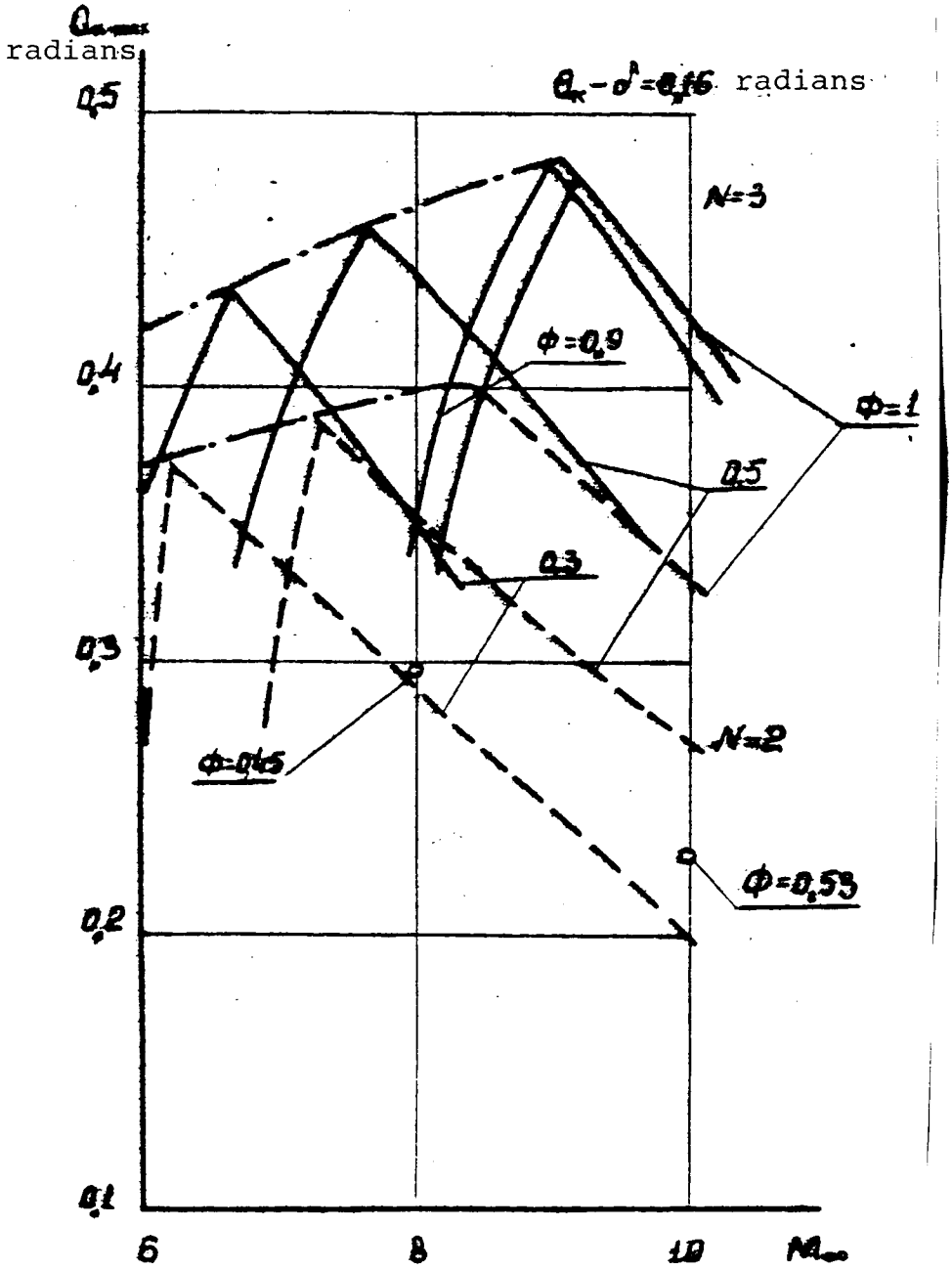
radians
radians
0,5
0,4
0,3
0,2
0,1
6
8
10
N=3
N=2
Φ=1
Φ=0,9
Φ=0,5
Φ=0,3
Φ=0,65
Φ=0,53

Fig. 3.

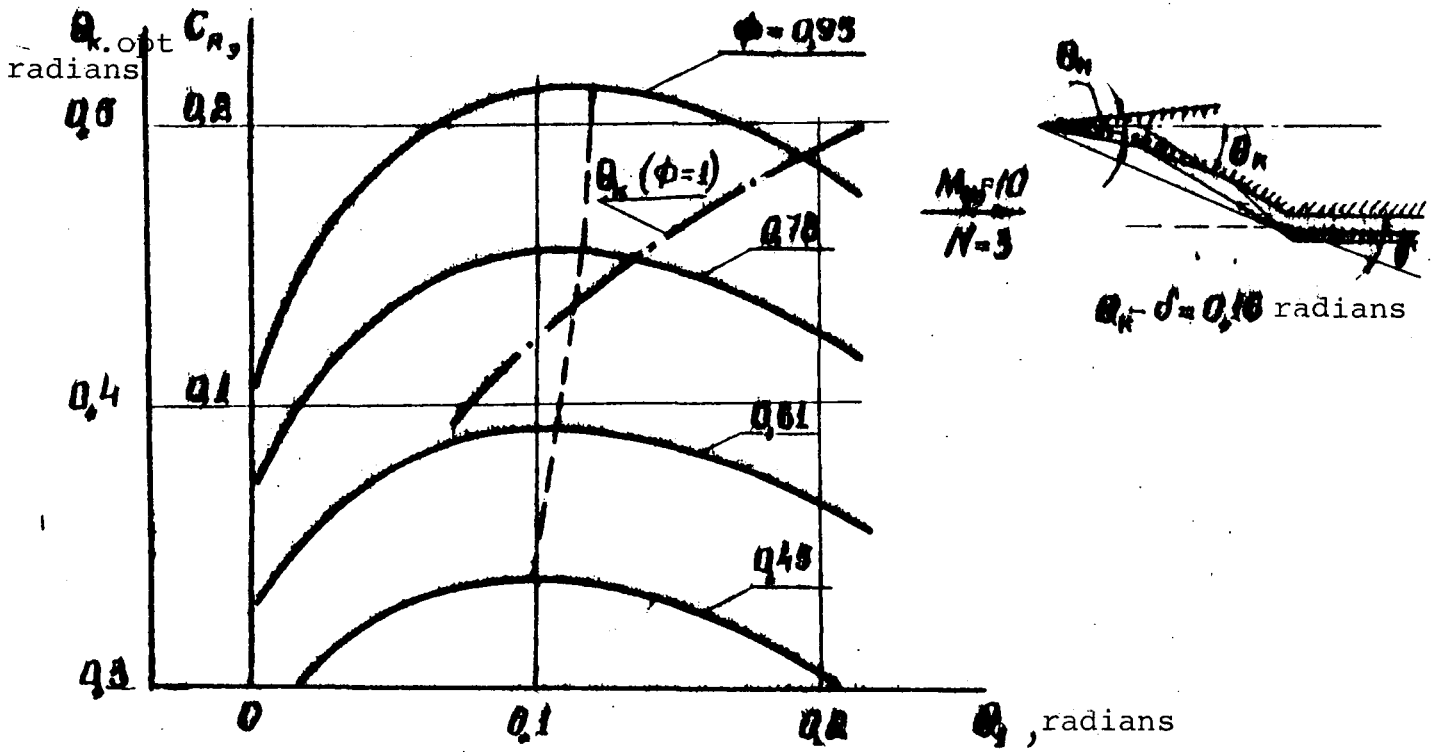
$\alpha_{k.opt}$ radians
C_n,
0,6
0,4
0,2
0,1
0
0,1
0,2
α_1, radians
$\varphi = 0,93$
α_k (φ=1)
0,78
0,61
0,48
$M_{кр}$=10
N=3
α_n
α_k - δ = 0,16 radians

Fig. 4.

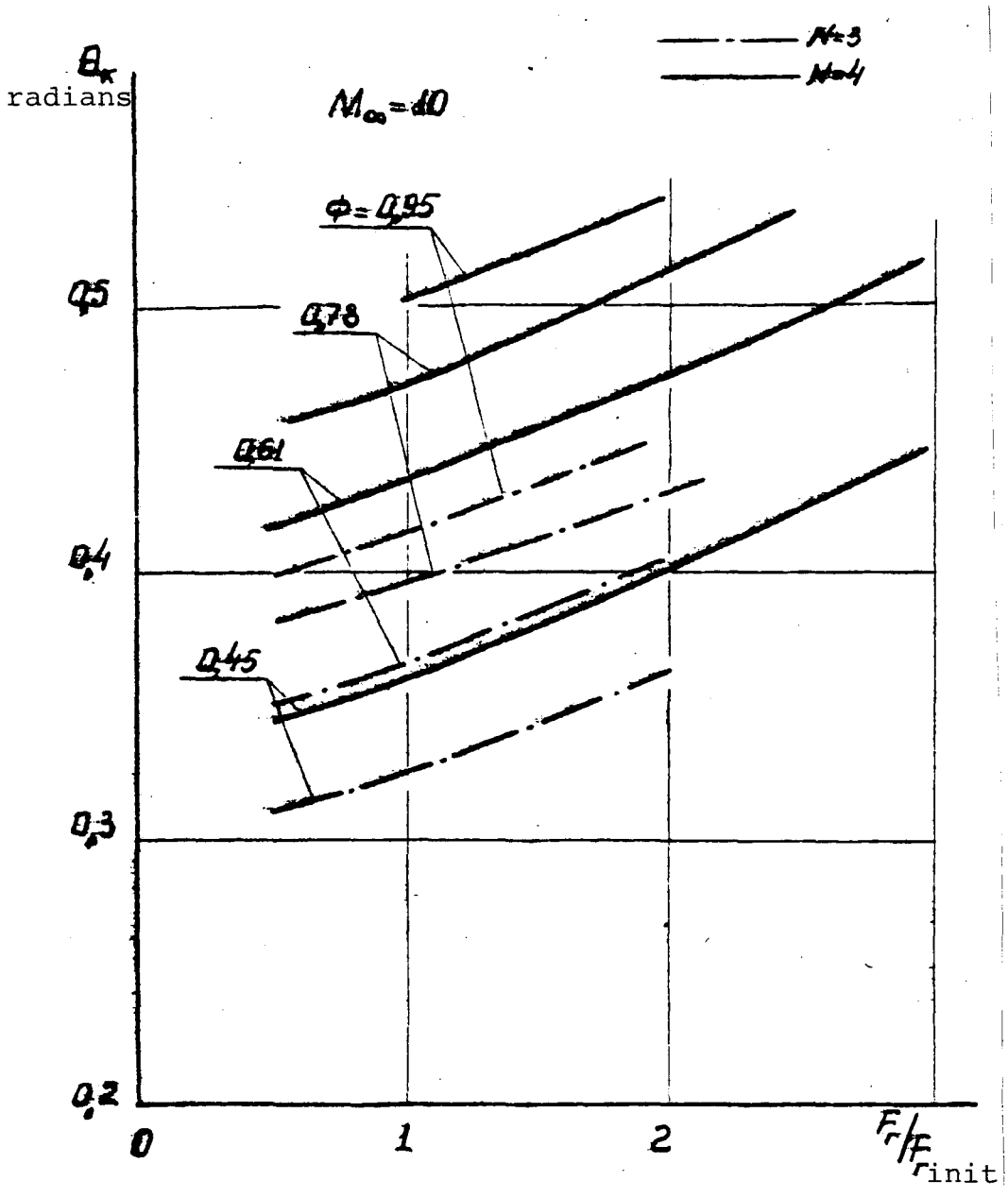
N=3
N=4
$\theta_к$
radians
$M_\infty = 10$
$\varphi = 0{,}95$
0,78
0,61
0,45
0,5
0,4
0,3
0,2
0
1
2
$F_r/F_{r\,init}$

Fig. 5.

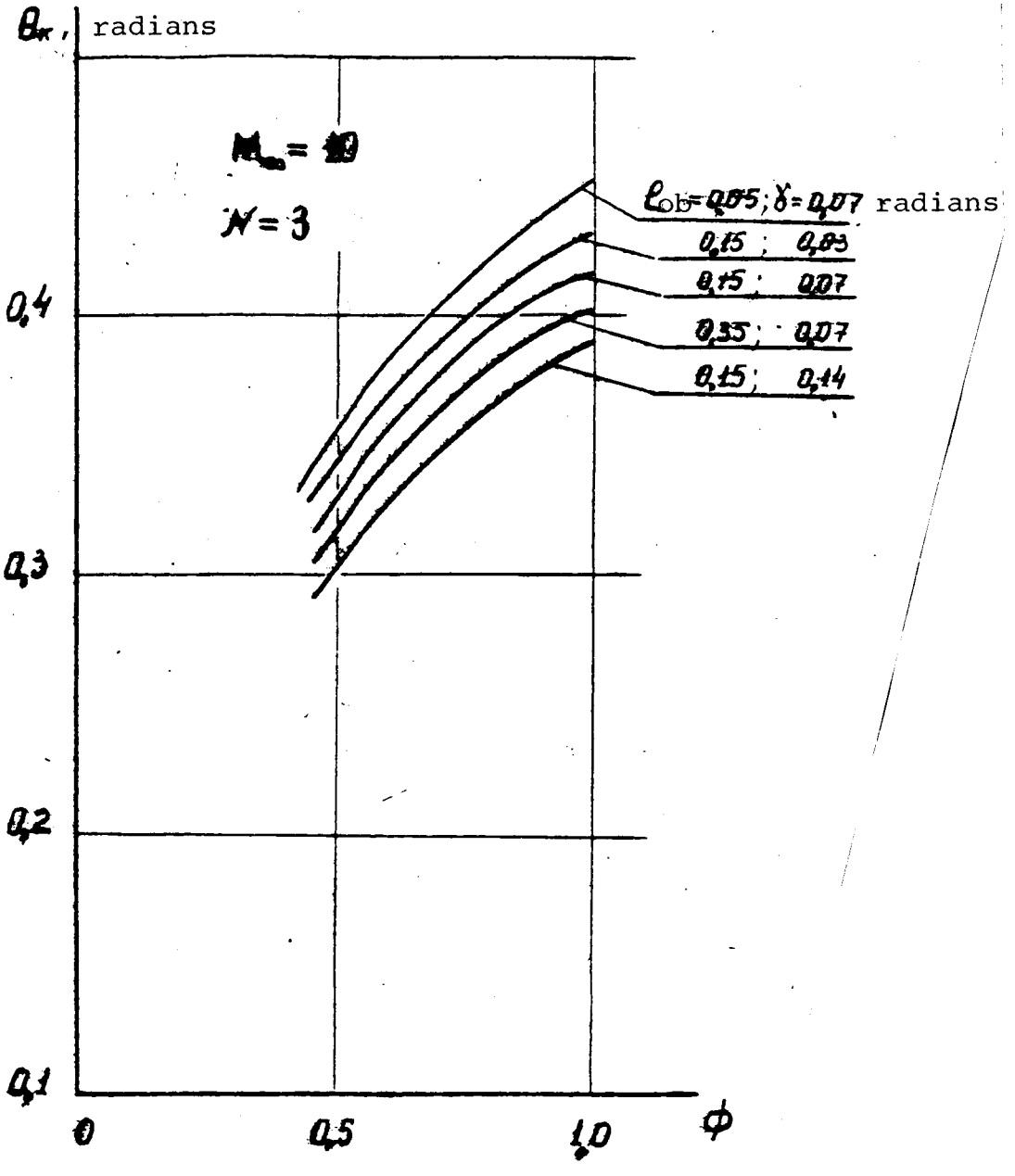
radians
$M_\infty = 10$
$N = 3$
c_{ob}=0,05; δ=0,07 radians
0,15 ; 0,03
0,15 ; 0,07
0,35 ; 0,07
0,15 ; 0,14
0,4
0,3
0,2
0,1
0
0,5
1,0
ϕ

Fig. 6.

Figure 5 shows the relations between $\theta_{K.opt}$ and relative throat area of three- and four-shock air inlets at various values of Φ. An increase in the throat area leads to a slight increase in $\theta_{K.opt}$, since the actual difference between F_r and the initial value is significantly smaller than that shown in Fig. 5. For example, the actual air-inlet throat area in the condition of turbulent flow in the boundary layer exceeds the initial value by approximately 8% [3]. The need for air inlet operation at M_∞ = M [symbol omitted] -3 leads to an approximately 20-30% increase in F_r. Considering that the slope of the curves of re- /80 lation $\theta_K = \theta_K(F_r/F_{r.init})$ is practically independent of Φ, a 30% increase in F_r leads to a 0.01-radian increase in $\theta_{K.opt}$. Because of the small change in the thrust coefficient C_a near the maximum with change in θ_K, when determining $\theta_{K.opt}$ in parametric calculations we can use the initial value of the air inlet throat.

In conclusion, we note the effect of the shape of the fore part of the lip on $\theta_{K.opt}$. Figure 6 shows relations between $\theta_{K.opt}$ and Φ for various values of $\bar{l}_{ob}$ and γ at M_∞ = 10 and N = 3. Change from the shortest and "thinnest" ($\bar{l}_{ob}$ = 0.05 and γ = 0.07 radians) to the longest and "thickest" ($\bar{l}_{ob}$ = 0.15 and γ = 0.14) fore part of the lip at Φ = 1 leads to a 0.07-radian reduction of θ_K.

REFERENCES

1. Penzin, V. I., "Optimality conditions of supersonic flows with diagonal shock waves and subsequent heat input," Izvestiya vysshikh uchebnykh zavedeniy. Aviatsionnaya tekhnika, Kazan', No. 4, 114-120 (1966).

2. Penzin, V. I., "A hypersonic ramjet engine as a Buseman biplane with heat input," Trudy I Chteniy F. A. Tsander. Sektsiya "Teoriya i konstruktsiya dvigateley" [Proceedings of the 1st F. A. Tsander Lectures: "Theory and Construction of Engines" Section], Moscow-Riga, 1972, pp. 22-32.

3. Gurylev, V. G., A. K. Ivanyushkin, Ye. V. Piotrovich, "Experimental study of the effect of M number on air intake start at high supersonic flow velocities," Uchenyye zapisiki TsAGI 4/1, 33-34 (1973).

4. Walker, R. C., "Configuration optimization of a class of hypersonic vehicles," ARL paper No. 70-0342, 1970.

THE IDEAS OF F. A. TSANDER AND ASSESSING THE USE OF JET ENGINES FOR ACCELERATING AEROSPACE AIRCRAFT

Yu. M. Annushkin

1. Basic Ideas of F. A. Tsander and the Future of Aerospace Science[1]

A basic idea that can be ascribed to F. A. Tsander is the /81
suggestion that atmospheric air be used in jet engines to accelerate aerospace aircraft. His design [1] published in the 1920's is widely known today.

Of course, the level of development of aviation and rocket technology at that time made it impossible to carry out space flights with a rocket or an aircraft launch. The creation of space-rocket systems became possible only in the 1950's, and creation of more economical winged aerospace booster systems is apparently a matter of the near future [2].

In the 1930's reaction-engine technology was split into two distinct fields: the first (use of VRD [jet engines] and winged craft) was assigned to aviation, the second (use of ZhRD [liquid-fuel rocket engines]) merged into independent rocket, and later aerospace technology. The problems of creating rockets with ZhRD in a system were simpler than those of creating vehicles using the Earth's atmosphere to produce VKS [aerospace plane] lift and VRD thrust. A significant role in this was played /82
by the fact that ballistic missiles were an even more important weapon than winged craft.

The development of aviation and aerospace science and technology is associated most of all with the development of aviation and rocket engine-building. Understanding this, Tsander, especially in the last years of his life, focused his attention on developments of and research on jet engines which could be employed to boost spacecraft. The status of aircraft engine-building in the 1920's did not allow him in his designs to examine engines using atmospheric air at speeds exceeding 400 m/sec. This apparently explains the fact that in his design for an air-launched vehicle he adopted propeller-driving powerplants [VMG] employing air.

---

[1] Materials from Yu. S. Voronkov, T. M. Mel'kumov, Yu. V. Biryukov, and I. A. Merkulov, published in collection [3], were used in the preparation of this section.

Aircraft engine-building theory and practice have now entered a region where we can examine the use of VRD, especially hydrogen VS [boost stages], in aerospace planes [VKS] and aerospace transport systems [TAKSi] at flight Mach numbers M_f = 10-12 [4, 5]. Present development of space-rocket technology is taking the road of designing cheaper recoverable spacecraft [KAMP], in the first generation traditionally employing ZhRD, in the second, VRD (TRD [turbojet engines], PVRD [ramjet engines], and GPVRD [hypersonic ramjet engines]).

Aerospace planes with hydrogen VRD as part of their SU [powerplants] may be single-stage with an air launch and airfield landing after returning from space flight; TAKSi may accelerate a rocket to velocities V = 3000-3600 m/sec and return "to base."

Use of aircraft designs with VRD in space-rocket technology is, at the current stage, dictated considerably by the need conduct space research for assorted economic tasks. In this connection it is becoming important to carry out space flights that provide proper aircraft "comfort" for the crews and expand the range of "launch points." It is for this reason that work is under way to create winged booster rockets and aerospace planes, i.e., self-launched and -landing aircraft. These operations are, in principle, a continuation of the ideas of Tsander, who first pointed out the substantial energy and operational advantages of using an aircraft over a rocket launch, suggested and thoroughly substantiated by K. E. Tsiolkovskiy. It is even more significant /83 that Tsander proposed using aerodynamic braking of an air-transport craft when it returns from space flight (without starting the rocket engine). Tsiolkovskiy and Kondratyuk later referred to this idea many times [3, p. 28].

Hydrogen-powered VRD (or combined RD [jet engines] with hydrocarbon and boron hydride fuel for VKS) using ZhRD in the last stages are a new advance in the development of aerospace technology [5].

Without making an absolute out of experimentally obtained knowledge, we should note that it plays a definitive role in technology, especially aerospace technology, so practical creation of VKS and TAKSi will be possible only after prolonged and difficult basic and experimental research on test-beds and in flight, particularly on model VRD and VKS. Questions of providing the aerospace industry with scientific and practical projects are being given paramount importance throughout the world. Among the most important problems in engine design is that of setting up highly efficient fuel combustion in engines, with minimal longitudinal dimensions and provision of heat-resistance; also important is the porblem of cooling the airframe structure with fuel (hydrogen) during flights at high supersonic and hypersonic velocities (M_f = 3-12) within the atmosphere.

The problem of organizing the process in hydrogen PVRD combustors and providing their high economy is examined below.

2. Hydrogen Ramjet Engines for Boosting VKS and TAKSi

a) Peculiarities of VRD for VKS

Calculations for evaluating the economy of different types of engines relative to flight speed, taken from [5], reveal that VRD are much more economical than ZhRD (Fig. 1a). For example, use of a combination of a kerosene-powered TRD with a hydrogen PVRD, shifting to GPVRD mode at $M_f \simeq 6$, allows obtaining a ZhRD specific pulse 10-4 times higher than that of a ZhRD in the M = 0-12 range, respectively. Use of only high boiling-point components (of the kerosene or boron hydride type) as fuel for VRD also substantially increases the economy of the engine over a ZhRD, but it should be remembered that at $M_f > 4$ these fuels, /85 because of their low cold-margin, are incapable of ensuring operation of VKS engine structures and components to high M_f. Up to $M_f \sim 5$, however, use of such fuels is possible, and abroad they are viewed, with sufficient foundation, as the probable fuels for winged aircraft having various purposes. This is all the more attractive a proposition in that such use eliminates the problem of storing winged aircraft and SU in the fueled condition.

/84

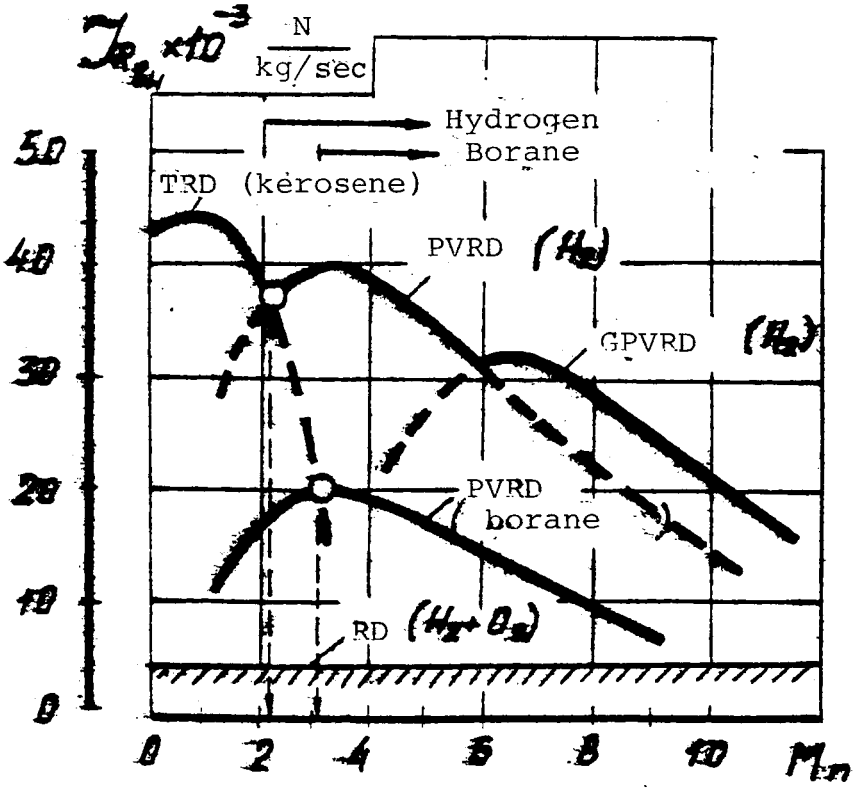

Fig. 1a.

Aerospace planes are large in volume and area, in terms of /85
their good aerodynamics, especially for high-altitude flights. They can be refueled with liquid hydrogen immediately before launch and there is no need to keep VKS in long-term storage in the fueled condition. Hydrogen is not the only fuel capable of assuring powerplant and airframe component cooling in hypersonic flight inside the atmosphere.

Combined and ramjet VRD for VKS and TAKSi may be extremely large and integrated with the aircraft's surfaces for their maximum use to compress air ahead of the intake and expand the gas behind the engine nozzle (see Fig. 1b).

To provide possibilities of experimental development on test-beds, the powerplant may consist of identical linear models, one of which (or a reduced-size, geometrically similar model) can undergo test-bed development or be studied on a flying laboratory (as is proposed for conducting research on two-dimensional GPVRD models in the U.S.A. on aircraft of the X-15 and X-24 type, see [5]).

The modular construction of VRD is very convenient for test-bed research, and as experience has shown, it allows obtaining reliable scientific data at low cost.

Discovery of the main criteria determining the efficiency of the process in VRD is at the top of the agenda for scientific experimentation; it is vital that modeling criteria be properly chosen and that experience in model research be employed in designing full-scale VRD. It is more important to discover the modeling principles for VRD than for other types of engines, since their thrust characteristics depend on a large number of factors [9], especially flight conditions (P_H, T_H, M_f), air-intake characteristics (ϕ, $\sigma^*_{\text{g max}}$), type of fuel (H_u, L_0), /87
relationships between air and fuel consumption ($\alpha = \sigma_B/\sigma_T L_0$ or $\beta = 1/\alpha$), relative flow-duct areas (see Fig. 2) (F_c/F_H, F_m/F_H, F_{cr}/F_H, F_{cr}/F_c, etc.), fuel combustion efficiency in the combustor, $\eta_{\Gamma ef}$, which is the main characteristic of the operating process.

The relative combustion efficiency in the engine ($\eta_{\Gamma ef}$) is determined by the thrust, measured in test-bed tests, and considers, in addition to chemical underburning, losses associated with irregular parameters at the nozzle exit and heat losses in the combustor, and it generally depends on almost all the aforementioned factors, especially α and combustor construction (number of nozzles in the fuel-nozzle unit, uniformity of their distribution by chamber section, chamber length, area, etc.). This specific feature is usually not accounted for in general VRD theory. Existing methods of calculating VRD parameters and thrust characteristics are either based on the presumption of

Lifting surface --
compression plane
Modular VRD
Gas expansion
plane

Fig. 1b.

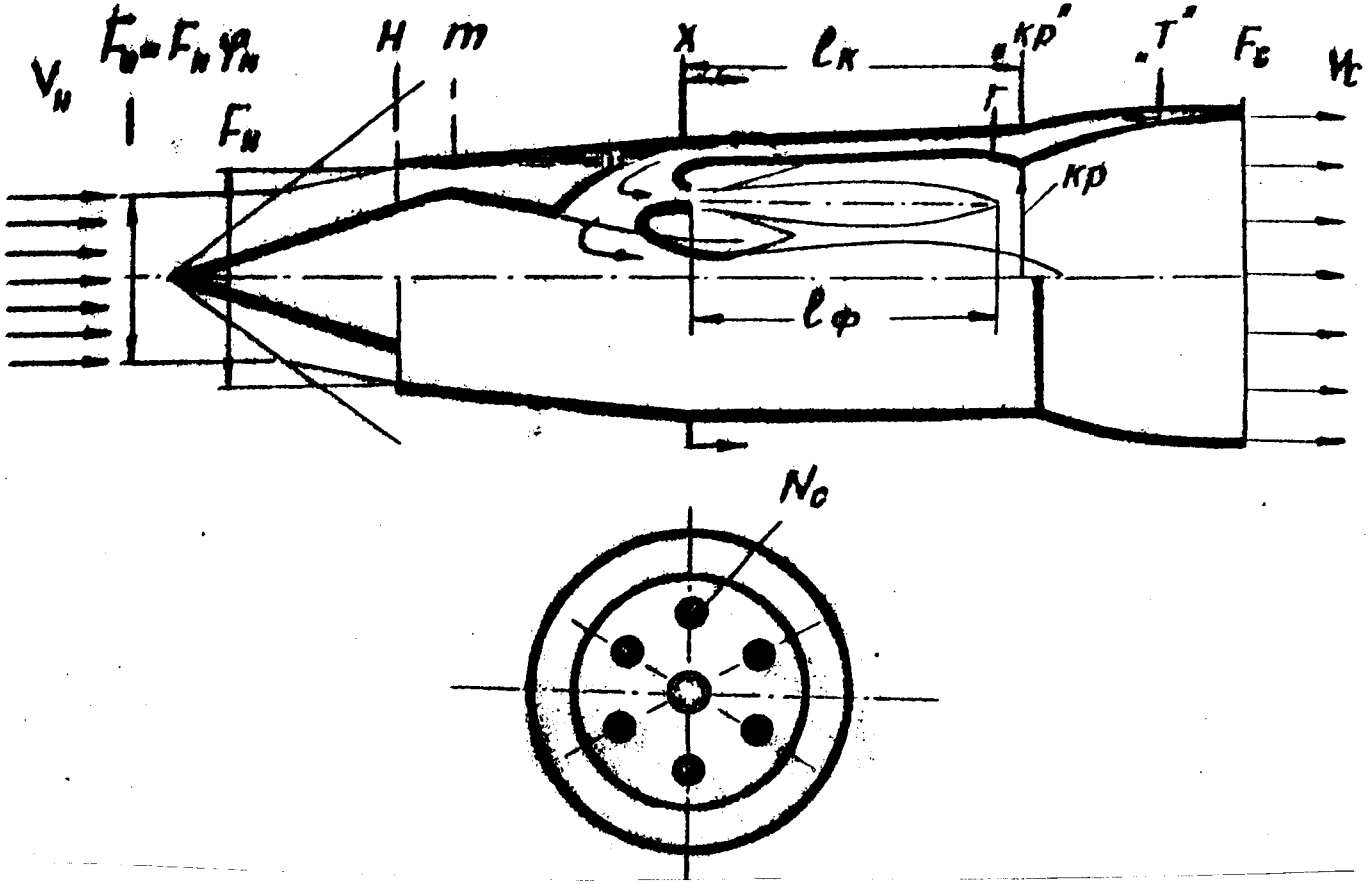

Fig. 2.

an ideal process in PVRD combustors ($\eta_{Tef} = 1$), and provide for /87
determining maximum possible thrust characteristics, or with parametric variation of η_{Tef} make it possible to discover the effect of η_{Tef} on VRD thrust characteristics (see [6], [7], [8], for instance). The question of the real thrust characteristics of VRD can be answered by direct engine tests on test-beds to determine engine characteristics. Calculation of the actual combustion rules can have a substantial effect on the choice of engine type, parameters, and characteristics. In comprehensive analysis, calculation of the actual values of η_T for an aircraft may provide results differing substantially from those of calculation analysis performed with η_{Tef} = const. In particular, calculation of actual values may have a substantial effect on choice of operating modes (β) along the flight trajectory, choice of engine length, and thus choice of engine mass and amounts of combustor cooled surface, which is of fundamental importance with a limited cooling margin. When choosing operating modes (β) it is also necessary to consider the possibility of providing (in these modes) cooling of powerplant and airframe components with hydrogen.

The thrust of a PVRD depends on many factors, in particular:

$$R_{out} = f(M_f, \beta, \eta_{Tef}, \varphi_{H\,max}, M_c, H, F_H, F_c, H_H, L_0).$$

The specific parameters are also functions of many factors, /89
especially for one fuel with a constant (invariable) flow duct:

$$J_{R_{GH}} = \frac{R_{GH}}{G_T} = f(M_f, \beta, \eta_{Tef}, M_c, \frac{F_c}{F_H})^*$$

$$C_{R_{GH}} = \frac{R}{q_H F_H} = f(M_f, \beta, \eta_{Tef}, M_c, \frac{F_c}{F_H}, \varphi_H).$$

Aircraft excess coefficients of fuel impulse and thrust depend on the aircraft's coefficient of external drag and are determined by relations

$$C_{R_u} = C_{R_{GH}} - C_{x\,ext}^{*H}$$

$$J_{R_u} = J_{R_{GH}}\left(1 - \frac{C_{x\,ext}^{*H}}{C_{R_{GH}}}\right) = f(M_f, \beta, \eta_{Tef}, \frac{F_{mid}}{F_H}, \text{form}),$$

Calculation of the actual values of η_{Tef} allows choosing the correct cruise ($J_{Ru} = 0$) and boost ($J_{Ru} > 0$) modes.

b) The Process in the PVRD and GPVRD Combustor

Under conditions providing aerodynamic stabilization of a hydrogen flame or its self-ignition (at high T_H^*, corresponding to high flight M, and at adequate pressures in the combustor before fuel delivery), kinetic factors, especially a gas time-

of-stay in a combustor over 100 mm long, may not have a substantial effect on process efficiency. Even at gas velocities in the chamber $W \simeq 1500$ m/sec with $l_K \geq 100$ mm the ratio of the gas time-of-stay to the chemical reaction time (at local $\alpha = 1$ and $T = T = 2500\text{-}2700$) is much larger than unity and equals

$$\bar{\tau} = \int_0^{l_K} \frac{dx}{w} \cdot \frac{1}{\tau_r} = 15 \div 20$$

and the combustion efficiency is often substantially lower than 1.0. We might assume that the combustion efficiency would be determined by fuel-air mixing.

The efficiency of hydrogen's combustion with its diffusion mixing with air when delivered in sprays is determined basically by turbulent mixing processes that do not depend on the absolute values of the parameters in the chamber (P_K, W_K) or the chamber's absolute length, but are determined by the ratio of the chamber's length l_K to the length of the diffusion flame in the duct l_ϕ, which (as in RPD [rocket-ramjet engines] [9]) is proportional to some complex -- the reduced relative length of the duct/90 $\bar{X}_{pr}$:

$$\eta = \frac{l_K}{l_\phi} \sim \bar{x}_{pr}.$$

Analysis of the change in $\bar{X}_{pr}$ from various relative parameters using turbulent-jet theory and also employing experimental regularities in flame-tongue change (in the accompanying flow of air and in unlimited space), obtained by Ferri-Zacchei [10] and corroborated by the author's experiments, revealed that for compressorless hydrogen VRD (PVRD, DGPVRD [dual-mode hypersonic ramjet engines], GPVRD) the reduced combustor length $\bar{X}_{pr}$ does not depend on the relative total outlet area of the fuel nozzles (F_{TC}/F_K) and does not depend on the relative temperature of the gaseous hydrogen fed into the chamber for combustion ($\theta_T = T_T/T_B$). When providing equal "access" of air to each of N_C nozzles in the fuel unit, if there is accompanying air ($\gamma = 0$) or if it is fed into the chamber at an angle or perpendicular to the engine's axis, the value of $\bar{X}_{pr}$ is determined basically by the relation of the components (α or β) and by the main geometric factor -- the equivalent length of the combustor:

$$\bar{X} = \frac{l_K}{D_{K\,eq}} \sqrt{N_C},$$

where $D_{Keq} = \sqrt{4F_K/\pi}$ is the equivalent diameter of a combustor of arbitrary cross-section.

The parameter that can be used to generalize the efficiency of the process in experiments with hydrogen PVRD and GPVRD with assorted designs is parameter $\bar{X}_{pr}$. The mathematical expression for the reduced length of the duct can be written as:

$$\bar{x}_{pr} = X \cdot F(\alpha). \qquad (I)$$

where function $F(\alpha)$ is determined by the engine's operating conditions, bound into 3 groups in accordance with change in the flame plume length:

$$\text{I. } \alpha < 1 \qquad F(\alpha) = \frac{\alpha^{-1}}{\tilde{\alpha}_\phi}\sqrt{\alpha}\ ; \qquad \text{2. } 1 < \alpha < 2.5 = \tilde{\alpha}_\phi \qquad F(\alpha) = \frac{\alpha}{\tilde{\alpha}_\phi}\sqrt{\alpha}\ ; \qquad \text{3. } \alpha > 2.5 = \alpha_\phi \qquad F(\alpha) = \sqrt{\alpha}\ .$$

The independence (for a hydrogen VRD) of the value of $\bar{X}pr$ from the total area of the fuel nozzles (at F_K = const.) from air temperature (determined by the flight M) and fuel temperature (determined by its heating in the structural-component convective cooling systems) is an extremely important circumstance permitting an arbitrary choice of nozzle area F_{T_C} with variation of N_C and experimental freedom from the requirement to provide simulation of T_B^* and T_T^*.

To obtain relation $\eta_{Tef} = f(\bar{X}pr)$ and check the theoretical conclusions, a number of studies were performed using two-dimensional models (at $\gamma = 0$) and with axially symmetric models. The studies were performed with external flow around the models of a hypersonic flow at T_H^* = 600-1500K and with an attached air duct at T_B^* = 1000-1200K. /91

Also employed in the analysis were foreign data from [4] and [5] (NASA and ONERA) at $\gamma = 90°$, obtained for axially symmetric PVRD with supersonic velocity in the chamber and mixed combustion ($M_K \lesssim 1$).

Experimental analysis revealed the correctness of using $\bar{X}pr$ as the modeling criterion. The obtained approximated (with 10% precision) relation $\eta_{Tef} = f(Xpr)$, shown in Fig. 3, is general and allows making a preliminary choice of combustor construction (N_C, l_K, F_K), and also performing calculations of engine thrust and VKS boost characteristics considering the actual efficiency of engine operation.

An approximation can be proposed for computer calculations: $\eta_{Tef} = 0.6 \log \bar{X}pr$.

A number of studies (including those of NASA and ONERA) imply that increasing $\bar{X}$ above 25-30 with limitations l_K/D_{eq} = 2-3 is very complicated because of the difficulty of cooling the combustor and nozzle, so the value $\bar{X}$ = 30 should be taken as a rough one when designing hydrogen PVRD (with subsonic, transsonic, and supersonic velocities in the combustors).

c) Thrust Characteristics of VRD and Assessing VKS and TAKSi Boost Characteristics

At $\bar{X}$ = 30 in PVRD and GPVRD there is combustion efficiency η_{Tef} = 0.95-0.65, depending on β (at β = 0.4-4), and regardless

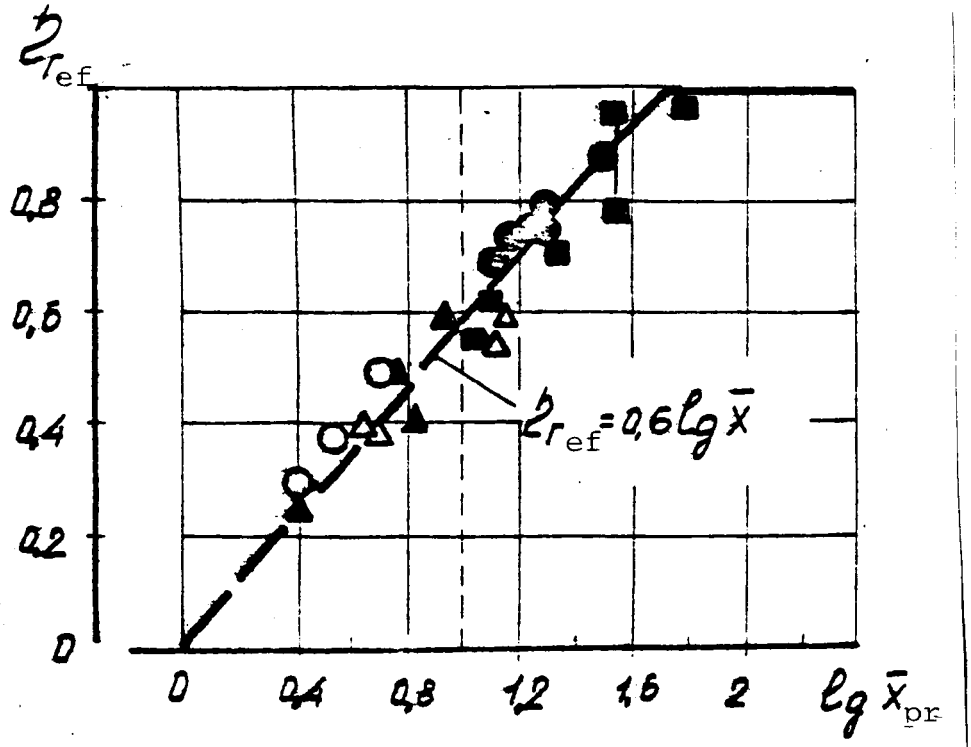

Linear plane modulus $B_H \times h_{II}$

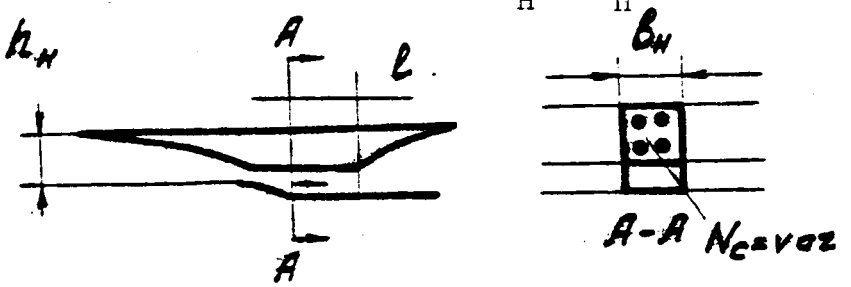

Fig. 3.

of $\bar{X}$ at $\beta = 1$ there is a combustion efficiency "gap" of fundamental importance for choosing engine operating modes (see below). /93
Figure 4 shows a comparison of calculated change in $\eta\Gamma_{ef}$ from β with the experimental data of ONERA [4], obtained in the $M_f = 5\text{-}7$ range. The calculated relation apparently agrees with the experimental data. This calculated relation is later taken for analysis of PVRD thrust characteristics (Fig. 4b, d) and aircraft excess /94
thrust parameters (Fig. 4b) (with $F_{mid}/F_H = 3$).

When the aircraft is accelerated, to improve VRD efficiency with increasing speed (M_f) it is expedient to provide engine afterburning (increase β); because of the combustion efficiency $\eta\Gamma_{ef}$ "gap" at $\beta = 1$ and $M_f \simeq 6$ it is expedient to shift "abruptly" to rich fuel-air mixture modes ($\beta > 1$). This peculiarity is apparently a general property of an actual engine, since it has already been noted when analyzing the acceleration of craft with an RPD. To provide for cruise flight ($J_{Ru} = 0$) of a hypersonic aircraft at $M_f = 6$, after acceleration along line β_{opt} at $J_{Ru_{max}}$ it is again necessary to throttle back "abruptly" from $\beta_{opt} \simeq 1.25$ to $\beta \simeq 0.45$ (see Fig. 4b).

We shall examine the approximate possibility of accelerating a VKS with a PVRD.

The PVRD fuel specific impulse and the fuel excess specific impulse J_{Ru} in the aircraft system depends very highly on the flight M (Fig. 5). In the M_f range from 2-3 to 10-12 in a hydrogen PVRD at $\beta = 1 = \text{const.}$ with $\beta = \beta_{opt}$ and J_{Ru}^{max}, the following relation can be employed:

$$\frac{J_{Ru}}{J_{Ru}^{init}} \approx \left(\frac{M_f^{init}}{M_f}\right)^{\xi}, \qquad (2)$$

where $\xi \simeq 2$ and J_{Ru}^{max} corresponds to the initial acceleration speed, which can be varied ($M_{init.} = 2\text{-}3$).

Generally, with $\beta = \text{var.}$ the value of ξ can be dependent on M_f; then in segments ΔM in the required range of the M interval we can make a numerical approximation $\xi = f(M_f)$, assuming the end of the preceding segment as the beginning of the next. Without introducing a large error, we can assume $\xi = 2 = \text{const.}$ in the $M_f < 12$ range. This method allows substantially simplifying the estimate of the aircraft's acceleration characteristics in computations, as compared to $\xi = \text{var.}$

From the general equation of aircraft motion, written as

$$m\frac{dV}{dt} = R_u\left[1 - \frac{m}{R_u}\sin v\right],$$

we can see that for rocket boost (when with a vertical launch $\sin v \simeq 1$, $m/Ru \ll 1$) and for aircraft boost (when $m/Ru \leq 1$, $\sin v \simeq 0$), for qualitative comparison under the same conditions

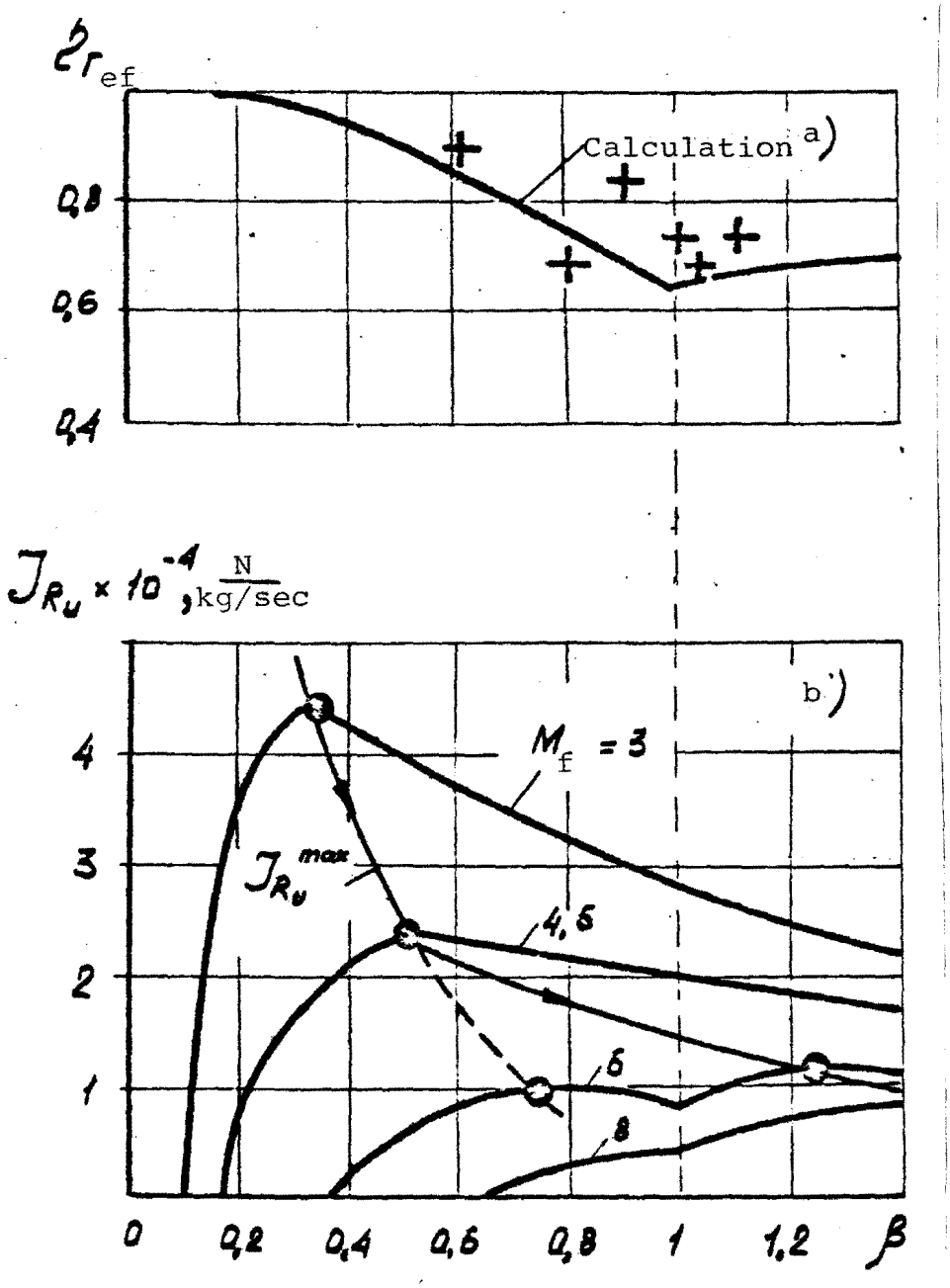
$2r_{ef}$
Calculation
a)
0,8
0,6
0,4
$J_{R_u} \times 10^{-4}$, $\frac{N}{kg/sec}$
b)
$M_f = 3$
$J_{R_u}^{max}$
4,6
6
8
4
3
2
1
0
0,2
0,4
0,6
0,8
1
1,2
β

Fig. 4a.

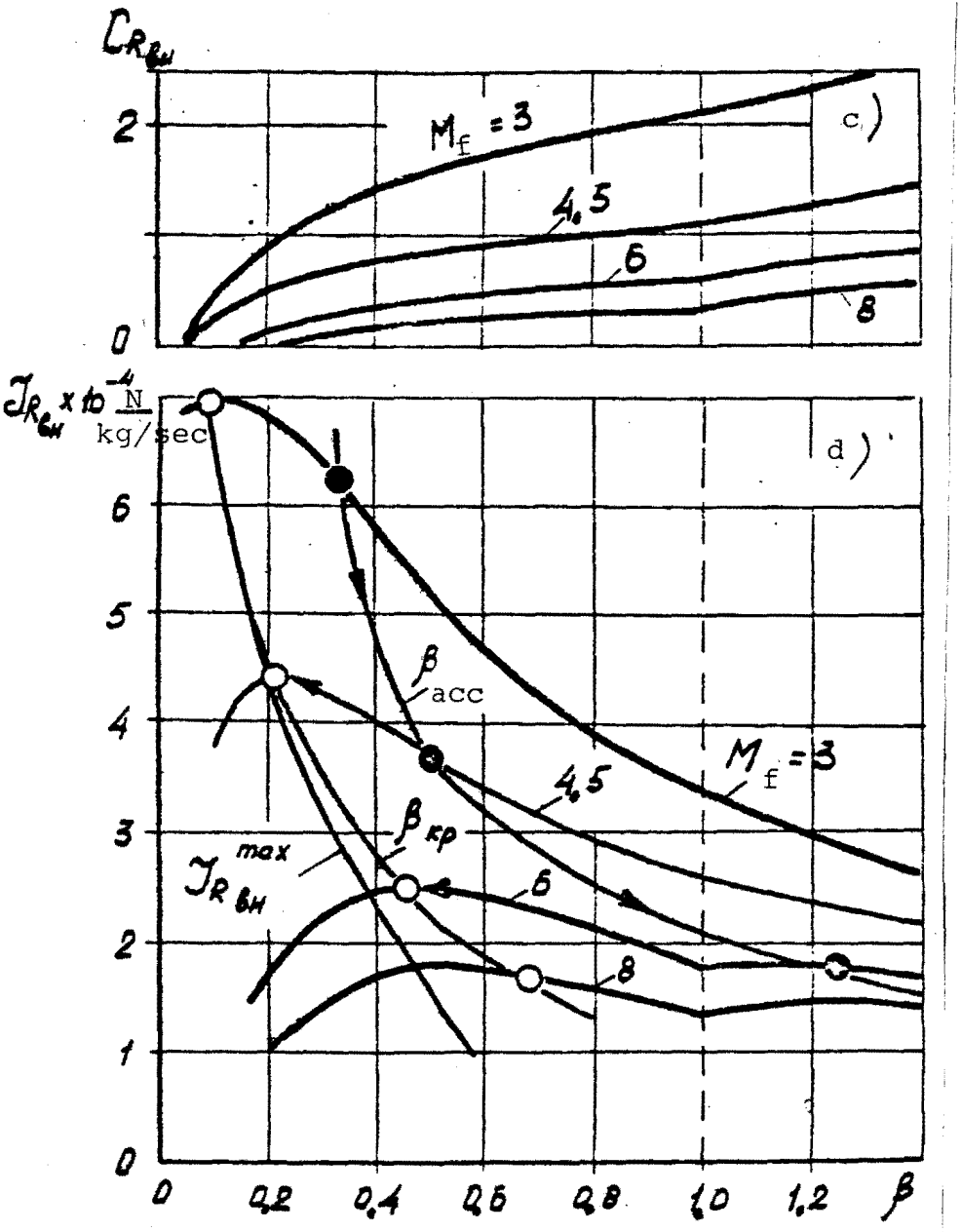
$C_{R_{BH}}$
2
0
$M_f = 3$
c)
4,5
6
8
$J_{R_{BH}} \times 10^{-4}$ N kg/sec
d)
6
5
4
3
2
1
0
β_{acc}
$M_f = 3$
4,5
β_{kp}
$J_{R_{BH}}^{max}$
6
8
0
0,2
0,4
0,6
0,8
1,0
1,2
β

Fig. 4b.

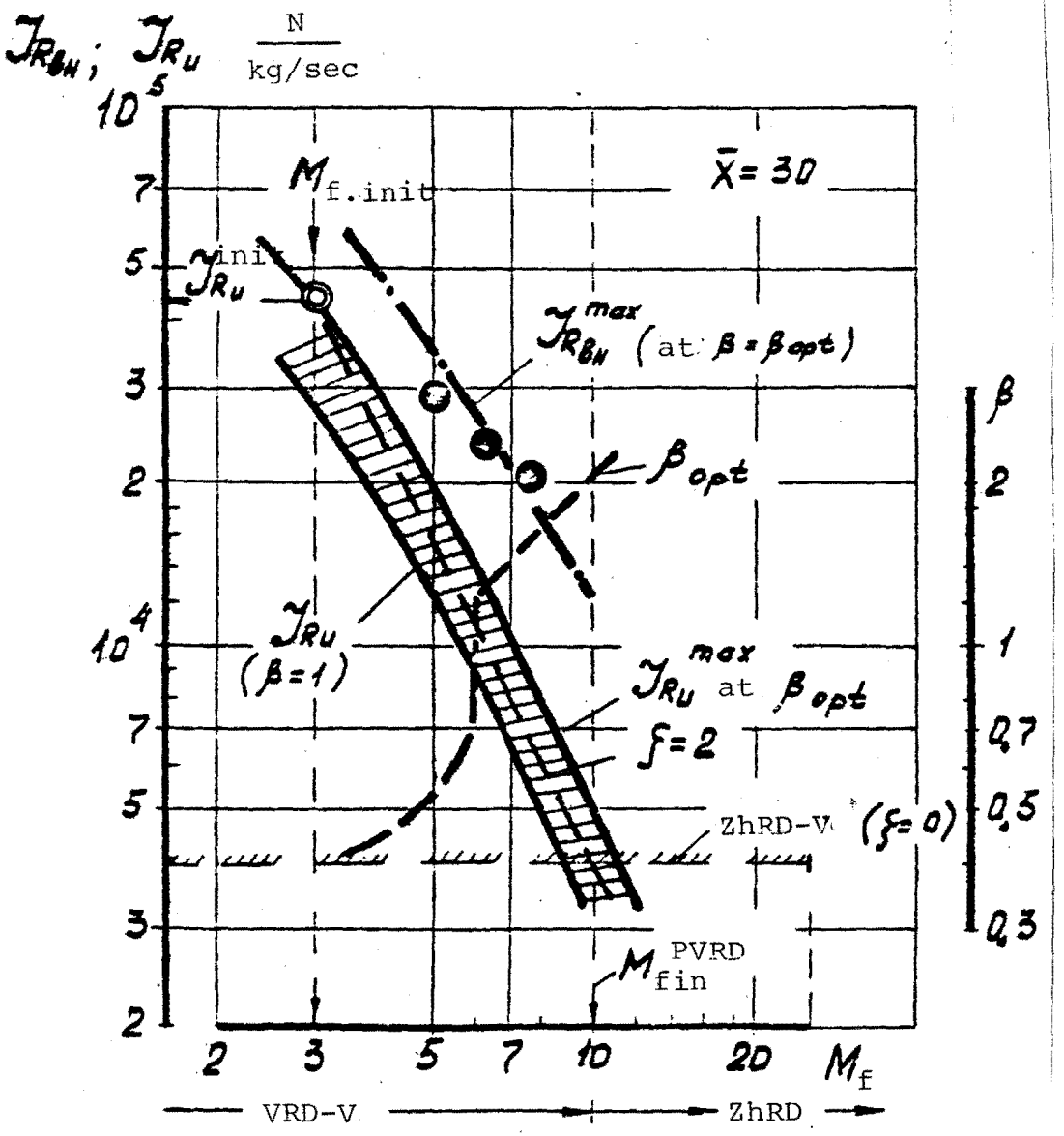
$J_{R_{BH}}$; J_{R_U} N/kg/sec
10^5
7
5
3
2
10^4
7
5
3
2
$M_{f.init}$
$\bar{X}$= 30
$J_{R_U}^{init}$
$J_{R_{BH}}^{max}$ (at $\beta = \beta_{opt}$)
β_{opt}
J_{R_U} (β=1)
$J_{R_U}^{max}$ at β_{opt}
f=2
ZhRD-V (f=0)
M_{fin}^{PVRD}
2 3 5 7 10 20 M_f
VRD-V
ZhRD
β
2
1
0.7
0.5
0.3

Fig. 5.

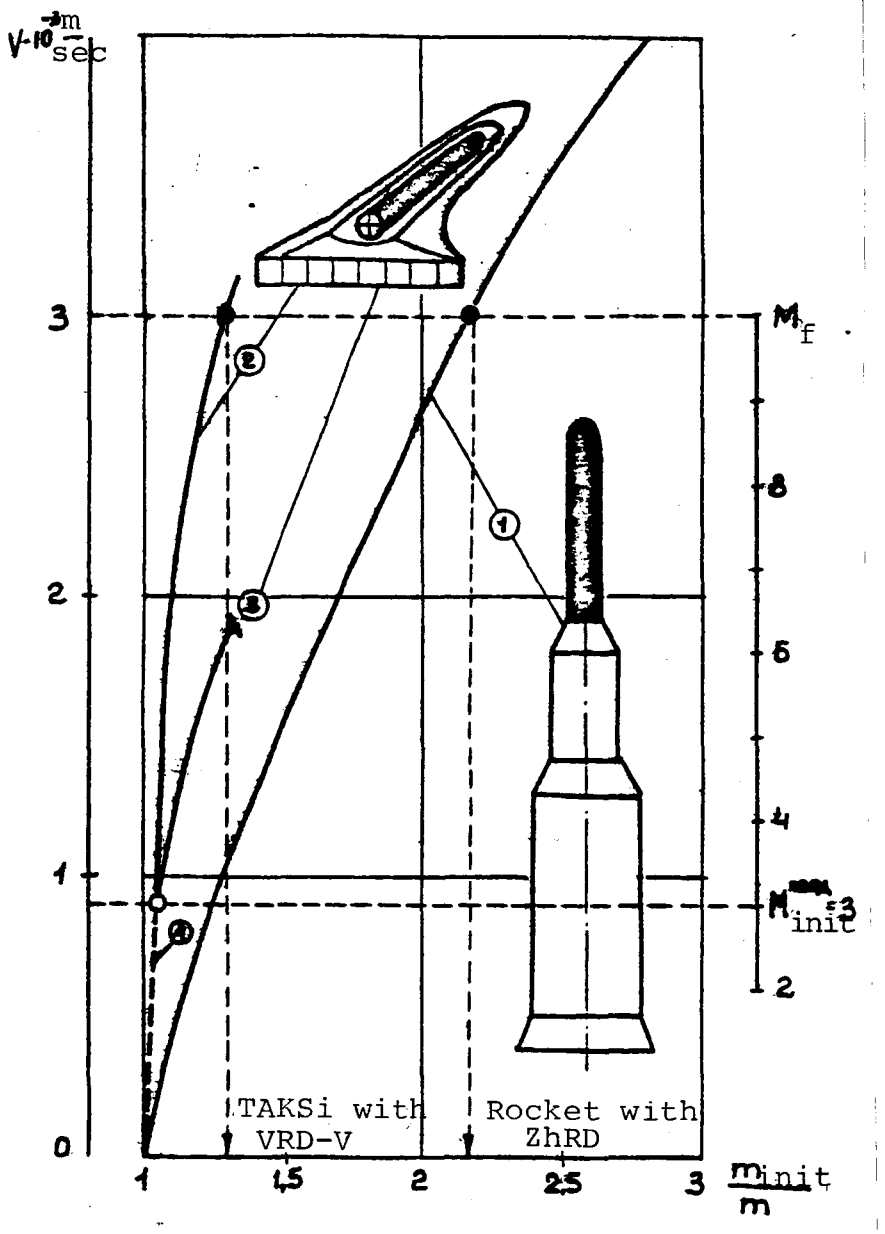
V·10⁻³ m/sec
3
2
1
0
1
1,5
2
2,5
3
m init / m
M f
8
6
4
M init
2
TAKSi with VRD-V
Rocket with ZhRD
1
2
3
4

Fig. 6.

the gravitational forces can be ignored. In this case, with conditions (2) for a craft with a VRD, considering that $R_u = G_T J_{Ru}$, it is easy to obtain a relation characterizing the craft's accleration when burning on-board fuel. /94 /98

After integrating the equation of motion from its initial parameters to the current ones, we obtain:

$$v = v_{init}\left[(1+\xi)\frac{J_{init}}{v_{init}}\ln\frac{m_{init}}{m}+1\right]^{\frac{1}{1+\xi}}. \qquad (3)$$

Relation (3) is general (for VRD and ZhRD) for the craft's boost segment where ξ = const. In particular, for acceleration with a ZhRD (or an RDTT), where $\xi = 0$ (J_{Ru} = const.), relation (3) is converted into the familiar equation of K. E. Tsiolkovskiy:

$$v = v_{init} + J_{Ru}\ln\frac{m_{init}}{m}.$$

Equation (3), like Tsiolkovskiy's, is convenient in that, without construction analysis and without fairly complicated trajectory calculations, it allows estimating the main parameters, in particular the required fuel reserve for accelerating a craft with a VRD. It is also convenient for comparative analysis of aerospace planes with ZhRD and VRD (PVRD).

A comparative evaluation of the acceleration characteristics of aircraft with ZhRD and VRD was performed in accordance with the characteristics of PVRD (Fig. 6). The comparison revealed that with acceleration to M_f = 10 with a ZhRD at J_{Ru} = 4000 N/kg-sec (J_{Ru} = 400 sec) the relative final mass of an aircraft m/m_{init} should be approximately 47%, and with acceleration of an aircraft with a TRD and hydrogen PVRD in the same velocity range, the final mass of the craft may be 78% of initial (22% of the initial mass of the craft should be fuel used for acceleration: 5% kerosene for the TRD and 17% hydrogen for the PVRD).

Thus, we can state that the theoretical advantages of hydrogen PVRD for boosting craft (of the VKS and TAKSi type) to M = 10-12 are indisputable.

REFERENCES

1. Tsander, F. A., "A description of the interplanetary spacecraft of F. A. Tsander's system," in Pionery raketnoy tekhniki [Pioneers of Rocket Technology], Moscow, 1964, pp. 271-276.

2. Shchuneyko, I. I., Krylatyye kosmicheskiye korabli [Winged Spacecraft], Moscow, 1966.

3. F. A. Tsander i sovremennaya kosmonavtika [F. A. Tsander and Modern Cosmonautics] (Collection of Articles), Moscow, 1976.

4. Contensou, P., R. Marquet, C. Huet, "Theoretical and experimental study of a mixed-combustion ramjet (Mach 3/7 flight range)," ICAS Paper No. 24, 1972.

5. Waltrup, P. I., B. Y. Anderson, F. D. Stull, "Supersonic combustion ramjet (scramjet) engine development in the United States," Paper No. 76-042, 3d Symposium on Jet Engines.

6. Shlyakhtenko, S. M., (ed.), Teoriya vozdushno-reaktivnykh dvigateley [Theory of Jet Engines], Moscow, 1975.

7. Kurziner, R. I., Reaktivnyye dvigateli dlya bol'shikh sverkhzvukovykh skorostey poleta [Jet Engines for High Supersonic Flight Speeds], Mosocw, 1977.

8. Zuyev, V. S., and V. S. Makaron, Teoriya pryamotochnykh i raketno-pryamotochnykh dvigateley [Theory of Ramjet and Rocket Ramjet Engines], Moscow, 1971.

9. Annushkin, Yu. M., L. N. Druzhinin, V. A. Sosunov, "Towards a theory of an optimal rocket ramjet engine with fuel afterburning in a wind chamber," Trudy I Chteniy F. A. Tsandera. Sektsiya "Teoriya i konstruktsiya dvigateley" [Proceedings of the 1st F. A. Tsander Lectures: "Engine Theory and Construction" Section], Moscow-Riga, 1972.

10. Ferri, A., Journal of the Royal Aeronautical Society 68/645, 575-597 (1964).

NUMERICAL CALCULATION OF THE SEPARATION AND JOINING OF TWO-DIMENSIONAL SUPERSONIC FLOWS IN DUCTS WITH DISCONTINUOUS BOUNDARIES

A. T. Berlyand and A. F. Chevagin

The question of numerical calculation of a flow within a jet engine has been taken up in works dealing with development of such engines (GPVRD [hypersonic ramjet engines], in particular). Lectures devoted to elaborating the legacy and developing the ideas of F. A. Tsander have in past years reported on a series of works [1-3] dealing with study of the possibility of using for such calculations the previously suggested numerical method using automatic division of separations [4]. However, both the programs implementing this numerical method and other programs used for these purposes (see [5, 6, 7], for example) were generally intended for calculating the flow in a simple single duct. When developing GPVRD it often becomes necessary to examine a duct with different kinds of partitions, slots, branches, etc. Use of ordinary programs (of the type described in [6]) to calculate such flows makes every such calculation a unique and very laborious operation and does not allow carrying out parametric calculations in an acceptable period of time. In connection with the requirements for such calculations, it became necessary to create a multipurpose program implementing one of the familiar methods of calculating supersonic flows for regions with complex separation boundaries. /100

This article deals with describing such a program implementing the numerical method in [4] and demonstrating its fitness using a number of examples. The choice of the calculation outline from [4] came about because it is specially oriented towards producing the most accurate solution near the solution features and, by omitting an outline of through calculation of the first order, it is devoid of a number of shortcomings present in ordinary through-calculation grid outlines [5]. An outline of the type in [4] can be used to construct generalized solutions of plane hyperbolic problems of gas dynamics in arbitrary regions for a fairly broad class of boundary conditions: solid boundaries, free surfaces, arbitrary incident flow, etc. [6]. The difficulties of using programs of the type in [5, 6] for calculating flows in separation boundaries is associated with the fact that we then lose the basic advantages of the through-calculation outline, the region under examination must be artificially divided into subregions, and the corresponding "joining" of solutions has to be performed, and this does not allow natural automation (an example of this kind of calculation is given in [6]). It should be noted that for /101

sustained outlines of the type in [4] the automatic joining and division of flows should not encounter great technical (algorithmic) difficulties. When such outlines are employed, at each moment in time the program processes parameters of only one current section of the flow.

Complete automation of sustained calculation of an arbitrary multiply connected region makes a very complex problem, generally leading to problems close in structure to those of image recognition theory. This apparently is because authors of the corresponding programs usually restrict themselves to calculating merely 1-connected regions and leave it to the user himself to analyze the flow in a complex region by employing the suggested program at some stages of this analysis (the exception is in periodic problems like the flow around grids of identical profiles, which reduce to analyzing the flow within one period). With this approach the user has to carry out both the part of the work actually difficult to formalize for computers, consisting of dividing the 1-connected subregions and of determining the sequence of their calculation, which is usually not particularly difficult for man, and the purely technical part of the work, consisting of sorting the results of calculating each isolated subregion for use as initial data to calculate other subregions. The second part of the work, on the other hand, does not present any difficulties for the computer and is extremely cumbersome for /102 man. This article offers a compromise approach to resolving this conflict. The user himself is assigned the division of a complex multiply connected region into a finite number of 1-connected subregions and determination of the order of calculating flow in these subregions. Figure 1 shows several examples of possible flow configurations which can be calculated using this program and means of breaking down the corresponding regions into subregions with the required numeration of their calculation sequences. Here the boundaries of all the subregions consist of solid walls and free surfaces.

Information about the breakdown results is entered in the TABL secondary file, elements of which are entered into the computer at the very beginning of the calculations as part of the initial data. Using the TABL file parameters as an indicator, the program itself sorts the calculation results for each subregion, and in those cases where they have to be initial data for calculation of other subregions it enters them into secondary file AOB, where they are stored until it becomes necessary to use them.

For hyperbolic problems it is obvious that this breakdown is always possible, since for each subregion a mixed Cauchy problem is set up and there is strict demarcation and absence of reverse effects between the initial data at the left boundary of the subregion and the calculation results at its right boundary.

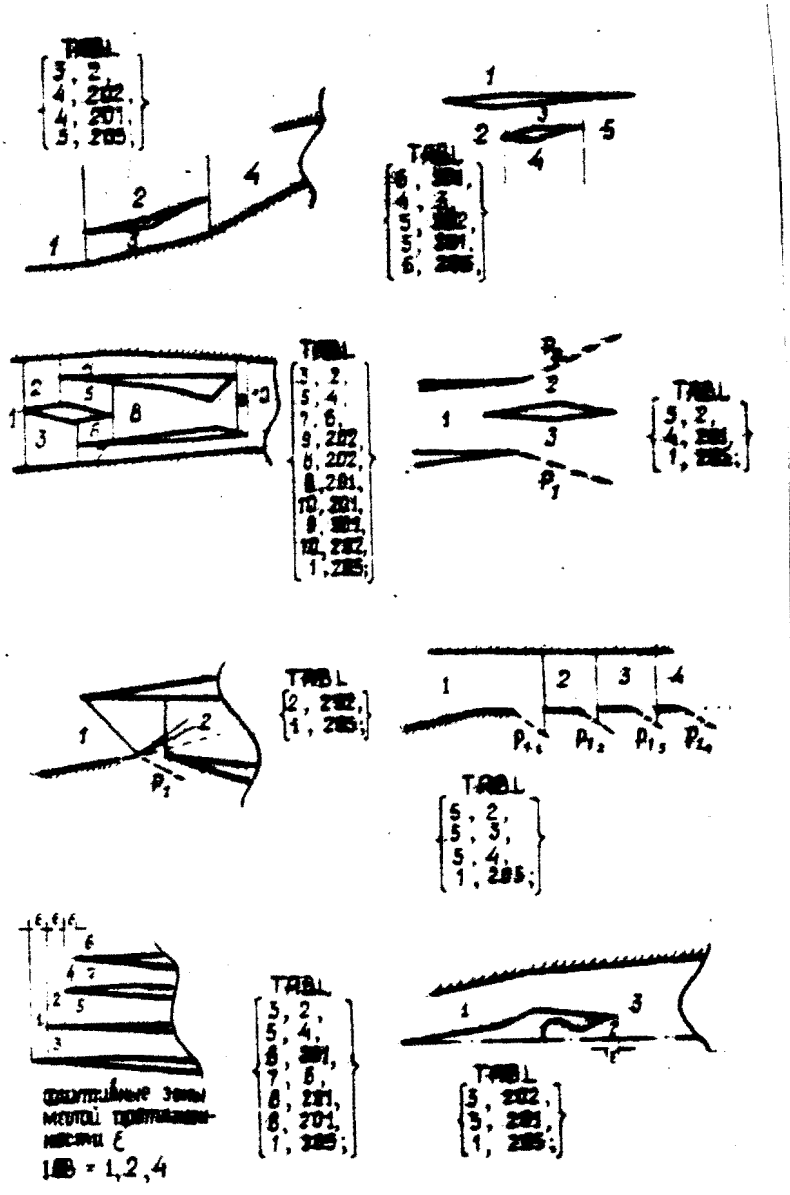

Fig. 1.

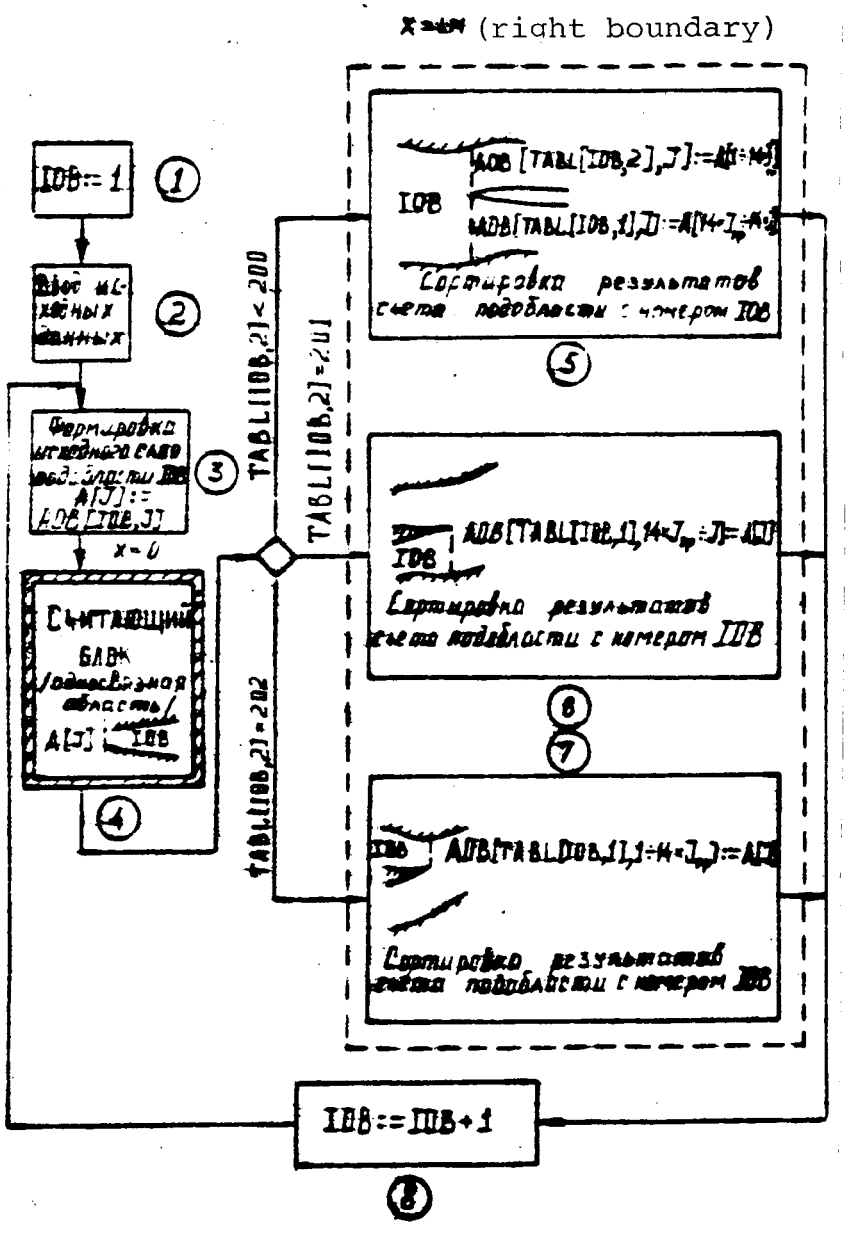

Fig. 2.

KEY: (2) Initial data input
(3) Generation of initial words of IOB subregion
(4) Counting assembly [1-connected region]
(5) Sorting of counting results of subregion with number IOB
(6) Sorting of counting results of subregion with number IOB
(7) Sorting of counting results of subregion with number IOB

A block diagram of the program is shown in Fig. 2. Its nucleus is the basic reference unit (block 4), which consists of a program for numerical calculation of the flow in a 1-connected subregion with a sequential number (program identifier IOB). In our case this block is practically equivalent to the program given in [6]. If necessary, it can easily be replaced by a subroutine implementing any other calculation outline. The main program is made in the form of a "binding" of block 4, and into its function go preparation of initial data for solving the problem in the subregion with number IOB, triggering block 4, sorting of calculation results for this subregion, and entering of them into file AOB for storage and use in solution of the problem in subregions with numbers higher than AOB.

Now a few words about the meaning and structure of the TABL and AOB files. Because of BESM-6 computer primary-storage limitations, the program is designed for solving problems in complex regions consisting of no more than 10 1-connected subregions. /105
Files TABL and AOB are two-dimensional with the scale of TABL (1:10, 1:2) and AOB (1:10, 1:2100). Generally speaking, the values of TABL (IOB, 1) and TABL (IOB, 2) designate the number of the subregions in which the calculation results at the right boundary of the subregion with number IOB would be used as initial data. If TABL (IOB, 2) > 200, the value of TABL (IOB, 2) is not the number of a real subregion and is used as as indicator whose meaning will become clear from the following. The fact that in file TABL the second index of its elements assumes only values 1 and 2 does not restrict the generality of the program and retains the possibility of calculating flow around grids consisting of several bodies, since we can always introduce an infinitely small (not equal to computer zero) difference in X -- the coordinates of the leading edge of each body forming the grid -- and thereby introduce into the examination the corresponding number of additional theoretical subregions of infinitely short length (Fig. 1g). When two flows have to be united in any subregion, the calculation results for each of them should be transfered into the initial data for only one subregion in the upper or lower part of the corresponding initial layer. If the entire field of parameters in the last section of the subregion with number IOB is included in the field of initial parameters, in its lower part for the following subregion, the number of this subregion is entered by the user into TABL (IOB, 1), and the number 201 is entered into TABL (IOB, 2); if it is included in its upper part, however, the number of this subregion is also entered into TABL (IOB, 1), but the number 202 is entered into TABL (IOB, 2). Thus, in accordance with the values of the elements of the TABL file, which by their meaning are only numbers of the corresponding subregions, during the calculation we can form elements of file AOB whose physical meaning is as profiles of gas-dynamic parameters at the entry to each of the isolated subregions.

When calculating subregions with number IOB the program operates in the following manner (see Fig. 2). Before operation of basic computation block 4, block 3 is used to form a field of initial parameters at the input to the subregion with number IOB, which is taken as AOB [IOB, j] (j = 1-2100). After this, computation block 4 operates, which calculates the isolated 1-connected subregion. When the right boundary of the subregion with number IOB is reached, the calculation of this subregion is /106 curtailed and the calculation results are sorted in accordance with the values of TABL [IOB, 1] and TABL [IOB, 2]. In blocks 5 and 7 the parameters obtained as a result of operation of block 4 are sent to the appropriate place in file AOB, after which the number of the next calculated subregion IOB is increased by one (block 8) and the program sets about calculating the next subregion.

With increase in the number of IOB and sequential calculation of the corresponding subregions, file AOB is gradually filled with the values of the initial parameters for calculating all the isolated subregions. On the other hand, as IOB increases, the values already entered into file AOB would gradually be used in calculating all the isolated subregions. This implies that the isolated subregions should be numbered by the program user so that all the subregions whose calculation results are needed for calculating subregions with number IOB would have a lower number than IOB. Then by the time that it is necessary to calculate the subregion with number IOB the corresponding elements of file AOB (IOB, j) would already be generated. Quite obviously, this kind of numeration is always possible.

Let's examine numerical solution of some model problems. Figure 3 shows the solution of a problem whose structure is close to that of interference of flows between two profiles, given in [6], whose solution was obtained using "manual joining" of the solution for different subregions. In the interference problem examined in [6] it proved possible to calculate only the flow pattern between the profiles, because of the extremely cumbersome "manual" preparation of data for further flow calculation. The problem solution shown in Fig. 3 produced a detailed picture of the flow pattern in the region behind one of the profiles, the complexity of which is produced just by the mere presence of flow interference in the preceding subregions, each of which separately has a relatively simple structure. Similar calculations were also performed for a number of complicated configurations of solid surfaces, and the obtained flow patterns have a similar character.

Another typical example of problems in which it is expedient to employ this program is calculation of flow in a duct with perforated boundaries and a given pressure behind the perforations. An example of calculating this kind of flow is shown in

/107

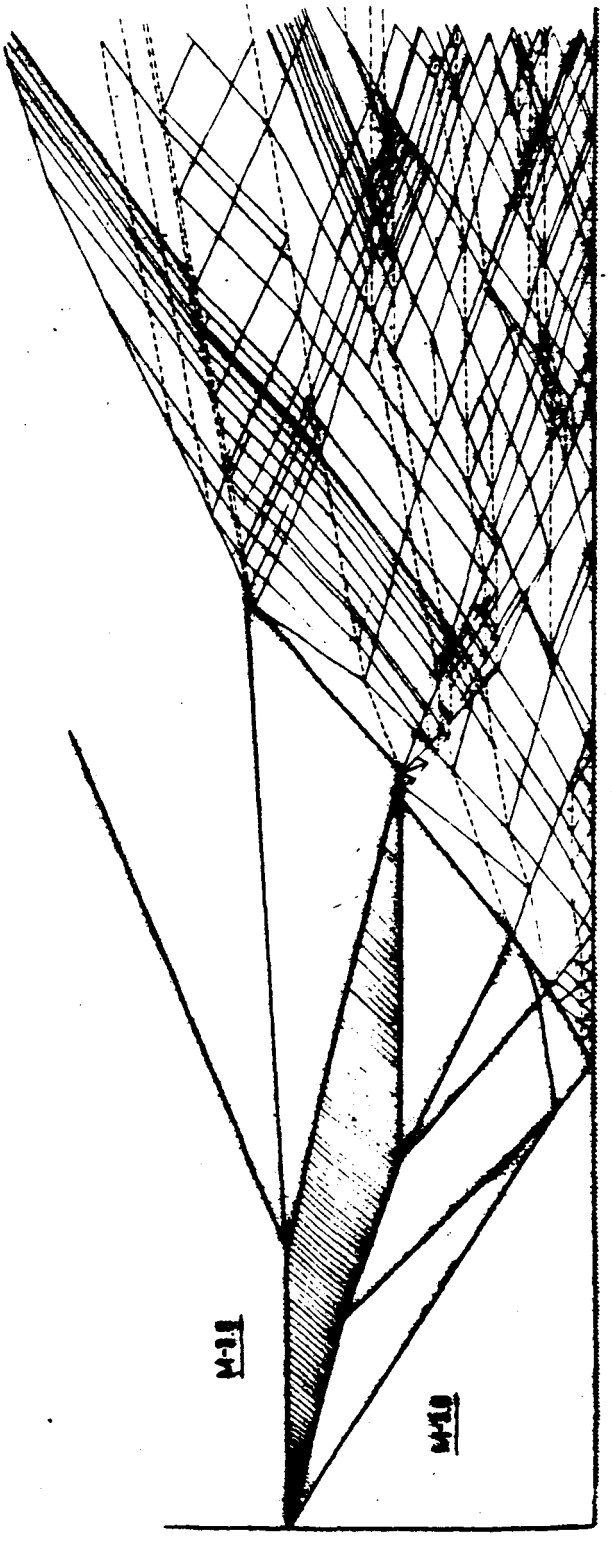

Fig. 3.

Fig. 4.

Fig. 4. The characteristic feature of these problems is the fact that the boundaries of some of the isolated subregions /109 partially are free surfaces. In distinction to the problems with free surfaces solved using the program in [6], in this case only a part of the surface is free and, as before, non-flow-through boundary conditions have to be set up for the remaining part. The program provided for special measures ensuring automatic transition at the necessary point from one boundary condition to another. Obviously, with this approach to calculation of flow in perforated boundaries the maximum number of perforation openings is limited to the maximum size of file TABL, since introduction of each new opening is associated with isolation of an additional subregion. It should be noted that problems concerning supersonic flow in perforated boundaries were quite successfully solved using the program given in [7]. There are, however, certain differences in the capabilities of these programs. So in some cases it is convenient to use the program in [7] and in others to use this one. If there is a need for accuracy of calculations, characteristic of technical problems, and for evenness of incident flow, the program in [7] allows, without exiting to a peripheral storage device, calculating a flow with a large number of perforation openings. Because the program in [7] does not provide for use of conditions at a free surface, however, in those cases where a disturbance from the flow enters a perforation opening and may, by being reflected from the free boundary, affect the flow pattern within the main duct, a correct solution cannot be obtained using the program in [7]. A particularly unfavorable circumstance here is the fact that normally we cannot know beforehand whether or not such a situation arises. Our program is free of this shortcoming (see Fig. 4). Moreover, it can be used to calculate flow both above a perforation and below it, if all the flow remains supersonic.

The convenience of employing this program for calculating two-dimensional double-flow air intakes of aircraft power plants is quite demonstrative. One possible design for such an air intake, widely used in the U.S.A. in designs for a hypersonic aircraft, is shown in Fig. 5. A power plant with the air intake shown in Fig. 5 provides acceptable characteristics in cruise flight at high supersonic and low hypersonic speeds (Mach 3-7) [8, 9].

Calculation of the flow in the lower duct, as in a normal air intake, can be performed both "manually", by relations for shock waves in an inviscid flow, and based on many known numerical methods, and it obviously presents no additional difficulties. But calculation of the upper duct, which operates in an essentially uneven flow field behind a series of shock waves from the compression wedge which interact with rarefaction of waves from the partition separating the ducts, becomes complicated and cumbersome for both "manual" calculation and the familiar

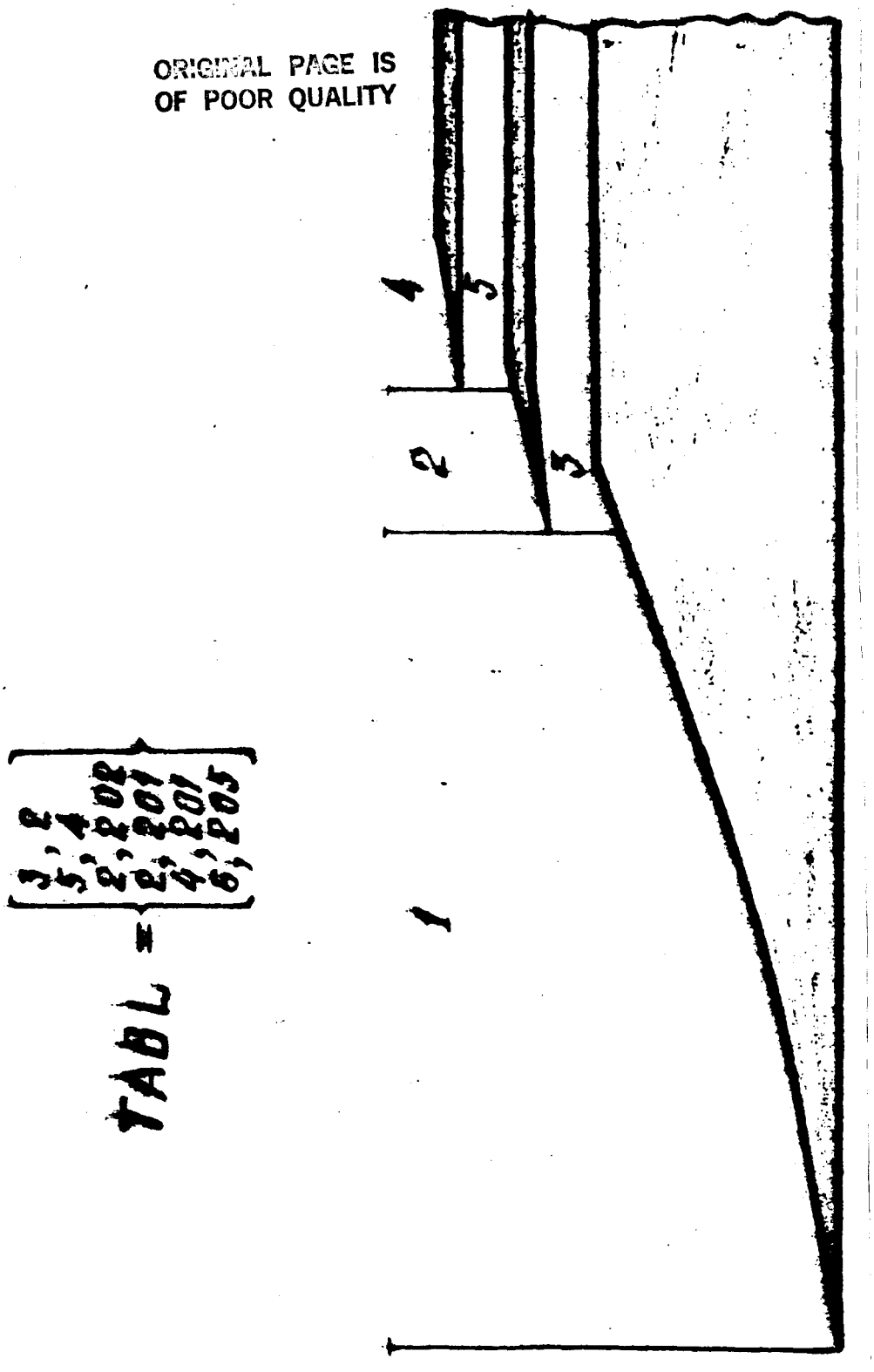

Fig. 5

/110

/112

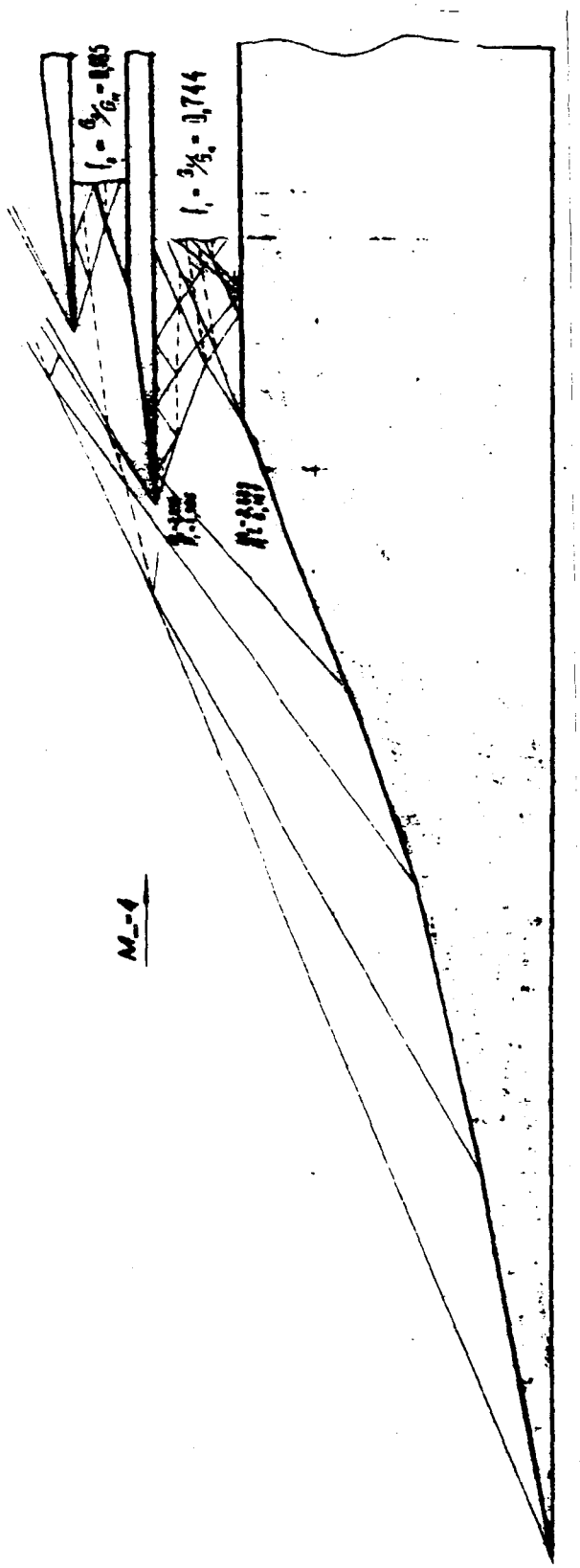

Fig. 6.

C-2

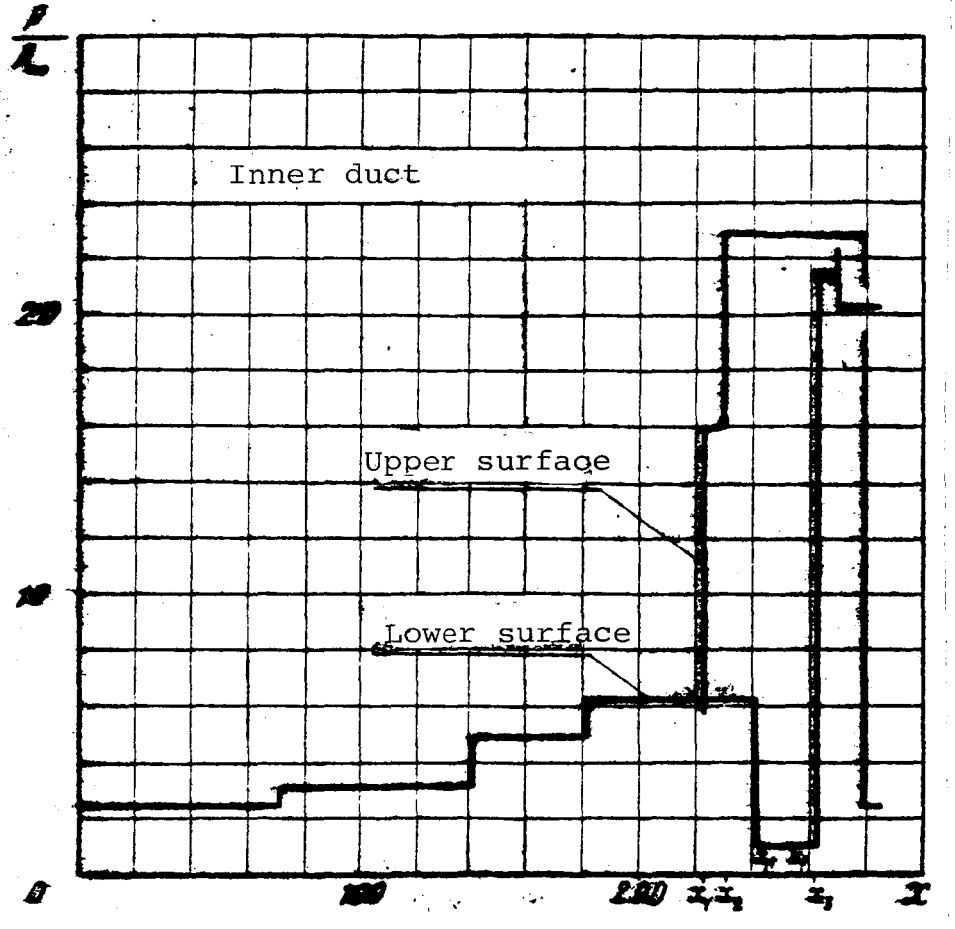

Fig. 7.

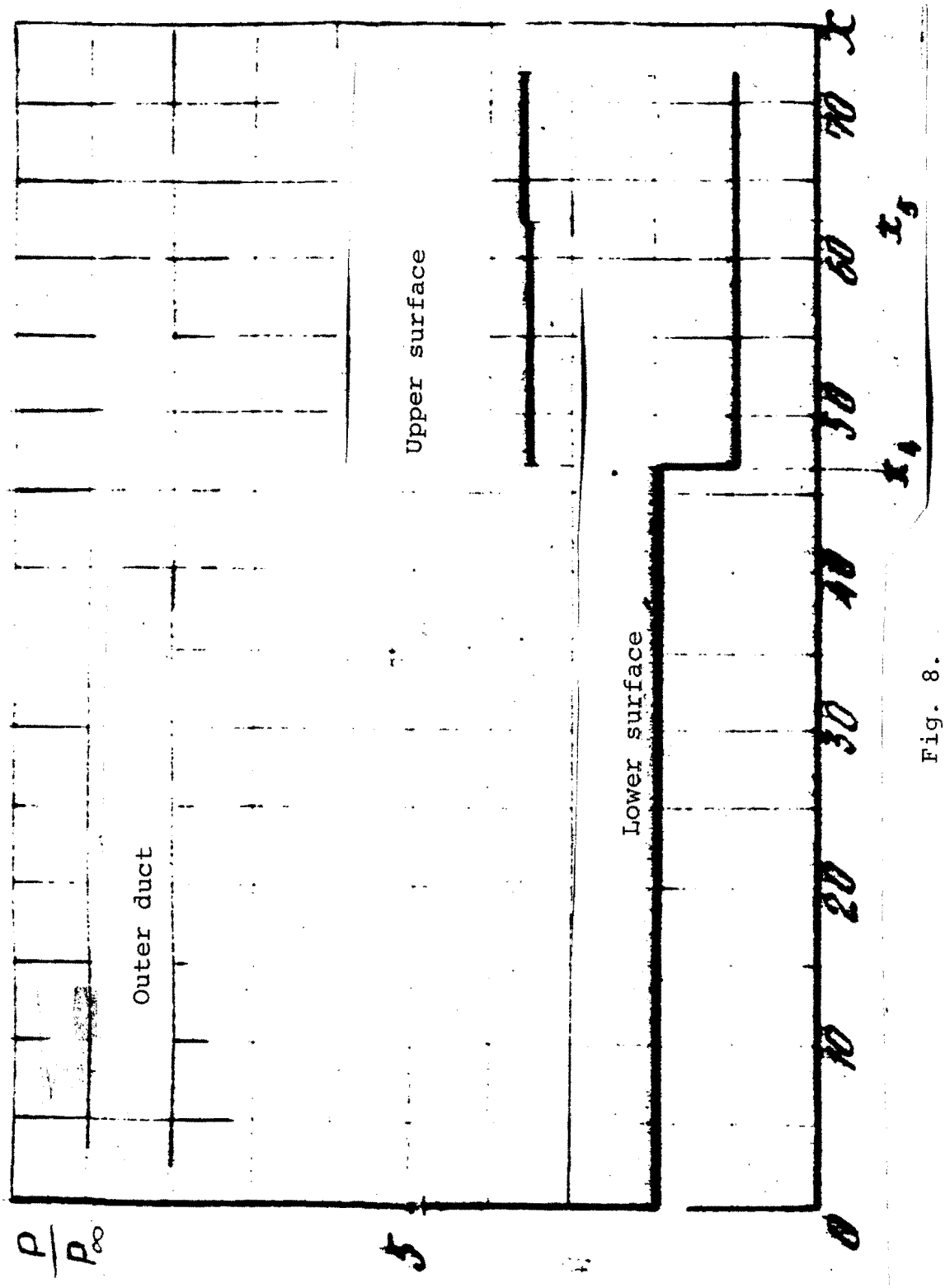

Fig. 8.

numerical methods with "joining" of the solution at the boundary passing through the leading edge of the separating partition. In parametric calculations of flows in the ducts of this air intake, work would be extremely laborious and inefficient, depending on the air intake's geometry (compression wedge geometry, shape and location of separating partition and upper lip, etc.) in a wide range of flight Mach numbers and angles of attack.

The complexity of flow calculation is significantly curbed using our program. Here it is sufficient to break down all of the flow field of interest to us into subregions and to generate file TABL in the following manner (Fig. 5):

$$\text{TABL} = \left\{ \begin{array}{l} 3,2 \\ 5,4 \\ 2,202 \\ 2,201 \\ 4,201 \\ 6,205 \end{array} \right\}$$

The obtained calculation flow pattern in the air intake at M = 4 and angle of attack $\alpha = 0$ is shown in Fig. 6. The shock waves from the forward panel of the compression wedge pass in front of the edges of the lips of both air intake ducts, so the calculated flow factors through the air inlet ducts are fairly small: $f_1 = 0.774$, $f_2 = 0.185$. The flow in front of the inlet into the lower duct is fairly highly decelerated. The Mach numbers in this section vary from 1.832 to 2.683. Accordingly, the ratio of static pressure in the duct inlet section to the static pressure in the incident flow p/p_∞ varies from 4.925 to 6.187.

The upper duct operates in the flow field with local Mach numbers at the inlet exceeding the corresponding Mach numbers at the inlet to the lower duct, because of the ring of shock waves formed at the leading edge of the separating vane. For this /115
reason, strong shock wave reflections from the lip form in the duct, which leads to high losses of total pressure.

The distributions of pressure at the surfaces of both ducts are shown in Fig. 7 and 8. Formation of shock waves at the lip (separating partition) in the lower duct is manifested in a sharp stepwise pressure increase in sections $X = X_1$ and $X = X_2$. A similar picture is also observed in the upper duct. The pressure on the panels of the compression wedge increases practically monotonically and in section $X = X_3$ (throat section) reaches the maximum value $p/p_\infty = 21.5$. Small changes in p/p_∞ in sections X_4 and X_5 on the lip are evidence of the formation of weak shock waves.

REFERENCES

1. Berlyand, A. T., B. I. Penzin, V. A. Eysmont, "The possibility of employing construction units as fuel and other features of a hypersonic ramjet engine," in F. A. Tsander i sovremennaya kosmonavtika [F. A. Tsander and Modern Cosmonautics], Moscow, 1976, pp. 94-100.

2. Berlyand, A. T., and V. A. Eysmont, "Generalization of a method of calculating two-dimensional nozzles of arbitrary configuration with shocks in the case of equilibrium dissociation," in Trudy III chteniy, posvyashchennykh razrabotke nauchnogo naslediya i razvitiyu idey F. A. Tsandera. Sektsiya "Teoriya i konstruktsiya dvigateley i letatel'nykh apparatov" [Proceedings of the 3d Lectures Devoted to Elaborating the Scientific Legacy and Developing the Ideas of F. A. Tsander. Section "Theory and Construction of Engines and Aircraft"], Moscow, 1975, pp. 50-64.

3. Berlyand, A. T., "Some specific difficulties in numerical computations of flows in VRD [jet engine] ducts," Trudy V Chteniy F. A. Tsandera. Sektsiya "Teoriya i konstruktsiya dvigateley i letatel'nykh apparatov" [The 5th F. A. Tsander Lectures. Section "Theory and Construction of Engines and Aircraft"], Moscow, 1980.

4. Berlyand, A. T., and V. A. Frost, "A method of calculating plane supersonic flows with automatic separation of discontinuities and stepwise approximation of rarefaction flows," in Chislennyye metody v mekhanike sploshnoy sredy [Numerical Methods in Solid Mechanics], vol. 3, no. 3, VTs SO AN SSSR Press, Novosibirsk, 1972, pp. 3-12.

5. Ivanov, M. Ya., and A. N. Krayko, "Some results of numerical solution of internal and external gas dynamics problems," Report read at the 4th F. A. Tsander Lectures (Section "Theory and Construction of Engines and Aircraft") in March, 1975.

6. Berlyand, A. T., "Computer implementation of a numerical method for calculating plane supersonic flows with automatic separation of discontinuities," Trudy TsAGI, issue 1807, 3-28 (1977).

7. Kotov, V. D., "A program in ALGOL-60 language for calculating plane supersonic flow of an inviscid gas in a duct using the two-dimensional graph construction method," Trudy TsAGI, issue 1807, 29-86 (1977).

8. Henry, I. R., and H. Lee Beach, "Hypersonic air-breathing propulsion systems," NASA SP-292, 1971, pp. 157-177.

9. Waters, M. S., "Turbojet-ramjet propulsion system for all-body hypersonic aircraft," NASA TN D-5993, 1971.

ON THE THEORY OF AN ELECTROMAGNETIC RESONATOR ENGINE

A. S. Dmitriyev

In connection with the intensive development of laser and /117
SVCh [microwave] technology, the literature widely discusses the idea of emloying a powerful source of electromagnetic radiation outside an accelerated craft for creating jet propulsion. For example, in [1, 2] there are examinations of reaction engine designs based on an evaporative mechanism of thrust, and [3] proposes accelerating a craft through the pressure of an expanding plasma obtained as a result of laser breakdown of the air and atmosphere near the craft. A diagram of a power plant combining the fundamental possibility of accerating an LA [aircraft] to relativistic velocities and a high factor of converting radiation energy into the kinetic energy of aircraft motion -- an electromagnetic resonator engine (EMRD) -- is given in [4].

This article examines some aspects of this engine's theory.

A schematic diagram of the EMRD is shown in Fig, 1. The LA is accelerated through the pressure of electromagnetic radiation on an open resonator, formed by mirrors 2 and 3 on the LA mirror (3). The electromagnetic radiation is pumped by source 1 into the resonator through rectifier 4. Equilibrium pressure of electromagnetic radiation [*sic*]. Here 0 means the Q factor of the resonator. For an ideal system without loss, the Q factor is determined by the size of the resonator and the speed of the moving mirror. Acceleration of the craft continues asymptotically/119 until the electromagnetic oscillations in the resonator are completely damped after source 1 is switched off. When there is no side scattering and no losses in the mirrors and medium, the energy of electromagnetic oscillations is transformed into LA kinetic energy. During the transfer of energy the radiation entering the resonator gradually "reddens."

The engine system provides for the presence in the fixed source and the LA of focused and strictly mutually oriented mirrors. This allows multiple use of the waves reflected alternately from each mirror to increase the LA momentum. It is through the multiple use of the momentum of photons imparting a small fraction of their energy to the LA with each reflection from its moving mirror that a high coefficient of converting electromagnetic oscillations into kinetic energy of the craft is achieved, wherein lies the critical advantage of EMRD over a photon engine.

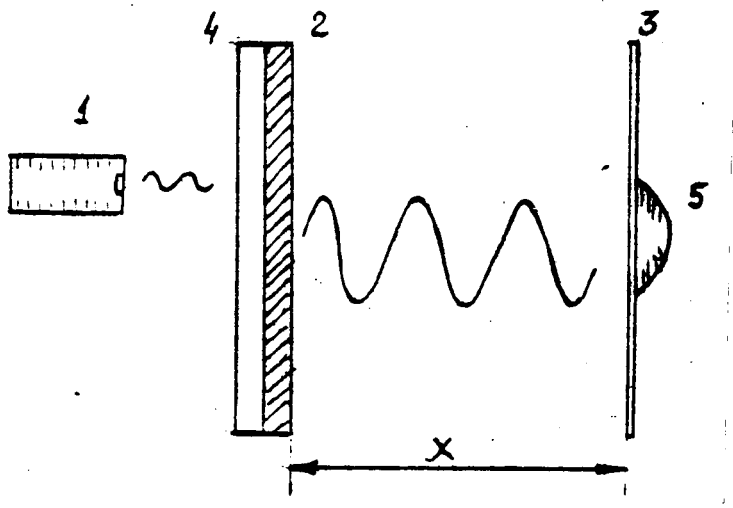

Fig. 1.

One other advantage of EMRD is the high rate of LA acceleration at a given source power, as a result of the practically inertia-free conversion of one type of energy into another.

For quantitative evaluation of EMRD efficiency we have to study the system's equation of motion. For the sake of simplicity, we shall examine a system without losses and introduce the following notations: m is the mass of the LA; X, F, and E are the size of the resonatorn the pressure force of radiation on the LA mirror, and the total energy of the electromagnetic field in the resonator, respectively.

The acceleration of an LA is determined by relation:

$$m\ddot{x} = F. \qquad (I)$$

In turn, the pressure of radiation in the resonator is expressed by the total energy of electromagnetic radiation in the resonator and the size of the resonator

$$F = E/x, \qquad (2)$$

and since there is no loss in the system, the value of E at each point in time can be found from the law of conservation of energy

$$E + \frac{1}{2} m\dot{x}^2 = \frac{1}{2} m\dot{x}_0^2 + E_0 + \int_0^t \varepsilon_0(t)\,dt, \qquad (3)$$

where X_0 is the initial velocity of LA motion, E_0 is the initial energy in the resonator; $\varepsilon_0(t)$ is the power of the radiation source. Substituting E from (3) into (2) and expression (2) into (1) and introducing the notation

$$\alpha = \frac{1}{2} m\dot{x}_0^2 + E_0$$

we obtain the desired equation of motion /120

$$m\ddot{x}\ddot{x} + \frac{1}{2} m\dot{x}^2 - \alpha = \int_0^t \mathcal{E}_0(t)\,dt. \qquad (4)$$

It is impossible to study analytically the nature of the solution of nonuniform nonlinear equation (4). But analysis of the system's dynamics when the source is switched on, i.e., for equation

$$m\ddot{x}\ddot{x} + \frac{1}{2} m\dot{x}^2 - \alpha = 0 \qquad (5)$$

can be performed analytically using the phase plane method [5].

The solution of equation (5) is:

$$\frac{\dot{x}^2}{2} - \frac{C}{x} - \frac{\alpha}{m} = 0,$$

where C is the integration constant. Consequently

$$\dot{x} = \pm \sqrt{\frac{2C}{x} + \frac{2\alpha}{m}}. \qquad (6)$$

Thus, the phase path of equation (5) consists of two branches, and the actual segments of the branches would exist only at those values of X for which

$$\frac{2C}{x} + \frac{2\alpha}{m} > 0$$

Considering that at the initial point in time $X = X_0$, we obtain

$$C = -\frac{E_0 X_0}{m}.$$

The phase path degenerates at $E_0 > 0$ into two straight lines parallel to the x axis. In this case the velocity of the craft is, of course, constant and independent of X (Fig. 2).

In the other physically realized cases E_0 0 [*sic*] and graphic representation reveals that the phase paths are open and for high X the velocity X asymptotically approaches the value

$$\dot{x}_\infty = \sqrt{\frac{2\alpha}{m}}.$$

It is interesting to note that in the absence of loss and with $E_0 > 0$ in the system, both conversion of electromagnetic

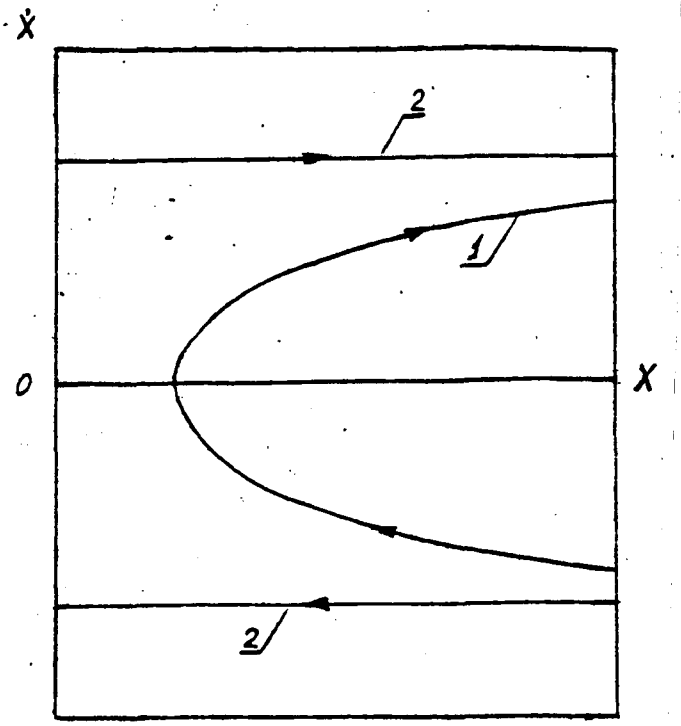

Fig. 2.

radiation energy into kinetic energy of LA motion and the reverse process are possible. Here the kinetic energy of the craft is totally converted into the energy of electromagnetic radiation at that point of the phase path with coordinates

$$x = x_0 / \left(\frac{m\dot{x}_0^2}{2E_0} + 1 \right), \dot{x} = 0.$$

The nature of LA motion when the source is switched on with $\varepsilon_0(t) \equiv \varepsilon_0$ and the dependence of the system's behavior on initial conditions can be obtained by numerically integrating equation (4).

The behavior of the phase paths relative to the initial conditions is qualitatively understood from Fig. 3. The closeness of the phase paths is evidence of the stability of the solutions with respect to the initial conditions. With the system parameters assigned for the graphs, in 15 min of acceleration the LA reaches orbital velocity. /122

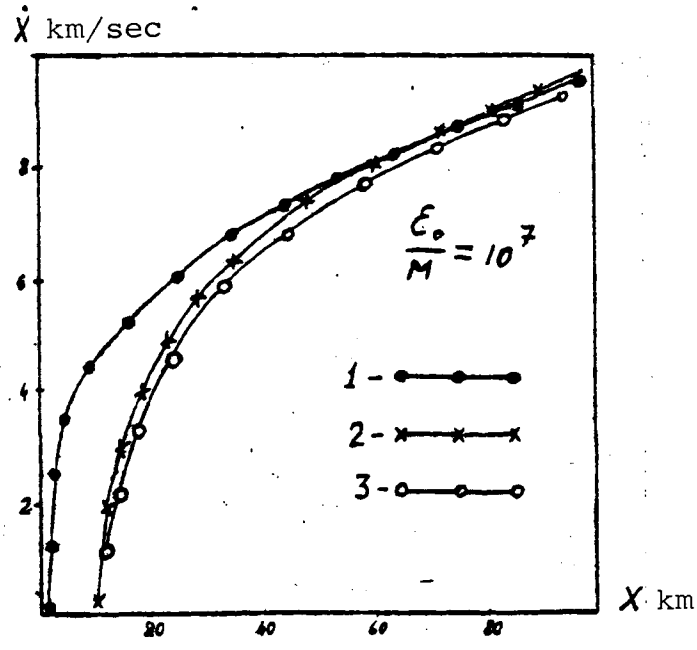

Fig. 3.

Of fundamental significance for the possibility if implementing EMRD is the law of radiation spectral-composition change with acceleration of the craft.

We shall study the dependence of the radiation spectral composition in the resonator as a function of time, in the assumption of absence of interaction between the radiation of different frequencies.

When a plane wave perpendicularly strikes a mirror surface moving at velocity, the frequency

changes in accordance with relation (the Doppler effect):

$$\omega' = \omega \frac{c - v}{c + v} \approx \omega \left(1 - 2 \frac{v}{c}\right), \qquad (7)$$

where ω is the frequency of the incident wave; ω' is the frequency of the reflected wave. One wall in the resonator is movable, and in time dt a wave with initial frequency ω strikes it $(c\,dt)/2x$ times. Therefore, the frequency of an electromagnetic wave at time $t + dt$ - $\omega(t + dt)$ is associated with the frequency of the wave at time t - $\omega(t)$ by relation

$$\omega(t + dt) = \omega(t) \cdot \left(1 - 2 \frac{v}{c}\right)^{\frac{c\,dt}{2x}}$$

or

$$\frac{\ln \omega(t + dt) - \ln \omega(t)}{dt} = \frac{c}{2x} \ln \left(1 - 2 \frac{v}{c}\right).$$

The left side of the last equation represents the total derivative of $\ln [\omega(t)]$ with respect to time and, consequently, equals

$$\ln [\omega(t)]' = \frac{\omega'(t)}{\omega(t)}.$$

Thus, the equation for $\omega(t)$ is:

$$\frac{\omega'(t)}{\omega(t)} = \frac{c}{2x} \ln \left(1 - 2 \frac{\dot{x}}{c}\right). \qquad (8)$$

Assume that at the initial point in time the spectral composition of the radiation in the resonator is $B(t)$ and no radiation arrives in the resonator from the source outside. For any frequency ω at the initial time, the law of its change over time is determined from equation (8). At time $t = 0$ the spectral density of $B(\omega)$ corresponds to frequency ω. We shall construct an equation for $B(\omega[t])$. Derivation of this equation is similar to that of equation (8). Upon reflection from the moving mirror, the amplitude of the original wave changes according to law /123

$$E' = E \cdot \left(\frac{1 - \frac{v}{c}}{1 + \frac{v}{c}}\right) = E \cdot \left(\frac{c - v}{c + v}\right) \sim \sqrt{B} \left(\frac{c - v}{c + v}\right) = \sqrt{B'}. \qquad (9)$$

Accordingly, the spectral density of the power, proportional to the square of the reflected wave's amplitude, equals

$$B' = B \cdot (1 - 4\frac{v}{c}). \qquad (10)$$

After transformations similar to those performed in the derivation of equation (8), we obtain

$$\frac{B'(t)}{B(t)} = \frac{c}{2x} \ln(1 - 4\frac{\dot{x}}{c}). \qquad (11)$$

Using the obtained equations we can calculate the spectral density of the radiation. To do this, we need to break down the spectral range into small segments and integrate equation (8) for the frequencies of all intervals with the initial conditions at the left end. We thereby find frequencies $\omega_i(t)$ corresponding to frequencies $\omega_i(0)$ at time t.

$$\omega_i(0) \longrightarrow \omega_i(t).$$

Then, considering that the law of change of the square of the wave's amplitude (spectral density) with change in frequency is subject to equation (11), we can construct a curve of the spectral composition at time t using the curve of spectral composition at time t = 0. We can show that this process constitutes a solution using the method of characteristics ($\omega(t)$ plays the role of characteristic) of some equation in partial derivatives of the first order for $B(\omega, t)$.

Note that along each curve lying in plane (t, ω) we can treat ω and $B(\omega, t)$ as functions of t, so that the total derivative of function $B(\omega, t)$ equals

$$\frac{dB}{dt} = \frac{\partial B}{\partial t} + \frac{\partial B}{\partial \omega} \cdot \frac{d\omega}{dt}. \qquad (12)$$

We shall now examine curve $\omega(t)$ in plane (t, ω), which satisfies equation (8). From (8) we can obtain explicit relation $\omega'(t)$, which, for now, we shall conditionally write using $\omega(t)$, X, and X'

$$\omega'(t) = \frac{\omega(t) \cdot c}{2x} \ln(1 - 2 \cdot \frac{\dot{x}}{c}). \qquad (13)$$

On the other side, on curve $\omega(t)$, we can obtain an explicit expression for B'(t) from equation (11). We shall write it as

$$B'(t) = B(t) \frac{c}{2x} \ln(1 - 4 \cdot \frac{\dot{x}}{c}). \qquad (14)$$

Substituting (13) and (14) in (12), we obtain the equation sought for $B(\omega, t)$

$$\frac{\partial B}{\partial t} + \frac{\partial B}{\partial \omega} \cdot \frac{\omega(t) \cdot c}{2 \cdot x(t)} \ln\left(1 - 2 \cdot \frac{\dot{x}(t)}{c}\right) = B(t) \frac{c}{2 \cdot x(t)} \ln\left(1 - 4 \frac{\dot{x}(t)}{c}\right). \quad (15)$$

Considering that $X/c \ll 1$, equations (8), (11), and (15) can be simplified and written, respectively /124

$$\frac{\omega'(t)}{\omega(t)} = -\frac{\dot{x}(t)}{x(t)} \quad (8')$$

$$\frac{B'(t)}{B(t)} = -2 \frac{\dot{x}(t)}{x(t)} \quad (11')$$

$$\frac{\partial B}{\partial t} + \frac{\partial B}{\partial \omega} \cdot \frac{\omega(t)\dot{x}(t)}{x(t)} = -B(t) \frac{2\dot{x}(t)}{x(t)}. \quad (15')$$

We examined the process of obtaining a relation when the source is switched on, i.e., the Cauchy problem for equation (15'). The problem with switching on of the source is a typical boundary value problem, for which

$$B(\omega, t) = B(\omega) \quad \text{at} \quad \omega > 0,\ t = 0$$
$$\varepsilon_0(\omega, t) = \varepsilon_0(\omega_0, t) \quad \text{at} \quad t > 0,\ \omega = \omega_0$$

and the solution is sought in region $\omega > 0$, $t > 0$ [6]. Figure 5 shows the diagram corresponding to (t, ω). The characteristics begin at positive semiaxis ω and at positive semiaxis t. This solution can be linked with solution of the Cauchy problem in a manner based on the fact that this solution coincides with solution of the Cauchy problem, if the characteristic is continued through points $t = t_0$, $\omega = \omega_0$ to the ω axis and the intersection points are designated $\omega = \omega(0)$. Then the boundary value problem is formulated as a Cauchy problem.

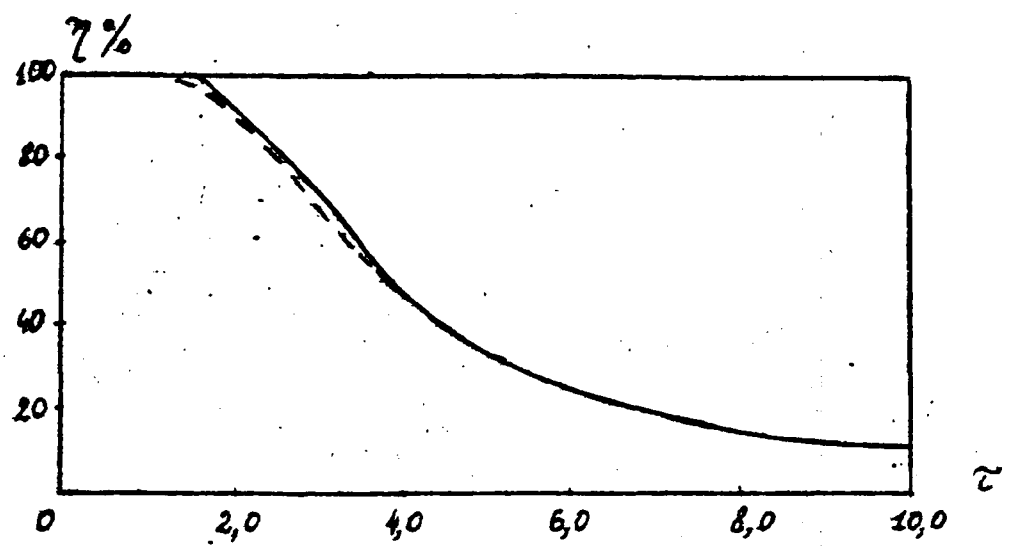

Fig. 4.

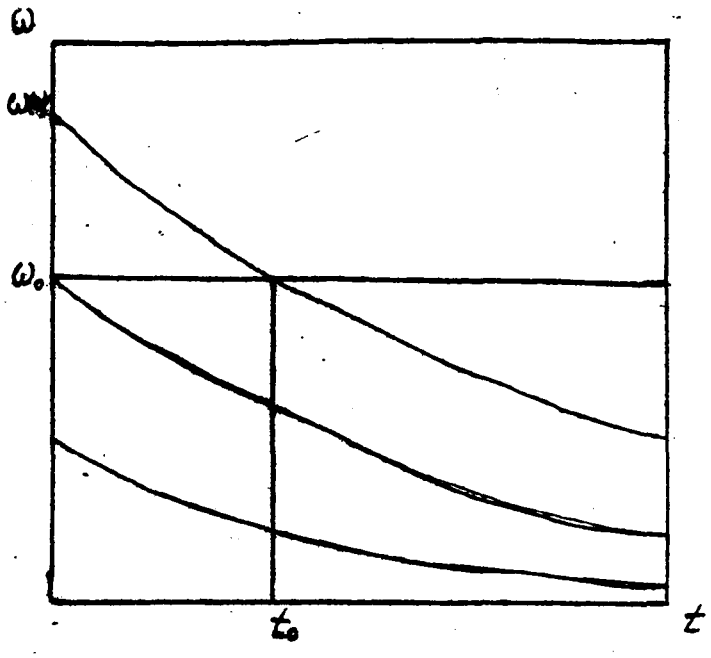

Fig. 5.

Analysis of the EMRD outline reveals that the basic parameters of the engine system are determined by the characteristics of the mirrors, the radiation source, and the precision of stationary installation and LA orientation. In turn, the efficiency of the EMRD is determined most of all by the maximum distance of the craft -- D -- at which the coefficient of electromagnetic radiation energy conversion into LA kinetic energy is still adequately high and by the power of the power source.

We can show that the maximum efficiency of energy conversion -- η -- between two mirrors through electromagnetic radiation depends only on parameter τ:

$$\tau = \lambda D / R_1 R_2.$$

where R_1 and R_2 are mirror dimensions [7]. Relation $\eta(\tau)$ for mirrors with round and square apertures is shown in Fig. 4. In the first case, lying along the x axis is value

$$\tau = \lambda D / R_1 R_2,$$

and in the second $\tau = (\pi/4)(\lambda D/L_1 L_2)$. /126

In both cases the parameter along the x axis can be written as $\tau = 2\pi(\lambda D/s)$, where s is the minimum total area of the receiver and transmitter mirrors' apertures needed to obtain the efficiency of transmission described by these curves.

For $\tau < 1.0$ the transmission efficiency equals practically 100%.

With increasing distance, the efficiency of the EMRD falls in proportion to the reduction in resonator Q factor

$$Q \sim \frac{E_c}{\varkappa \mathcal{E}} \gg 1.$$

The requirements for transmission efficiency are fairly strict. For example, with a 10% total efficiency of the system, the minimum allowable transmission efficiency is 99.9%.

The prospects for creation of full-scale EMRD should be linked first of all with work to create energy transmission systems. The combination of energy transmission systems with sail structures as a mirror on an LA may be the first full-scale realization of the idea of an electromagnetic resonator engine.

REFERENCES

1. Kantorovitz, A. R., Aeronautics and Astronautics, 9, 35 (1971); Aeronautics and Astronautics, 10, 74 (1972).

2. Pirri, A. N., M. I. Monsler, P. F. Nebolsin, AIAAI, 12, 1254 (1974).

3. Barchukov, A. I., F. B. Bunkin, V. I. Konov, A. M. Prokhorov, "A laser jet engine," Pis'ma v ZhETF, 23, 237 (1976).

4. Gayev, F. F., and A. S. Dmitriyev, "A high-efficiency engine system with an external source of electromagnetic radiation," Trudy XII chteniy K. E. Tsiolkovskogo. Sektsii "Problemy raketnoy i kosmicheskoy tekhniki" [Proceedings of the 12th K. E. Tsiolkovskiy Lectures. "Problems of Rocket and Space Technology" Sections], Moscow, 1979, pp. 70-76.

5. Moiseyev, N. N., Asimptoticheskiye metody nelineynoy mekahniki [Asymptotic Methods of Nonlinear Mechanics], Moscow, 1969.

6. Uizem, Dzh., Lineynyye i nelineynyye volny [Linear and Nonlinear Waves], Moscow, 1977.

7. Okress, E., (ed.), SVCh-energetika [Microwave Power], vol. 1, Moscow, 1971.

MODEL STUDIES ON THE DYNAMIC CHARACTERISTICS OF LIQUID FUEL ROCKET ENGINE PUMPS AND TURBINES IN TRANSIENT CONDITIONS

V. M. Kalinin and V. A. Sherstyannikov

Introduction. Launches of the first ZhRD [liquid fuel rocket/127 engines] were worked out basically empirically, by testing various launch outlines and cyclograms directly in engine firing tests. This required large expenditures of time and resources. The existing launch calculation methods failed to account adequately for the basic factors affecting the process, and could not serve as a reliable tool for its development. Over 30% of the accidents with ZhRD took place during the launch phase. As more powerful and complicated engines were produced it became necessary to create more efficient and cheaper methods of trying out launches. This problem was solved using the following procedures:

1) studying the physical picture of engine start;

2) creating methods of mathematical analysis of this process;

3) developing methods of hydrodynamic modeling;

Through development of the first and second areas, methods were mastered for high speed recording of basic engine parameters in start conditions, some important consistencies determining the chemophysical processes were discovered, and procedures for calculating launch using a computer were created which more fully accounted for the discovered consistencies.

Work performed in the third area allowed creating methods of hydrodynamic modeling which provided for developing specific /128 launch systems, especially for engines of complex design. Hydrodynamic processes have a major role in ZhRD starting. This conclusion was reached by almost all researchers investigating the operating process of actual engines. Hydrodynamic processes are virtually the only ones through which all other stages of the chemophysical process constituting ZhRD start can be affected. Thus, development of methods for studying and developing the ZhRD launch process traveled the road of thorough study of these processes and creating effective methods for their certain prediction and strict control.

Development of hydrodynamic methods for modeling the launch process allowed significantly expanding the information about physical processes occurring during launch and creating an effective tool for prior working out of launch even before engine firing tests [1-3].

The purpose of this article is to examine experimental methods based on hydrodynamic modeling of ZhRD systems and to describe the obtained results.

Modeling Methods and Similarity Criteria

Hydrodynamic modeling methods are used to study the space-time irregularity of engine accessory filling, irregularity of engine injector operation start, processes of emulsion feed of components, and the dynamic characteristics of pumps and turbines in start and transient conditions.

The modeling consists essentially in the following. The assembly being studied (combustion chamber, turbo-pump assembly (TNA), starting valve at the inlet to the engine, etc., for example) is mounted in the operating position in a hydraulic system with a modeling liquid, having fuel lines similar to the hydraulic lines of a rocket (Fig. 1). The fuel tank pressurization and the resistance and inertia of the hydraulic system are established in accordance with the similarity criteria discussed below. The modeling liquid is delivered by switching on the starter and automatic start equipment through the control panel using a test bed allowing assignment of different times for shifting starter and launch device commands. All of the basic parameters needed for determining the dynamic characteristics of the assembly under study are recorded during testing using high speed measuring equipment. /130

/129

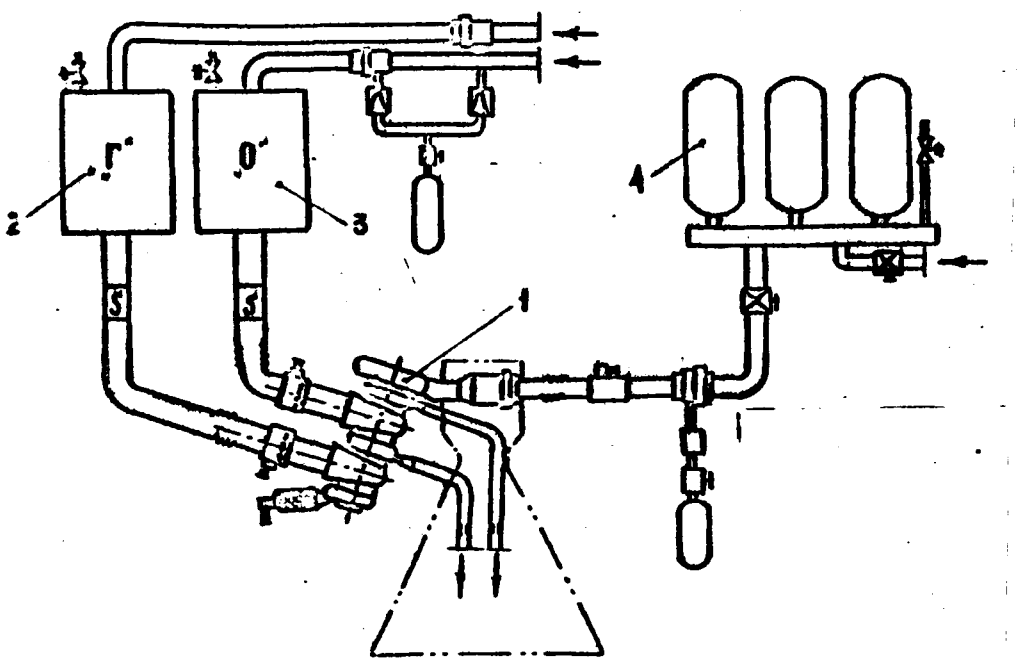

Fig. 1.

We use the following similarity criteria when modeling non-steady-state hydrodynamic processes:

1) Complete geometric similarity of the hydraulic system (a full-scale assembly is employed).

2) Equality of piezometric head at the inlet to the assembly:

$$\left(\frac{p_1}{\rho_\ell}\right)_M = \left(\frac{p_1}{\rho_\ell}\right)_H.$$

3) equality of inertial and effective hydraulic resistance input lines:

$$\sum_i \left(\frac{l_i}{F_i}\right)_M = \sum_j \left(\frac{l_j}{F_j}\right)_H; \quad \sum_i \Delta P_{iM} = \sum_j \Delta P_{jH}.$$

4) Equality of inherent self-oscillations of liquid in hydraulic system elements:

$$(\omega_i)_M = (\omega_j)_H,$$

where P_1 is the pressure of the liquid at the inlet, ρ_ℓ is the density of the liquid, $l_{i,j}$ represents the lengths of the line segments, $F_{i,j}$ represents the areas of the passage segments of the lines, $\Delta P_{i,j}$ represents pressure losses in the lines, M is the model system, and H is the full-scale system.

Meeting of these criteria provides identity of the temporal characteristics of the filling process, that is, the time needed for the components to reach the assembly and the amounts of fluid hammers and pressure dips in the full-scale and model systems. When these conditions are observed, simple calculation using the density of the model liquid is used to determine the expected expenditures of actual components.

Hydrodynamic tests are performed with thorough preparation of the assemblies being tested and detailed visualization of the liquid flow pattern (Fig. 2).

The firing assemblies, pumps, and TNA turbine are prepared with pressure, temperature, and phase sensors and transparent inserts for photographing the flow. Measured besides pressures and temperatures in the sections at the inlet and outlet of the assemblies are the pressures along the flow area (at the periphery of the spiral tap of the pump, in the radial clearance of the turbine, etc.).

The combustion chamber cooling lines and fuel component feed lines are prepared with high speed sensors of the delivery of the component and small-calibrated pressure strain-gauge

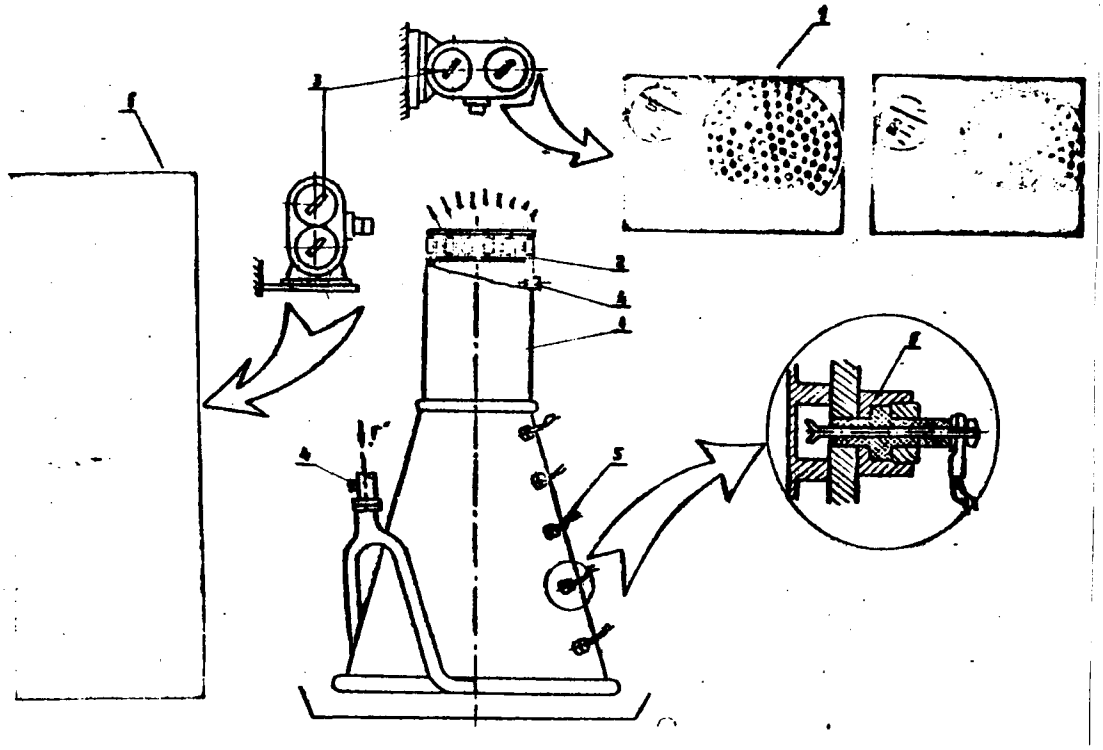

/131

Fig. 2.

transducers. To visualize the process of operation start of the fuel injector, the combustion chamber is made with an inverted injector -- with external outlet of the liquid from the injector (Fig. 2). This allows making motion picture films of the liquid emerging from the injector (in two projections) in the start process. /132

Displacement of the controller plunger piston in the start mode is determined by inductive pickups mounted on its housing. To measure pressure drops and flows in feed lines for the fuel and oxidant of the combustion chamber and gas generator, differential pressure pickups and induction turbine flowmeters are mounted.

Hydrodynamic modeling methods have found extensive use. These methods are used to study the characteristics of non-steady-state processes and elaborate a number of assumptions for efficient organization of pre-firing processes. Some of the obtaiend results are examined below.

II. Examples of Modeling

1. Hammer during Pump Filling

In the staring of engines in which the pumps are not filled with components before start, hammers accompanied by later wave

processes arise in the input hydraulic lines at the moment the pumps are filled. The allowable amounts of hammer are limited by the strength of the pump lines and housings. Modeling has revealed that two hammers develop when screw impeller pumps are filled. The first is associated with deceleration of the liquid in the screw, the second with generation of a critical flow condition in the volute diffuser. The second hammer is considerably greater than the first (Fig. 3). Measurements have established that the basic part of a pump's hydraulic resistance in the filling mode is concentrated on the volute diffuser and amounts to approximately 85% of the total pump resistance. The nodal points on the resistance distribution characteristic along the pump tract (Fig. 3) correspond to: (1) resistance of the screw, (2) of the screw with impeller, (3) of the entire pump. Within each of these pump elements we can adopt a linear law of resistance and inertia distribution by volume. This relation can be used to calculate hammers for a whole series of pumps. The calculation results provide satisfactory agreement with experimental data. Because of this it is possible correctly to predict the amounts of hammer upon ZhRD start and adopt and approve in timely fashion measures for reducing them to a safe level.

/133

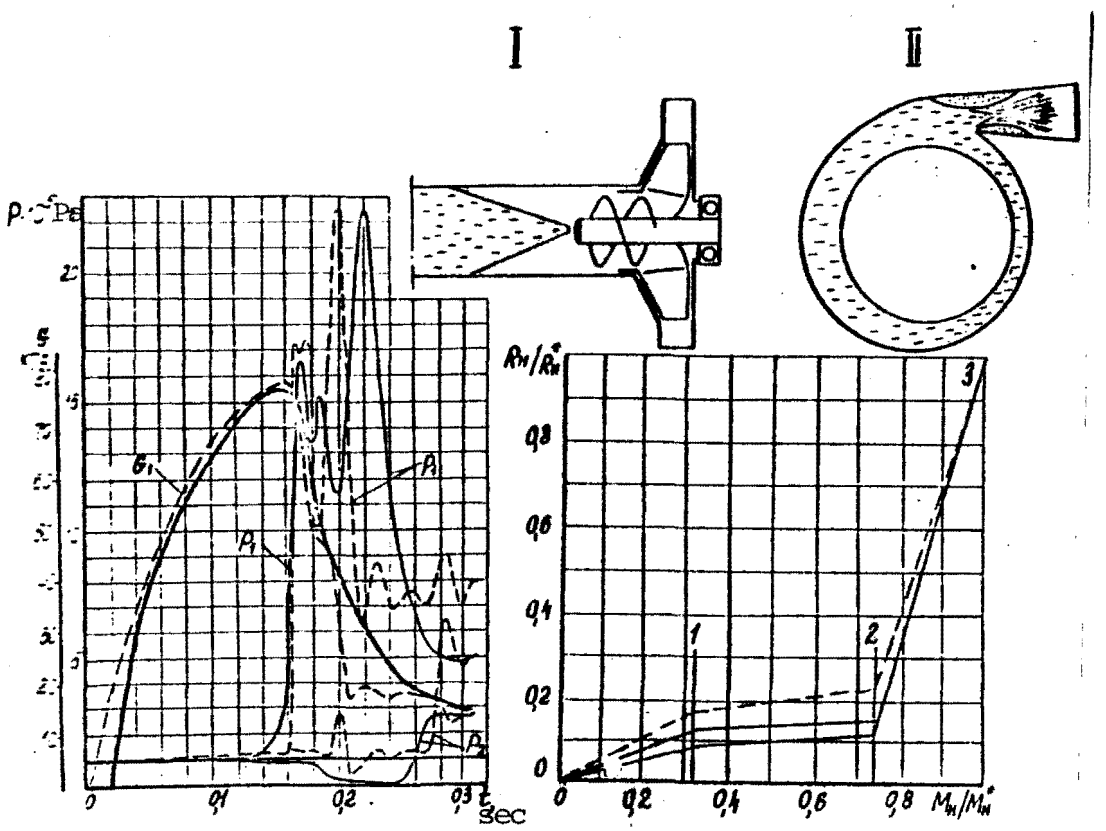

Fig. 3.

2. Pressure and Torque of Pumps in Non-steady-state Conditions /134

Non-steady-state processes upon start of ZhRD affect the operation of pumps basically as a consequence of the action of inertial masses of fluid in the flow part. In accordance with the equations of motion of the pump rotor liquid masses in its lines, the dynamic pressure and torque of the pump in transient modes are determined by expressions

where H_{CT} and M_{CT} are the pressure and torque of the pump in the steady mode, [illegible] are coefficients characterizing the pump's inertia:

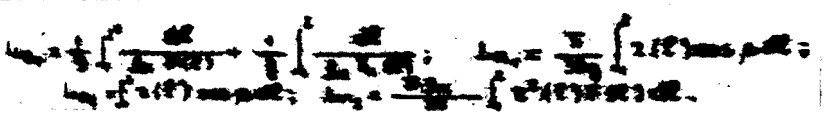

(l is the length of the path of movement of the liquid in the flow-through part of the pump, [illegible] is the area of the flow section of the element, z is the current value of the radius, β is the angle between the vectors of relative and circumferential velocities, g is the acceleration of gravity, [illegible] is the liquid density, "K" is the impeller). The above equations are approximate, since, of all the acting dynamic factors, only the inertia of the liquid and of the pump rotor is accounted for in them.

Hydrodynamic modeling of pump operation in non-steady-state conditions has confirmed the need for employing these approximate relations to calculate the pressure and torque of pumps in ZhRD start modes. At relatively low rates of flow increase ($dG/dt \leq 250$ kg/sec/sec) the reduction of pressure in the TNA acceleration process is relatively low and does not exceed 5% of the pressure in the steady condition. At high rates, obtained with even opening of the pump valve ($dG/dt = 2000$-3000 kg/sec/sec) the drop in pressure reaches 30-40% (Fig. 4). Pressure drop occurs basically because of inertial losses in the diffuser. With increasing pump speed, the effect of liquid inertia on the pump decreases as a result basically of increase in the relative area of the diffuser throat. Acceleration of the rotor [illegible] with real TNA acceleration rates has little effect on pump pressure. These conclusions have been tested on ZhRD pumps /136 with specific speeds of $n_s = 36$-75 at flow rate increases $dG/dt \leq 3500$ kg/sec/sec and rotor accelerations $dn/dt \leq 10^5$ r.p.m./sec.

The amount of torque on the pump shaft in transient modes (at $dG/dt \leq 500$ kg/sec/sec and in the absence of cavitation)

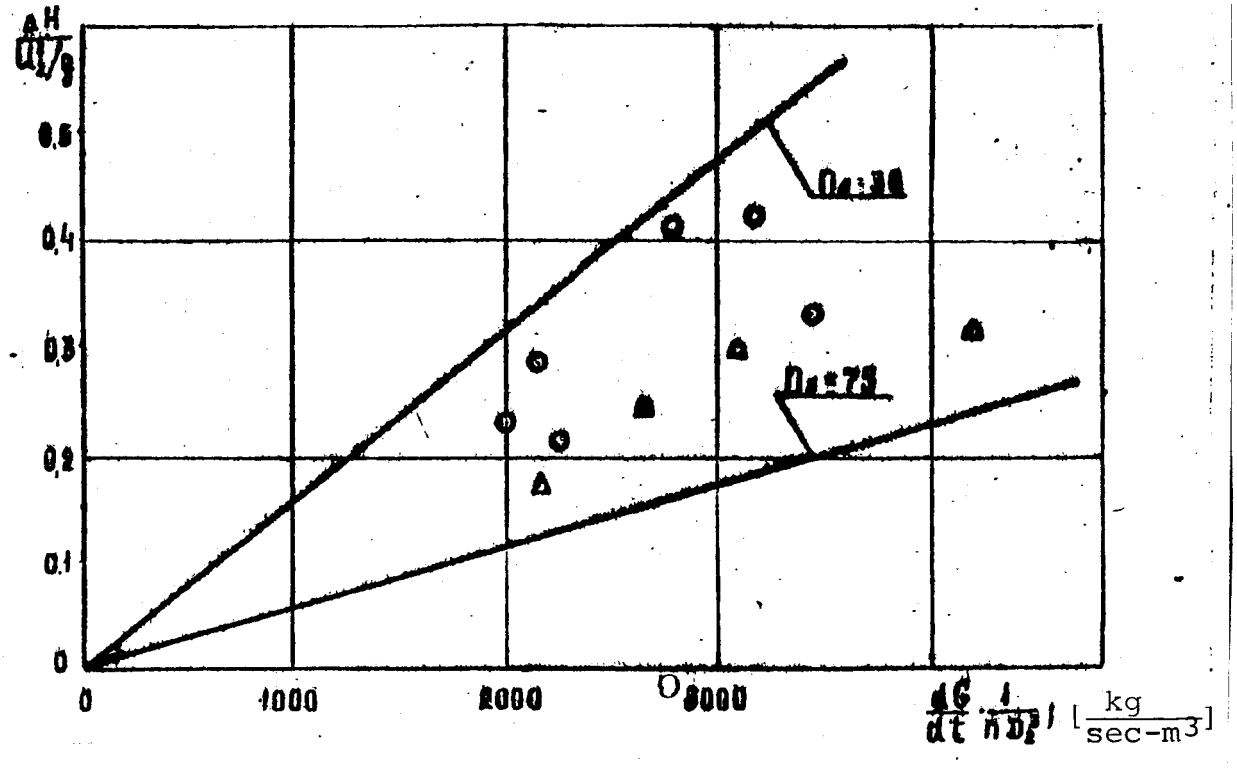

/135

Fig. 4.

differ little from the amount of torque in the steady state (the difference is no more than 1%). The obtained results lie at the foundation of mathematical modeling of ZhRD start. /136

3. Dynamic Characteristics of Turbines

Works studying the dynamics of ZhRD turbines in non-steady states have recently appeared in the literature. We have used the hydrodynamic modeling method to obtain some results related to assessing the dynamic properties of turbines at high rates of change in gas flow and turbine rotation speed. The parameters of combined resistance of the circuit following the turbine were varied. Five different types of turbines in the TNA system were tested -- two centrifugal turbines with small π_T = 1.5-1.8 and three partial axial-flow turbines with large π_T = 15-30. Research revealed that in a wide range of values of parameter u/Cag the dynamic factors of rotating rotor acceleration have no marked effect on turbine efficiency. Thus, at accelerations dn/dt $\leq 2\times10^6$ r.p.m./sec, characteristic of ZhRD start, the power characteristics of turbines can be considered quasi-steady.

The volume aft of the turbine substantially affects the developed turbine power during ZhRD start and acceleration. Figure 5 shows the consistencies in change of pressure in the gas duct

/137

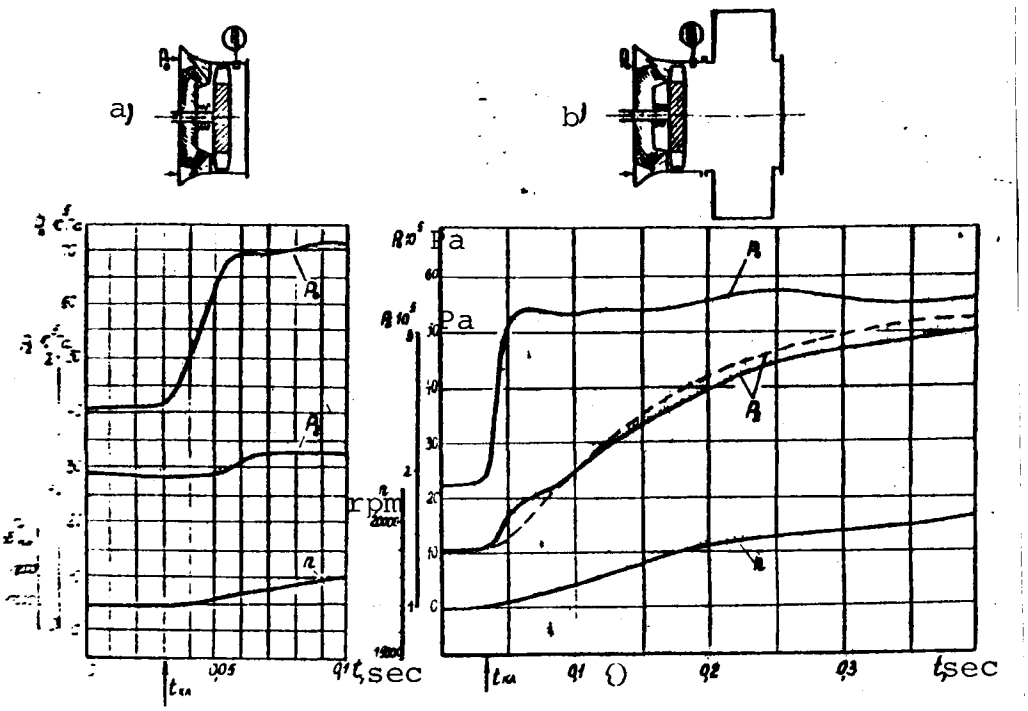

Fig. 5.

from the turbine over time at different volumes aft of the turbine./136 For a sharp change in turbine operation conditions during testing, a fast-acting two-position valve was used which provides for increasing the input pressure with acceleration dP_0/dt = (1000-1500) × 10^5 Pa/sec. Figure 5a shows the course of processes in a turbine with a short outlet line with exhaust to the atmosphere. Pressure was measured directly at the inlet to the turbine and aft of the impeller at its outlet. It can be seen that in this transient process, caused by an abrupt increase in pressure at the inlet to the turbine P_0^*, delay of pressure behind the turbine P_2 comprises a mere 0.002 sec. Similar results were obtained in tests of other turbines without a space aft of the turbine in a /138 wide range of turbine operating-mode changes. The delay time here was 0.002-0.005 sec.

Figure 5b shows the source of processes in tests of a turbine with a large volume aft of it in the form of a 60 L exhaust manifold at the outlet. In this case the delay time of the transient process for P_2 is ∿0.45 sec, which substantially exceeds the values recorded in the absence of a volume aft of the turbine. Estimates were made of the effects of an exhaust manifold attached aft of the turbine on P_2 pressure transient processes.

When calculating these processes we can use the continuity equation for the "turbine-gas duct" system with the assumption that this system consists of a simple pneumatic circuit comprising

the active hydraulic resistance of the turbine, a concentrated volume aft of the turbine, and a concentrated hydraulic resistance at the outlet from the volume. The results of calculations provide satisfactory agreement with model processes (Fig. 5b). This leads to the conclusion that in the low frequency region, characteristic of start processes and transient conditions of ZhRD (f = 0-100 Hz), the size of the volume aft of the turbine is one of the basic dynamic factors determining the transient process in a system with turbine.

4. Cavitation Interruptions of Pump Pressure

Cavitation interruptions of pumps, caused by sharp pressure drops at the inlet to the pump, have a substantial effect on the process of starting and other transient conditions of power plants with ZhRD. In multiengine installations the engines are found to affect each other, a fact associated with hydraulic disturbances arising in the fuel supply system. When designing and developing starting systems we have to account for the dynamics of development of pump cavitation interruptions caused by induced vibrations, solitary pressure drops in inlet lines, or presence of gas inclusions in them. The hydraulic modeling method has allowed thorough study of the features of these highly unsteady processes.

Figure 6 shows a typical picture of transient processes in a pump when a brief severe drop occurs in pressure at the inlet. With minor drops, the shape of the pressure curve behind the pump P_2 corresponds to the course of input pressure P_1, there is no phase shift, and the pump pressure does not change in the process of the transient condition. With severe drops the P_1 and P_2 pressure change curves are different. Pressure curves for P_K behind the impeller and P_2 behind the pump follow change in the curve of pressure P_1 at the inlet with a delay and distortion of shape. /140

Comparison of the nature of change in the integral flow rate difference

and the reduced pressure head indicates that change in pump pressure corresponds approximately to the change in cavity volume. Results of tests on a wide range of pumps confirm the described consistencies and allow presenting a generalized dependence of pump pressure change on the volume of the forming cavity in the flow part of the pump $\bar{H} = f(\bar{v}_K)$ (Fig. 7). The points designated by O refer to a pump tested with delivery of gas inclusions to the inlet. Points marked x were obtained in tests with abrupt changes in resistance in the pump lines, and points marked X correspond to conditions of developed cavitation self-oscillations. The following approximations were obtained as a result of processing all the experimental data using the least-squares method:

$$\bar{H} \approx 1 + 0{,}0529\,\bar{v}_K - 0{,}8766\,\bar{v}_K^2.$$

/139

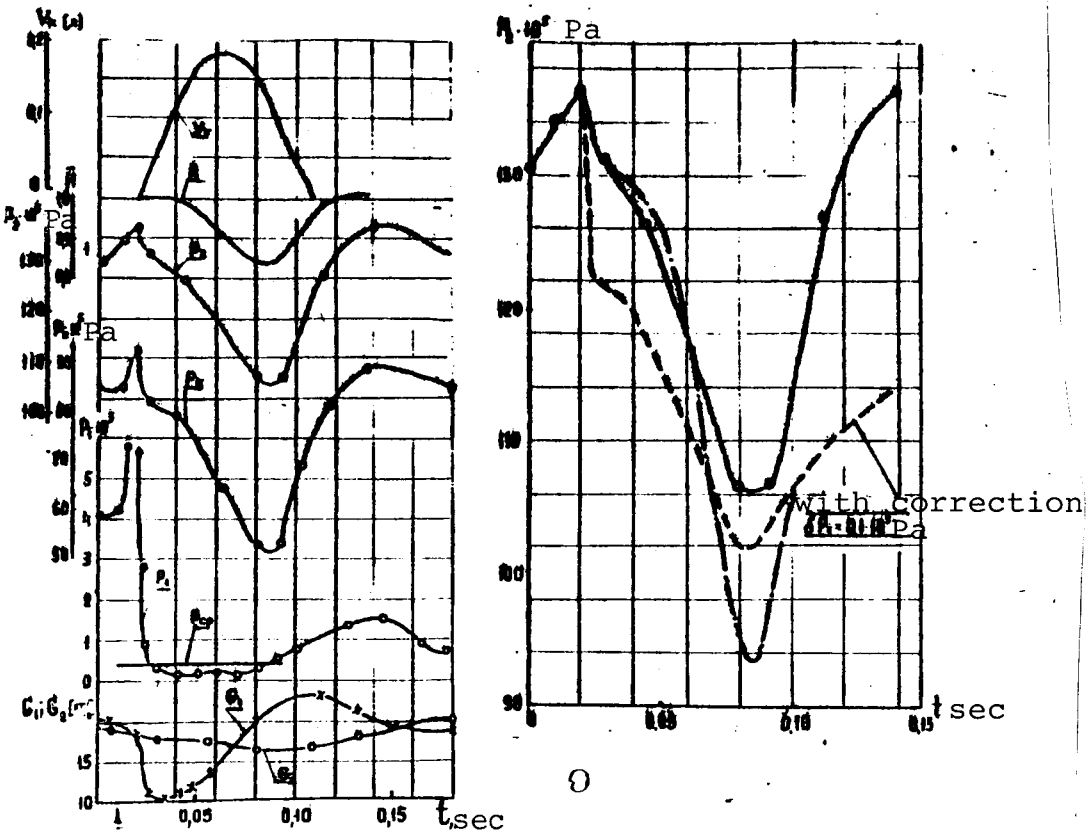

Fig. 6.

/141

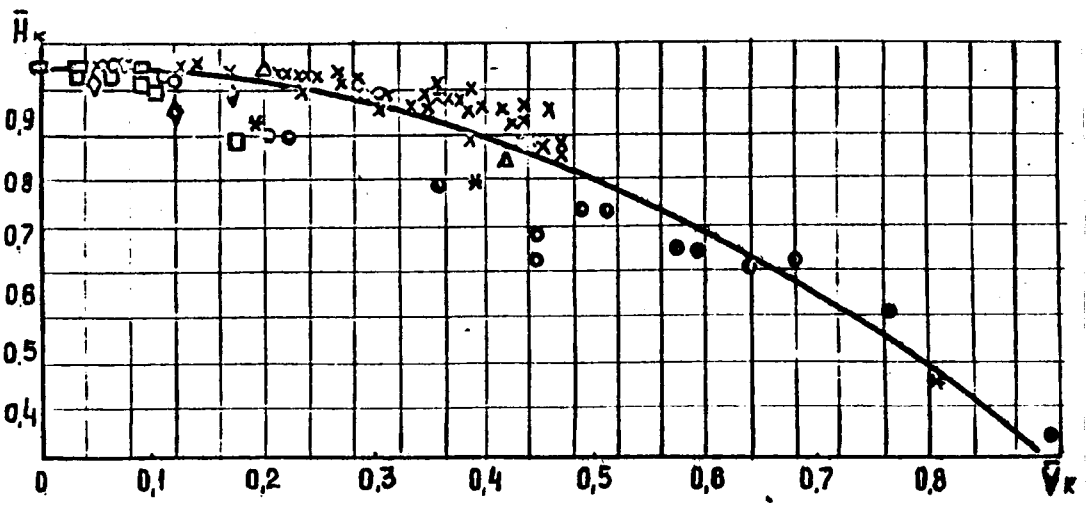

Fig. 7.

Based on the obtained generalized relation, mathematical models of the dynamics of cavitation interruptions of pump pressure were constructed: /140

Model I

$$\Delta P_H = \Delta P_H^{\delta_K} \cdot \bar{H};$$

$$\frac{d\bar{H}}{dt} = \frac{\bar{H}_{CT} - \bar{H}}{\tau_H};$$

$$\tau_H = \frac{\rho_\ell V_H^K}{G_1 f'(\bar{V}_K)};$$

Model II

$$\Delta P_H = \Delta P_H^{\delta_K} \cdot \bar{H}$$

$$\bar{H} = f(\bar{V}_K);$$

$$\frac{d\bar{V}_K}{dt} = \frac{G_2 - G_1}{\rho_\ell V_H^K}.$$

Here $\Delta P_H^{\delta_K} = n^2 \Phi\left(\frac{Q}{n}\right)$ is the pump pressure according to the universal pressure characteristic; ΔP_H is the pump pressure during cavitation; $\bar{H} = f(\bar{v}_K)$ is the relative reduction of pressure during cavitation; $v_K = v/v_H^K$ is the relative volume of the cavity; v_H^K is the volume of the screw and impeller; G_1 and G_2 represent the liquid flow at the inlet and outlet of the pump. The static cavitation (interruption) characteristics of pump pressure are used in the first model.

$\bar{H}_{CT} = f\left(\frac{p_1 - p_s}{\rho_\ell n^2}, \frac{Q}{n}\right)$ and the variable of liquid stay time in the band τ_H = var. at $G_1 = G_2$. In the second model the static cavitation characteristics of maximum flow rates through the pump $G_{np} = f\left(\frac{p_{np} - p_s}{\rho_\ell n^2}\right)$ are used:

$$G_1 = \begin{cases} G_2 \text{ at } G_2 < G_{pr} \text{ and } \bar{V}_K = 0 \\ G_{pr} \text{ at } G_2 > G_{pr} \text{ and } \bar{V}_K = 0 \\ G_{pr} \text{ at } G_2 \leq G_1, \quad \bar{V}_K > 0 \end{cases}$$

The first model is valid for conditions with relatively minor cavitations ($1 \geq \bar{H} \geq 0.6$), the second for the entire range ($1 \geq \bar{H} \geq 0$). Figure 6 gives the results of a comparison of experimental transient processes with calculated ones. There are some differences in the quantitative indices of the processes. Introduction into the first model of correction $\delta P_1 = 0.1 \times 10^5$ Pa for accuracy of measuring pressure $P_1(t)$ provides better agreement. Thus, the obtained mathematical models allow accounting for the dynamics of cavitation interruptions of pump pressure in calculations of the start and other transient conditions of ZhRD. /142

5. Diagnosing TNA Transient Conditions

Technical diagnostics have been widely developed in aviation gas-turbine engines and have recently begun use in ZhRD. We used the following methods for diagnosing TNA in model conditions:

-- recording and analysis of TNA rotor mechanical vibrations produced by its hydrodynamic loads, mass imbalance, shaft

/143

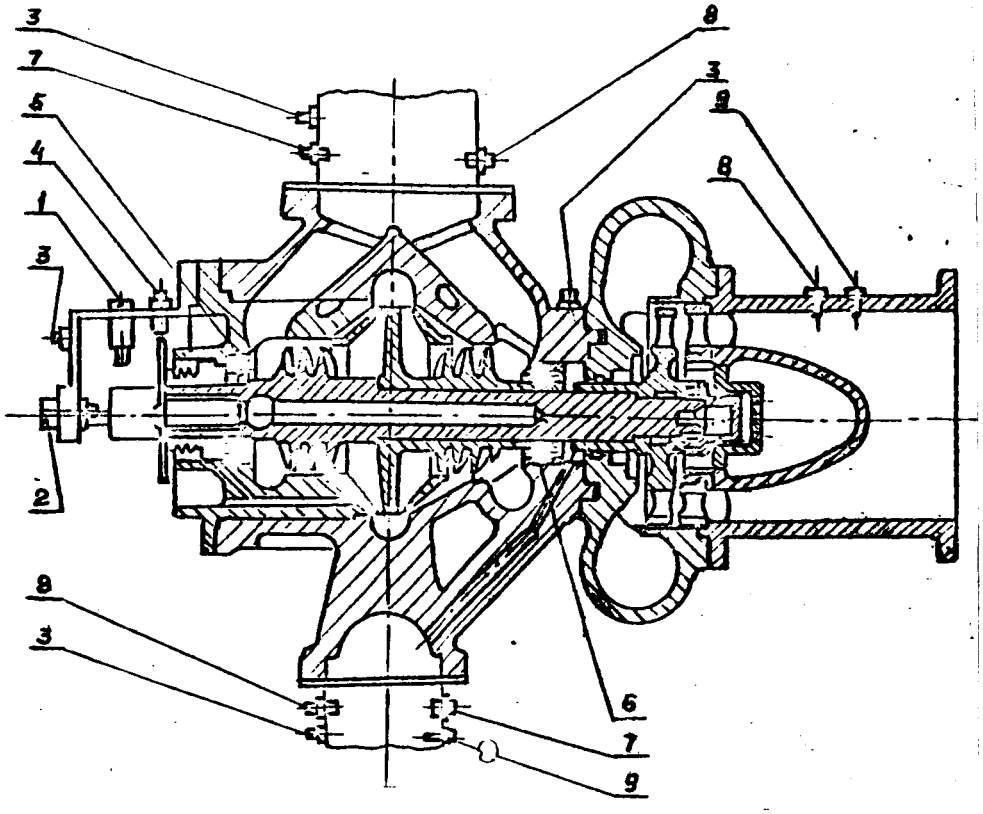

Fig. 8.

elasticity and support pliability; /142

-- experimental calculation determination of hydrodynamic loadings of the rotor according to measurement of mean values of parameters of steady and transient conditions. To understand the complex interaction of hydrodynamic and mechanical forces, the pattern of combined action of the housing vibrations, radial and axial forces of shaft displacements, and the thermal state of the bearing are studied. The combination of measuring equipment implemented on a full-scale TNA includes strain gauges of radial forces, built into the bearing, a multijunction annular thermocouple, current vortex sensors of shaft radial and axial displacements, vibration tranducers on the housing in the area of the support, and pressure-pulsation sensors at the pump's inlet and outlet. Figure 8 shows a diagnostic diagram of TNA preparation. Under modeling conditions, research is conducted by replacing the actual fuel components with water and the producer gas with air. Various methods of varying the loads on the TNA rotor are then used. A convenient means of simulating dynamic phenomena under these conditions is artificially bringing the pump into cavitation conditions. This method makes it possible, in

/144

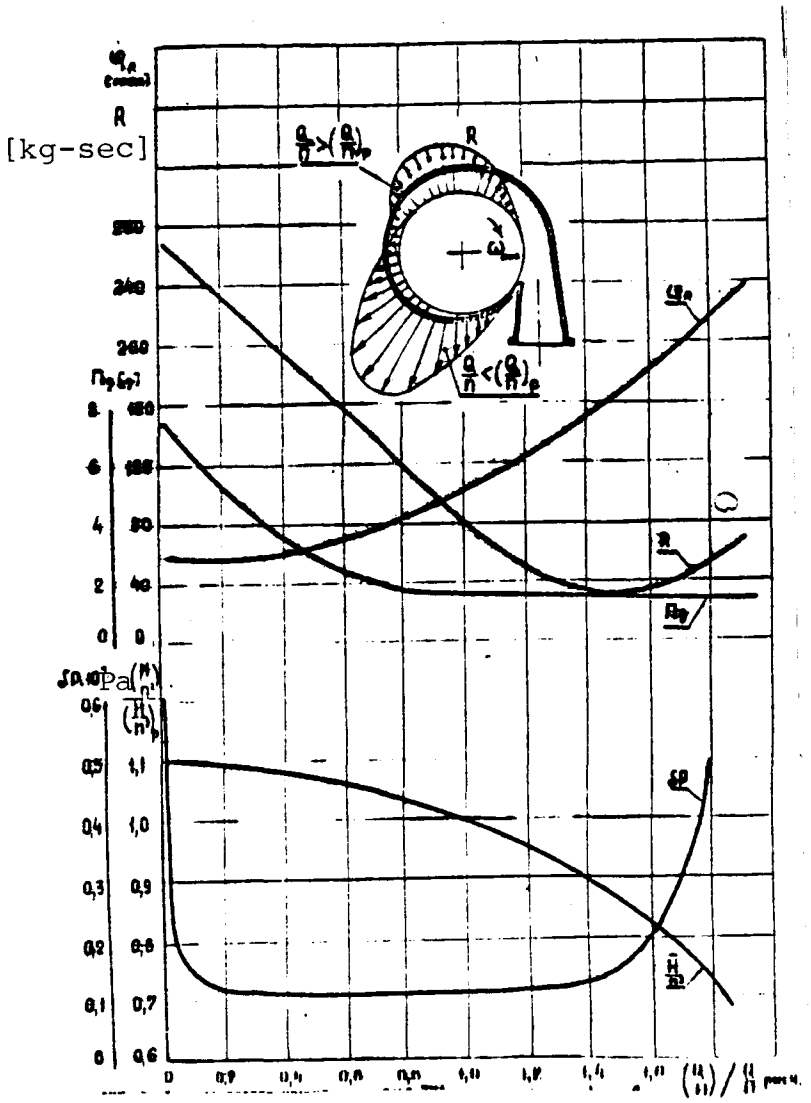

Fig. 9.

particular, to change the hydrodynamic loads on the rotor within /142
wide limits and to assign the desired level of modal parameters, including with respect to flow rate of cooled liquid through the bearing. This equipment allows obtaining complex information about the dynamic loadings and displacement of the rotor with errors /145
not exceeding 10% in the 5-2000 Hz frequency range.

Research has shown that significant increase in loads on the bearing and vibration displacements of the rotor are observed in transient conditions only with severe throttling of the pump -- at low values of parameter Q/n (Fig. 9). Here even the direction of the radial force is altered. If in condition Q/n nom. the force is directed towards large cross-sections of the diffuser

then in throttling conditions there is a change in direction towards smaller diffuser cross-sections. At $Q/n = 0.1$ the change in force direction is $\sim 50°$. Cavitational self-oscillations in the "pump-inlet line" system do not lead to substantial additional loadings of the bearing. The obtained data are used to develop a mathematical model of a TNA as a diagnostic object.

REFERENCES

1. Glikman, B. F., Avtomaticheskoye regulirovaniye zhidkostnykh raketnykh dvigateley [Automatic Control of Liquid Fuel Rocket Engines], Moscow, 1974.

2. Makhin, V. A., N. P. Milenko, L. V. Pron', Teoreticheskiye osnovy eksperimental'noy otrabotki ZhRD [Theoretical Foundations of Liquid Fuel Rocket Engine Experimental Development], Moscow, 1973.

HIERARCHY OF MATHEMATICAL MODELS OF AIRCRAFT CONTROL MOTORS

V. N. Gladkova, V. V. Kokorin, Ye. V. Solov'yev

Introduction. The modern approach to designing complex sys- /146
tems, including motors (DU) for controlling aircraft (LA), is based on comprehensive calculation of the interaction between both system components and external conditions. This leads to the need for discovering quantitative associations of DU operating processes with control system (SU) characteristics and the properties of the controlled motions of LA. This problem can be solved only using modeling methods, and particularly mathematical modeling methods, widely used in modern engineering practice. Mathematical modeling lies at the foundation of automated design, the methodology of which is based on use of a systems-technical approach. This approach, in turn, relies on the hierarchic principle, which provides a description of the operating processes of functional assemblies in complex systems with different degrees of simplification. Thus, for automated design of optimal DU for LA control we need to construct a hierarchic structure of a complex of mathematical models (MM) distinguished by a different level of simplification in describing DU function. This level is associated with the need for retaining in the MM those processes and phenomena selected as definitive during design. These processes have to be provided essential similarity with the original and insubstantial difference of the model with respect to other indices of operating process quality which are not definitive. The limiting conditions in /147
developing MM are cost and time factors. The former are determined by the available computer facilities and the second by the time allotted to the design process.

Problem statement and solution methods. The question of constructing a hierarchic complex of MM of the functioning of LA control system DU is associated most of all with providing a foundation for the choice of structure and parameters to identify models ensuring that the modeled processes are equal to the real ones. Assume that the real process of DU function and its model are characterized by change over time of value $\bar{x}(t) = \{x_\theta(t)\}$, where $\theta = 1, 2, \ldots, L$ and $\bar{x}_M(t) = \{x_{mq}(t)\}$, where $q = 1, 2, \ldots, h_{i-1}, \ldots, l$, which are mutually associated by relations $F_j[\bar{x}(t)] = C_j(t)$, where $j = 1, 2, \ldots, P$ and $F_{MK}[\bar{x}_M(t)] = C_{MK}(t)$, where $K = 1, 2, \ldots, P_M$, L and l are the total number of parameters characterizing the real process and its model, respectively, h is the number of parameters determining the existence of similarity between the studied process and the real ones; $C_j(t)$ and $C_{MK}(t)$ are known parameters,

$P_u P_M$ is the number of discovered interrelations between the real process and those processes implemented in the model, respectively (generally $P_M << P$); then the condition of adequacy of the modeled process to the real one can be written as:

$$\sup(\inf) \mathcal{F}[\Phi\{x_\theta(t)\}, \Phi_i\{x_{m\,h_i}(t)\}, \text{ at } \delta\Phi_i[\{x_\theta(t)\}, \{x_{m(q_i-h_i)}(t)\}] \leq \varepsilon,$$

where δ_i is the specific functional, $\delta\Phi_i$ is the constraint, and ε is a constant preassigned to the bounded quantity.

The form of the specific functional and of the constraints is determined by the tasks of the modeled system in the design process and the characteristics of the computer support equipment. The form of the specific functional generally determines the form of the model and, in turn, the hierarchic structure of the complex of models is determined by the hierarchy of the specific functionals.

When examining the DU as an element of the system controlling the motion of various LA relative to their centers of mass, in most cases it turns out that the operating process of aircraft control motors is pulsed in nature [1]. The pulsed nature of control motor operation is provided by SU command signals sent to the motor input with various durations t_K and various intervals t_n (Fig. 1). The sum $t_K + t_n = T$ characterizes the period of alternation of pulsed motor actuations, and the inverse, $1/T = f$ is the frequency of pulsed motor actuations.

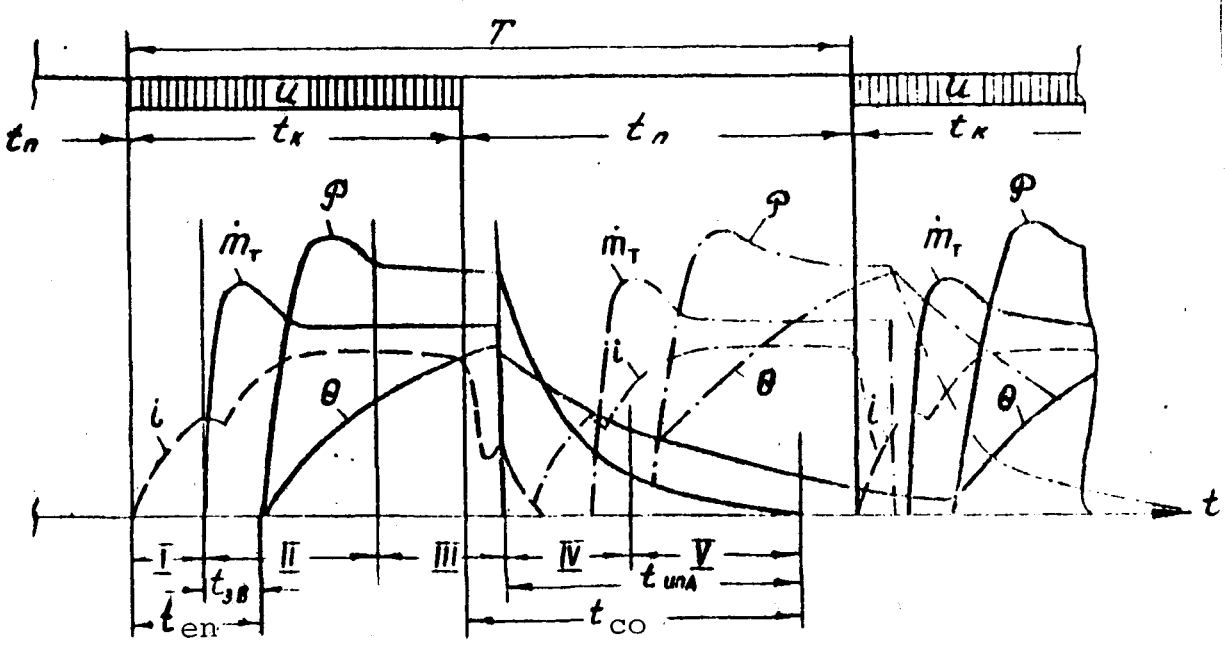

Fig. 1.

The output signals of the motor as an executive component /149
in response to SU command are: the thrust momentum of the motor $J_{gb} = \int_0^T P\,dt$, characterizing the force of the motor on the LA and the required fuel expenditure on its production $m_T = \int_0^T m(t)\,dt$. In this connection, the idea of completeness of modeling the functioning of control motors has to be associated with completeness of description of the thrust change over time -- $P(t)$ -- and the fuel consumption $m_T(t)$. Since the actual output signals of the motor are shifted in time in models of DU functioning, we also have to account for lags of thrust -- t_{en} -- and cutoff t_{co} (see Fig. 1). The nature of change over time of $P(t)$, $\dot{m}_T(t)$, and the lag times t_{en} and t_{co} are, to some extent, determined by the features of control motor construction and the type of fuel employed. Many works [2, 3] have shown, however, that the change of output signals over time is also largely determined by condition factors, i.e., the characteristics of combination of times t_K and t_n. When modeling this effect we have to examine both an account of the prehistory of the motor's state, which considers the presence of heat and mass exchange between adjacent motor engagement pulses. This circumstance necessitates reproducing in the models the connection between the modeled values and the current values of $t_K(t)$ and $t_n(t)$. Three characteristic cases determining the conditions of heat-mass exchange in pulsed motor operation conditions have to be examined: independent pulses (isolated engagements), pulses associated by heat exchange (shown in Fig. 1 by solid lines), and pulses associated by heat and mass exchange simultaneously (shown in Fig. 1 by solid and dot-and-dash lines).

The entire process of one act of control motor engagement can be represented as consisting of a minimum five consecutive time segments (Fig. 1): I -- the segment of electromagnetic valve gear operation delay; II -- the segment of valve opening delay, fuel ignition lag, and non-steady thrust output to the nominal level; III -- the segment of nominal thrust and fuel expenditure; IV -- the segment of motor combustion chamber evacuation; V -- the segment of fuel evaporation from the motor spaces aft of the valve.

Depending on the duration of the input signals and their /150
different combinations, in the process of DU functioning we may encounter different combinations of their linkage: I, II, III, IV, V, I, II ...; I, II, IV, I, II, ...; I, II, III, I, II, ..., etc. Proper description of the changes over time of the modeled parameters P, $\dot{m}_T$, t_{en}, and t_{co} in all possible combinations of input signals is provided by the structure of MM construction, a typical block diagram of which is shown in Fig. 2. The form of the approximating relations for each segment can be chosen in different ways. The degree of complexity of the description of

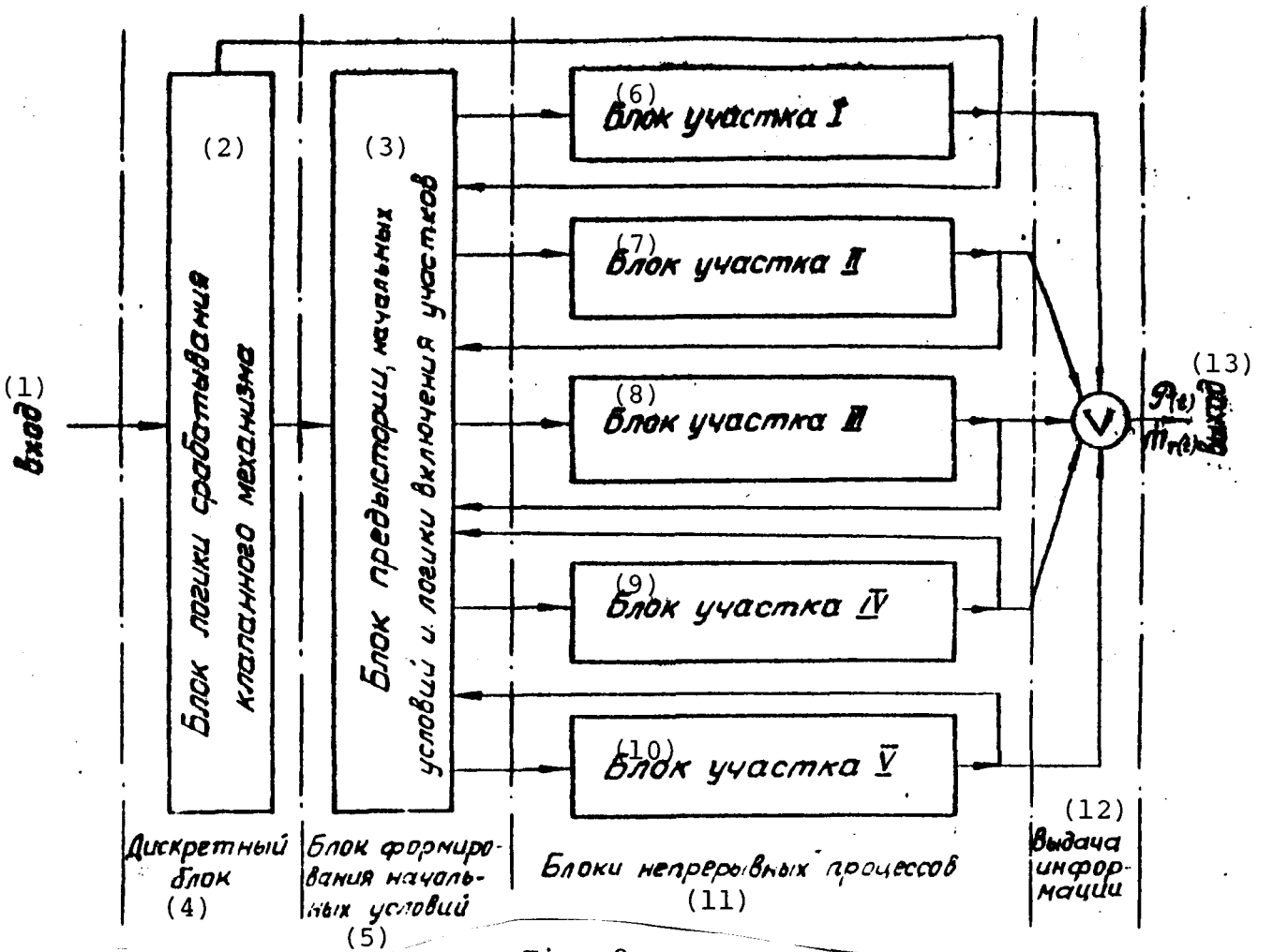

Fig. 2.

Key: (1) Input
(2) Valve mechanism operation logic block
(3) Block of prehistory, initial conditions, and section inclusion logic
(4) Discrete block
(5) Generation of initial conditions block
(6) Section I block
(7) Section II block
(8) Section III block
(9) Section IV block
(10) Section V block
(11) Continuous processes block
(12) Data supply block
(13) Output

operating processes is determined by the required accuracy of reproduction of the modeled values and by the operating range of input signal combinations. The construction of MM of control motor function is based on the principles of structural and parametric identification of the modeled values to the real ones and is implemented using one method of regression analysis according to the outline shown in Fig. 3. The basic role in the process of identifying modeled and real processes is played by goodness of fit. /150

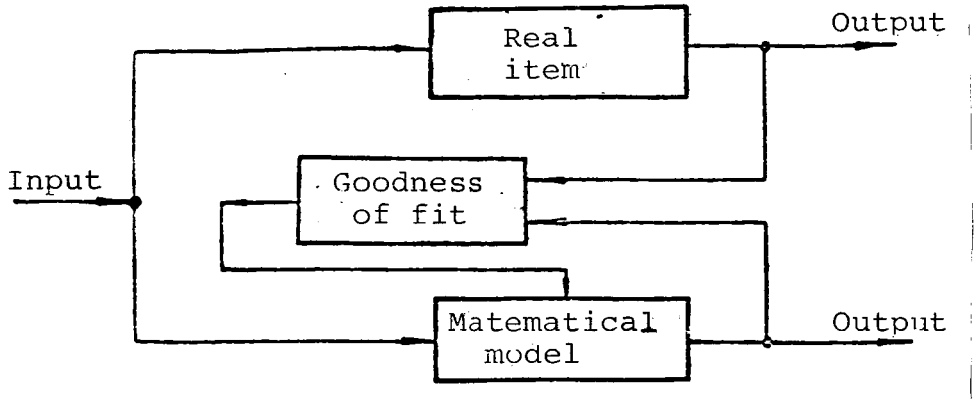

Fig. 3.

Analysis of the operating processes in control motors [2, 3] indicates that each engagement of a motor in the pulsed mode of operation for all possible combinations of command signals corresponds to a certain value of the specific thrust pulse, obtained in the form of ratio

$$J_{y\,imp} = \frac{\int_0^{t} P(t)\,dt}{\int_0^{t} \dot{m}(t)\,dt}.$$

J_{yimp} accounts for the force of the motor on the LA and the fuel expenditures needed to produce it. At the same time, the specific thrust pulse characterizes, with a given type of fuel, the degree of motor perfection. The specific thrust pulse obtained for any number of engagements (n) in a series of pulses reflects firstly the losses associated with the non-steady nature of triggering and cutoff processes, the proportion of which increases with diminishing duration of the command signal. The value J_{yimp} also accounts for heat and mass exchange between adjacent pulses, associated with the duration of the interval between engagements, that is, it accounts for the prehistory of the motor's state. Thus, J_{yimp} is determined by any of a set of mode factor combinations: J_{yimp} [t_K, t_n, n]. The maximally possible value of the specific thrust pulse of a control motor is determined in the continuous mode of its operation (J_{ycont}). Its value is stable and determined by the type of fuel employed and the degree of motor construction perfection. The ratio $J_{yimp}/J_{ycont} = J_y$ retains the properties of complex assessment

of the effect of the pulsed mode with respect to the ratio to the continuous mode and thereby characterizes the proportion of losses produced by the pulsed operating mode. Thus it is expedient to adopt a dimensionless complex as the goodness of fit of the mathematical model to a real item. /152

The degree of completeness of the accounting in this criterion of the heat and mass exchange characteristics, associated with the prehistory of motor condition, can be used to construct its hierarchic structure, which reflects the different level of detail in description of operating processes in pulsed modes in mathematical models.

Taken as lowest level of the hierarchy is the goodness of fit correponding to the condition of production of independent pulses by the motor. Corresponding to this case is condition $\bar{J}_y = F(t_k, n)$, for each single engagement $n = 1$. The MM of this level reproduce the continuous mode of operation and single motor engagements between which there is no heat or mass exchange.

The next higher level is taken as complication of the goodness of fit, which considers the connection between the specific thrust pulse and pulse mode parameters, $\bar{J}_y = F(t_K, t_n, n)$ under the condition that $t_K = \text{const.}$, $t_n = \text{const.}$, and $n \geq n_{est}$. Thus, for each combination of t_K and t_n the specific thrust pulse of the motor has a specific value with an established heat exchange of the motor in the pulsed operating mode. The MM of this level are capable of reproducing established pulsed operating modes considering an established heat and mass exchange process. /153

The next hierarchic level is associated with accounting for the goodness of fit of an unestablished pulsed mode or its non-steady state. An unestablished pulsed mode is manifested in the goodness of fit by accounting for the specific thrust pulse of the motor, associated with the sequential number of the engagement $\bar{J}_y = F(t_K, t_n, n)$, under the condition that $t_K = \text{const.}$, $t_n = \text{const.}$, and $n \geq 1$. The non-steady nature of the pulsed mode is accounted for by the dependence of the goodness of fit on the values of t_K and t_n, which can be in any combination at any point in time, but under the condition that each combination corresponds to a quasisteady pulsed mode. In this case $\bar{J}_y[t_K, t_n, n]$ under the condition that $t_K = \text{var.}$, $t_n = \text{var.}$, and $n \geq n_{est}$. The MM of this level are capable of reproducing either unsteady pulsed modes, considering an unsteady process of heat and mass exchange, or an unsteady nature of change in established modes considering an established process of heat and mass exchange.

At the highest hierarchic level in the goodness of fit we need simultaneous accounting of the effects of both the unestablished pulsed mode and the unsteadiness of change in the

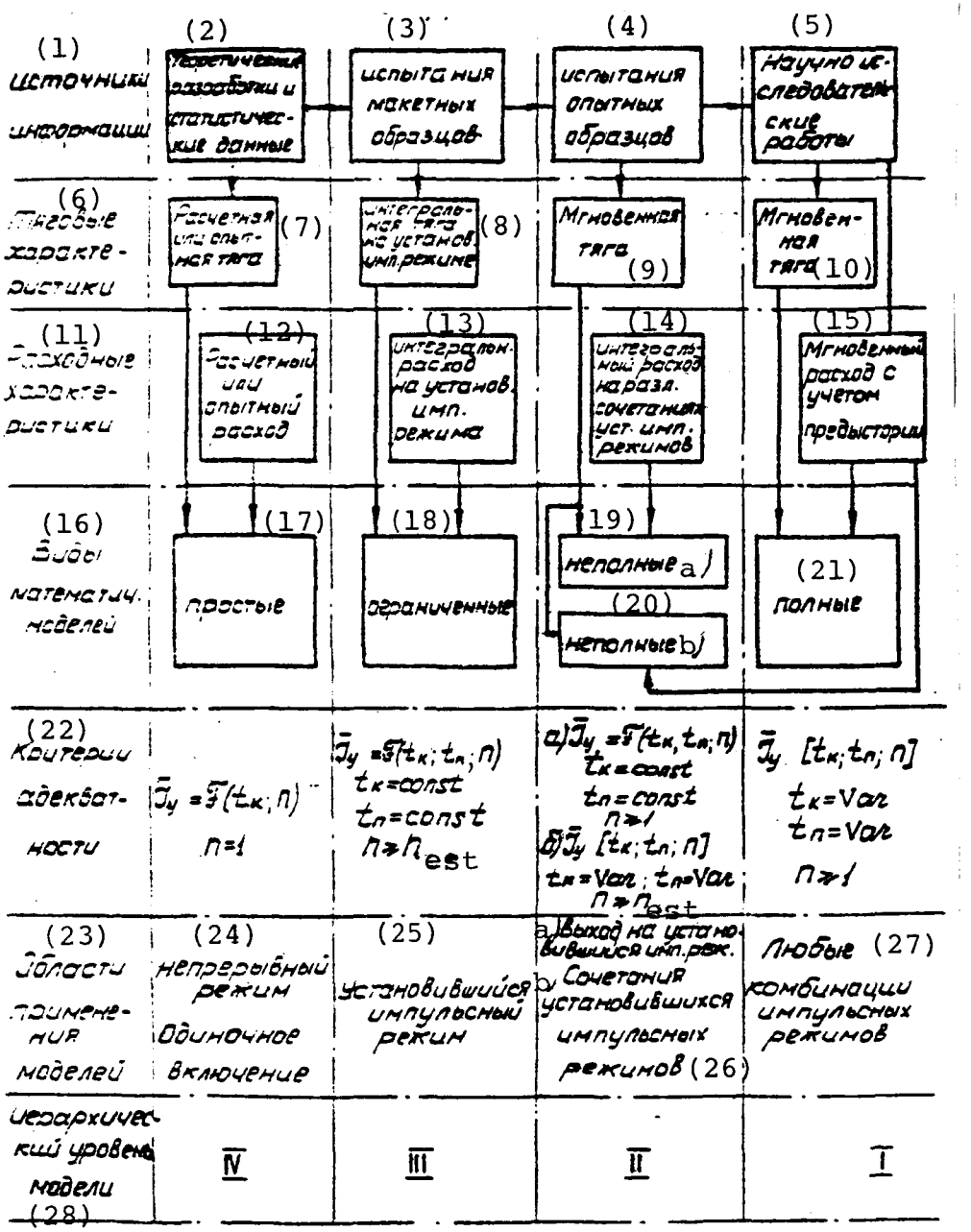

Fig. 4.

KEY: (1) Data source
(2) Theoretical development and statistical data
(3) Tests of mockups
(4) Test of experimental models
(5) Scientific research
(6) Thrust characteristics
(7) Calculated or experimental thrust
(8) Integral thrust in established pulse mode
(9), (10) Instantaneous thrust
(11) Consumption charateristics
(12) Calculated experimental consumption
(13) Integral consumption in established pulse mode
(14) Integral consumption in different combinations of modes
(15) Instantaneous thrust considering prehistory

(Continued on next page)

Caption for Fig. 4 (continued):

(16) Types of mathematical models
(17) simple
(18) limited
(19) incomplete a)
(20) incomplete b)
(21) complete
(22) Goodness of fit
(23) Areas of application for models
(24) Continuous mode, Single engagement
(25) Established pulsed mode
(26) a) Exit to established pulsed mode
b) Combinations of established pulsed modes
(27) Any combinations of pulsed modes
(28) Hierarchic level of model

unestablished modes. In determining the criterion this appears /153
as $\bar{J}_y[t_K, t_n, n]$, if t_K = var., t_n = var., and $n \geq 1$. The MM of the highest level are capable of reproducing any combinations of pulsed operating modes of a motor, considering heat and mass exchange processes.

Results. The mathematiccal models are constructed in accordance with the hierarchy of the adopted criterion. Depending on the degree of completeness of description of pulsed mode characteristics in MM, models are called: simple, limited, incomplete, and complete (Fig. 4).

In turn, a different degree of description detail of the /155
modeled values is possible at each level of the hierarchy. As an example, Fig. 5 shows a comparative assessment of the lowest level MM with a different degree of detail in description of the modeled values with their reproduction of single engagements. In model 1 the processes of change in thrust and consumption over time are idealized by a relay function considering delay. In model 2 the process of thrust change is taken as the real one, but with a delay constant over time, and the change in consumption is idealized by a relay function. In Model 3 the process of thrust and consumption change is take as real with delay. In addition, a relation is introduced which reflects the connection between the process of pulse aftereffect with a prehistory of motor state with respect to the duration of the command signal. Experimental points obtained by calculation in [3] are given for comparison. We can see from comparison of the modeling results that the simplest models (1) can reproduce single engagements for a command signal duration of over 0.6 sec. At lower durations the error of determining fuel consumption increases. Model 2 has a systematic $\bar{J}_y$ reproduction error that increases as the duration of the command decreases, a fact showing the inadequacy of modeling only of real thrust. Model 3 indicates the modeled value of $\bar{J}_y$ in a field of experimental point scatter and uniquely correctly reflects the real process.

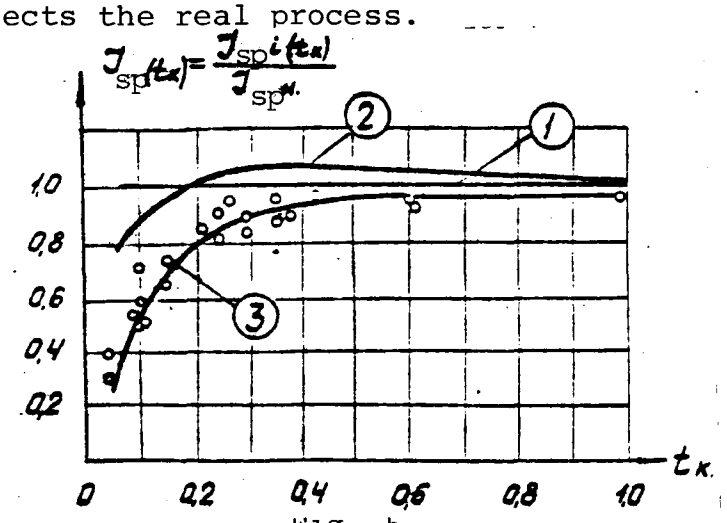

Fig. 5.

Similar results are observed in comparative assessments of models of higher levels of MM hierarchic structure. /157

Conclusion. The development of MM is associated first of all with choice of information sources. For the obtained hierarchic structure of MM the continuity is displayed both by the goodness of fit criteria and by the information sources (see Fig. 4). The goodness of fit criteria of each lower level are a special case of higher level MM criterion. The information used to construct the MM of higher levels includes the information sources of lower level MM.

The cyclicity of MM development consists in the fact that information for higher level MM development can be partially obtained using models of the lower level. A shortage of information is filled in in the process of step-by-step DU design (Fig. 6).

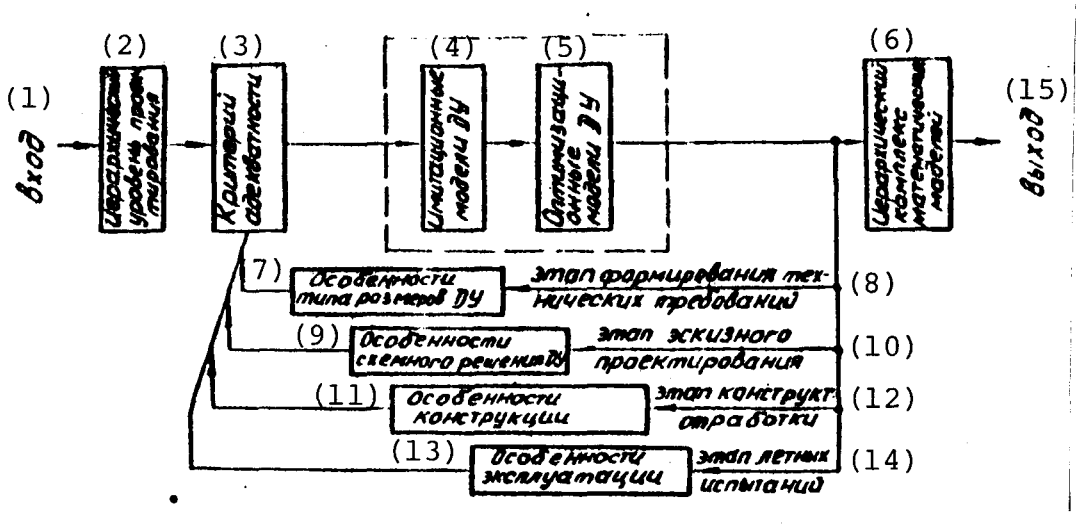

Fig. 6.

KEY: (1) input
(2) Hierarchic level of design
(3) Goodness of fit
(4) DU simulation models
(5) DU optimization models
(6) Hierarchic complex of mathematical models
(7) Features of DU size type
(8) stage of technical requirements formulation
(9) Features of DU outline solutions
(10) stage of draft design
(11) Structural features
(12) stage of structral development
(13) Operational features
(14) stage of flight tests
(15) output

REFERENCES

1. "Cosmonautics," Malen'kaya entsiklopediya [Concise Encyclopedia], Moscow, 1970.

2. Belyayev, N. M., and Ye. I. Uvarov, Raschet i proyektirovaniye reaktivnykh sistem upravleniya letatel'nykh apparatov [Calculation and Design of Aircraft Reactive Control Systems], Moscow, 1974.

STANDARD TITLE PAGE

1. Report No. NASA TM-88583	2. Government Accession No.	3. Recipient's Catalog No.
4. Title and Subtitle THEORY AND DESIGN OF FLIGHT-VEHICLE ENGINES		5. Report Date April 1987 6. Performing Organization Code
7. Author(s) V. T. Zhdanov and R. I. Kurzinor, Eds.		8. Performing Organization Report No. 10. Work Unit No.
9. Performing Organization Name and Address Leo Kanner Associates, Redwood City, California 94063		11. Contract or Grant No. NASW-4005 13. Type of Report and Period Covered Translation
12. Sponsoring Agency Name and Address National Aeronautics and Space Administration, Washington, D.C. 20546		14. Sponsoring Agency Code

15. Supplementary Notes

Translation of Teoriya i konstruktsiya dvigateley letatel'nykh apparatov, USSR Academy of Sciences, Moscow, 1979. 158 pages.

83A22651

16. Abstract

Papers are presented on such topics as the testing of aircraft engines, errors in the experimental determination of the parameters of scramjet engines, the effect of the nonuniformity of supersonic flow with shocks on friction and heat transfer in the channel of a hypersonic ramjet engine, and the selection of the basic parameters of cooled GTE turbines. Consideration is also given to the choice of optimal wedge angle for the air intake of a hypersonic ramjet engine, the use of jet engines for the acceleration of aerospace vehicles, etc.

17. Key Words (Selected By Author(s))	18. Distribution Statement Unclassified-Unlimited		
19. Security Classif. (of this report) Unclassified	20. Security Classif. (of this page) Unclassified	21. No. of Pages 139	22.